Klimaänderung I
2. Das sich verändernde Klimasystem

Robert Sausen

Institut für Physik der Atmosphäre
Deutsches Zentrum für Luft- und Raumfahrt
Oberpfaffenhofen

Vorlesung WS 2022/23

LMU München

Technical information

- http://www.pa.op.dlr.de/~RobertSausen/vorlesung/index.html
  - Most recent update on the lecture
  - Slides of the lecture (with some delay)

  - See also LSF https://lsf.verwaltung.uni-muenchen.de/

- Contact: robert.sausen@dlr.de

- Further information:
  - www.ipcc.ch
  - www.de-ipcc.de

Contents of IPCC AR 6 2021: Working Group I: the Physical Science Basis

Chapters

IPCC 2021

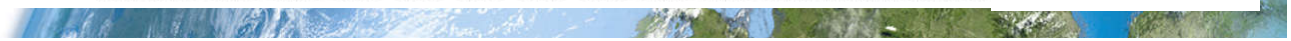

Chapter 2: Changing state of the climate system

Coordinating Lead Authors:

Sergey K. Gulev (Russian Federation), Peter W. Thorne (Ireland/United Kingdom)

Lead Authors:

Jinho Ahn (Republic of Korea), Frank J. Dentener (EU/The Netherlands), Catia M. Domingues (Australia, United Kingdom/Brazil), Sebastian Gerland (Norway/Germany), Daoyi Gong (China), Darrell S. Kaufman (United States of America), Hyacinth C. Nnamchi (Nigeria,Germany/Nigeria), Johannes Quaas (Germany), Juan A. Rivera (Argentina), Shubha Sathyendranath (United Kingdom/Canada, Overseas Citizen of India, United Kingdom), Sharon L. Smith (Canada), Blair Trewin (Australia), Karina von Schuckmann (France/Germany), Russell S. Vose (United States of America)

Chapter 2: Changing state of the climate system

Contributing Authors (1):

Guðfinna Aðalgeirsdóttir (Iceland), Samuel Albani (Italy), Richard P. Allan (United Kingdom), Richard A. Betts (United Kingdom), Lea Beusch (Switzerland), Kinfe Beyene (Ethiopia), Jason E. Box (Denmark/United States of America), Denise Breitburg (United States of America), Kevin D. Burke (United States of America), Michael P. Byrne (United Kingdom/Ireland), John A. Church (Australia), Sloane Coats (United States of America), Naftali Cohen (United States of America), William Collins (United Kingdom), Owen R. Cooper (United States of America), Pedro Di Nezio (United States of America), Fabio Boeira Dias (Finland/Brazil), Ed J. Dlugokencky (United States of America), Timothy Dunkerton (United States of America), Paul J. Durack (United States of America/Australia), Tamsin L. Edwards (United Kingdom), Veronika Eyring (Germany), Chris Fairall (United States of America), Vitali Fioletov (Canada), Piers Forster (United Kingdom), Gavin L. Foster (United Kingdom), Baylor Fox-Kemper (United States of America), Qiang Fu (United States of America), Jan S. Fuglestvedt (Norway), John C. Fyfe (Canada), Marie-José Gaillard (Sweden/Switzerland, Sweden), Joelle Gergis (Australia), Nathan P. Gillett (Canada), Hans Gleisner (Denmark/Sweden), Nadine Gobron (EU/France), Nicholas R. Golledge (New Zealand/United Kingdom), Bradley Hall (United States of America), Ed Hawkins (United Kingdom), Alan M. Haywood (United Kingdom), Armand Hernández (Spain), Forrest M. Hoffman (United States of America), Yongyun Hu (China), Dale F. Hurst (United States of America), Masao Ishii (Japan), Samuel Jaccard (Switzerland), Dabang Jiang (China), Christopher Jones (United Kingdom), Bror Jönsson (United Kingdom/Sweden), Andreas Kääb (Norway/Germany), Ralph Keeling (United States of America), Noel S. Keenlyside (Norway/Australia, United Kingdom), John Kennedy (United Kingdom), Elizabeth Kent (United Kingdom), Nichol S. Khan (Hong Kong, China/United States of America), Wolfgang Kiessling (Germany), Stefan Kinne (Germany), Robert E. Kopp (United States of America), Svitlana Krakovska (Ukraine), Elmar Kriegler (Germany), Gerhard Krinner (France/Germany, France), Natalie Krivova (Germany), Paul B. Krummel (Australia), Werner L. Kutsch (EU/Germany), Ron Kwok (United States of America), Florian Ladstädter (Austria), Peter Landschützer (Germany/Austria), June-Yi Lee (Republic of Korea), Andrew Lenton (Australia), Lisa A. Levin (United States of America), Daniel J. Lunt (United Kingdom), Jochem Marotzke (Germany), Gareth J. Marshall (United Kingdom), Robert A. Massom (Australia), Katja Matthes (Germany), Damon H. Matthews (Canada), Thorsten Mauritsen (Sweden/Denmark), Gerard D. McCarthy (Ireland), Erin L. McClymont (United Kingdom), ...

IPCC AR6 WG I, 2021, Chapter 2

Chapter 2: Changing state of the climate system

Contributing Authors (2):

... Shayne McGregor (Australia), Jerry F. McManus (United States of America), Walter N. Meier (United States of America), Alan Mix (United States of America), Olaf Morgenstern (New Zealand/Germany), Lawrence R. Mudryk (Canada), Jens Mühle (United States of America/Germany), Dirk Notz (Germany), Lisa C. Orme (Ireland/United Kingdom), Scott M. Osprey (United Kingdom), Matthew D. Palmer (United Kingdom), Anna Pirani (Italy/United Kingdom, Italy), Chris Polashenski (United States of America), Elvira Poloczsanka (Australia/United Kingdom), Anthony Richardson (Australia), Belén Rodríguez-Fonseca (Spain), Joeri Rogelj (United Kingdom/Belgium), Steven K. Rose (United States of America), Yair Rosenthal (United States of America/Israel, United States of America), Alessio Rovere (Germany/Italy), Lucas Ruiz (Argentina), Ulrich Salzmann (United Kingdom/Germany, United Kingdom), Bjørn H. Samset (Norway), Abhishek Savita (Australia/India), Margit Schwikowski (Switzerland), Sonia I. Seneviratne (Switzerland), Isobel J. Simpson (Canada), Aimée B. A. Slangen (The Netherlands), Chris Smith (United Kingdom), Olga N. Solomina (Russian Federation), Joshua H. P. Studholme (United States of America/United Kingdom, New Zealand), Alessandro Tagliabue (United Kingdom), Claudia Tebaldi (United States of America), Jessica Tierney (United States of America), Matthew Toohey (Canada, Germany/Canada), Andrew Turner (United Kingdom), Osvaldo Ulloa (Chile), Caroline C. Ummenhofer (United States of America/Germany, United States of America), Axel von Engeln (Germany), Rachel Warren (United Kingdom), Kate Willett (United Kingdom), John W. Williams (United States of America)

IPCC AR6 WG I, 2021, Chapter 2

Chapter 2: Changing state of the climate system

Review Editors:

Timothy J. Osborn (United Kingdom), Azar Zarrin (Iran)

IPCC AR6 WG I, 2021, Chapter 2

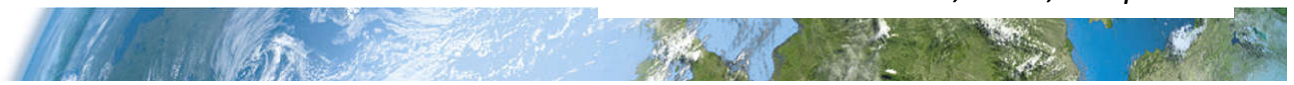

Evaluation and communication of degree of certainty in AR6 findings

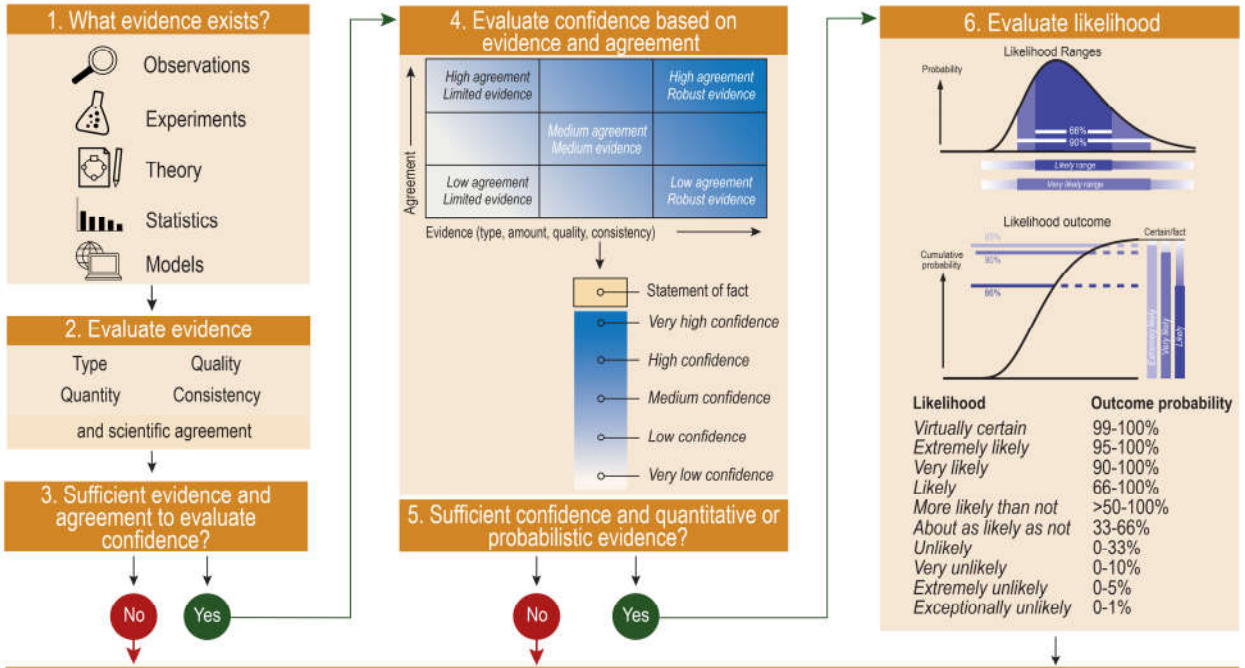

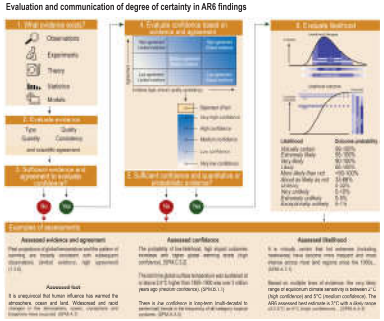

4. Evaluate confidence based on evidence and agreement

Agreement \ Evidence (type, amount, quality, consistency)		
		High agreement Robust evidence
	Medium agreement Medium evidence	
Low agreement Limited evidence		Low agreement Robust evidence
High agreement Limited evidence		

Statement of fact

- Very high confidence
- High confidence
- Medium confidence
- Low confidence
- Very low confidence

5. Sufficient confidence and quantitative or probabilistic evidence?

No

Yes

6. Evaluate likelihood

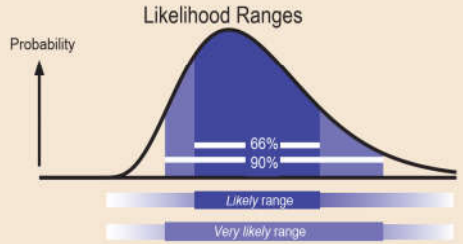

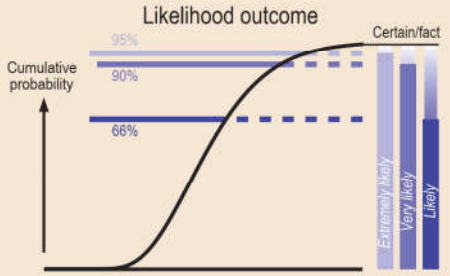

Likelihood	Outcome probability
Virtually certain	99-100%
Extremely likely	95-100%
Very likely	90-100%
Likely	66-100%
More likely than not	>50-100%
About as likely as not	33-66%
Unlikely	0-33%
Very unlikely	0-10%
Extremely unlikely	0-5%
Exceptionally unlikely	0-1%

IPCC 2021, Chap. 1

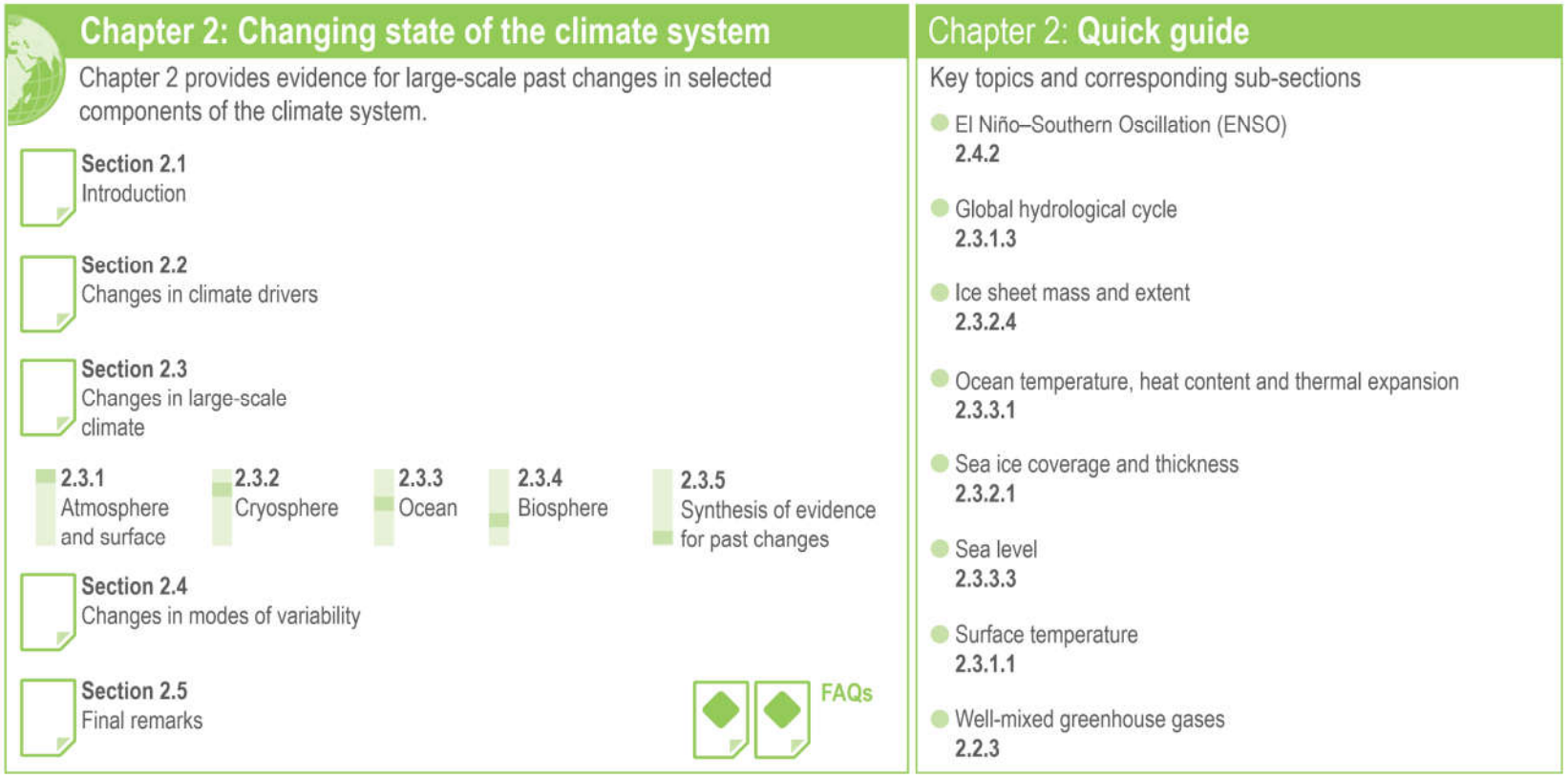

Figure 2.1 | Visual guide to Chapter 2.

IPCC 2021, Chap. 2

Chapter 2 Outline

Section 2.1 Introduction

Section 2.2 Changes in climate drivers

Section 2.3 Changes in large scale climate

2.3.1 Atmosphere and surface

2.3.2 Cryosphere

2.3.3 Oceans

2.3.4 Biosphere

Section 2.3.5 Synthesis of evidence for past changes

Section 2.4 Changes in modes of variability

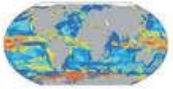

Section 2.5 Final Remarks

Cross-Chapter boxes:

CC Box 2.1 Paleoclimate reference periods (ch. 1, 3, 5–9)

CC Box 2.2 Large-scale indicators of climate change (ch. 3, 4)

CC Box 2.3 New estimates of global warming to date and key implications (ch. 1, 3, 4, 5, 7, 8, 9, 11, Atlas)

CC Box 2.4 The climate of the Pliocene (ch. 5, 7, 9)

Quick Guide

2.2.3 **Well-Mixed greenhouse gases**

2.2.8 **Effective radiative forcing**

2.3.1.1 **Surface temperature**

2.3.1.3 **Global hydrological cycle**

2.3.1.4 **Atmospheric circulation**

2.3.2.1 **Sea-ice coverage and thickness**

2.3.2.4 **Ice sheet mass and extent**

2.3.3.1 **Ocean temperature, heat content, and thermal expansion**

2.3.3.3 **Sea-level**

2.3.3.6 **Ocean deoxygenation**

2.4.1 **Annular modes**

2.4.2 **El Niño Southern Oscillation**

Figure 2.1: Chapter 2 visual abstract of contents.

IPCC 2021, Chap. 2

Statements in the Executive Summary

Chapter 2 assesses observed large-scale changes in climate system drivers, key climate indicators and principal modes of variability. Chapter 3 considers model performance and detection/attribution, and Chapter covers projections for a subset of these same indicators and modes of variability. Collectively, these chapters provide the basis for later chapters, which focus upon processes and regional changes. Within Chapter 2, changes are assessed from in situ and remotely sensed data and products and from indirect evidence of longer-term changes based upon a diverse range of climate proxies. The time-evolving availability of observations and proxy information dictate the periods that can be assessed. Wherever possible, recent changes are assessed for their significance in a longer-term context, including target proxy periods, both in terms of mean state and rates of change.

IPCC 2021, Chap. 2

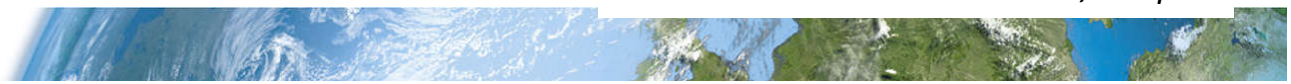

Global mean surface temperature over the past 60 million years

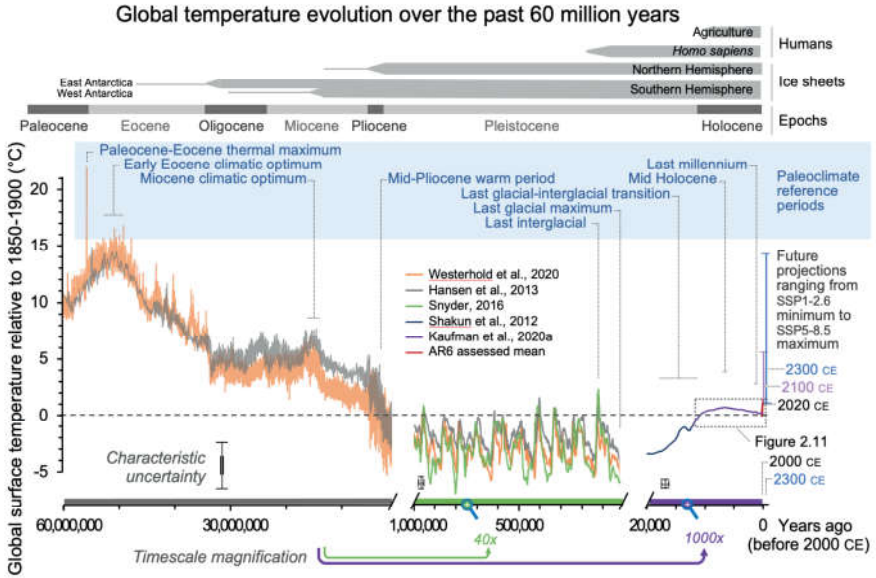

Cross-Chapter Box 2.1, Figure 1 | Global mean surface temperature (GMST) over the past 60 million years (60 Myr) relative to 1850–1900 shown on three time scales. Information about each of the nine paleo reference periods (blue font) and sections in AR6 that discuss these periods are listed in Cross-Chapter Box 2.1 Table 1. Grey horizontal bars at the top mark important events. Characteristic uncertainties are based on expert judgement and are representative of the approximate midpoint of their respective time scales; uncertainties decrease forward in time. GMST estimates for most paleo reference periods (Figure 2.34) overlap with this reconstruction, but take into account multiple lines of evidence. Future projections span the range of global surface air temperature best estimates for SSP1–2.6 and SSP5–8.5 scenarios described in Section 1.6. Range shown for 2100 is based on CMIP6 multi-model mean for 2081–2100 from Table 4.5; range for 2300 is based upon an emulator and taken from Table 4.9. Further details on data sources and processing are available in the chapter data table (Table 2.SM.1).

IPCC 2021, Chap. 2

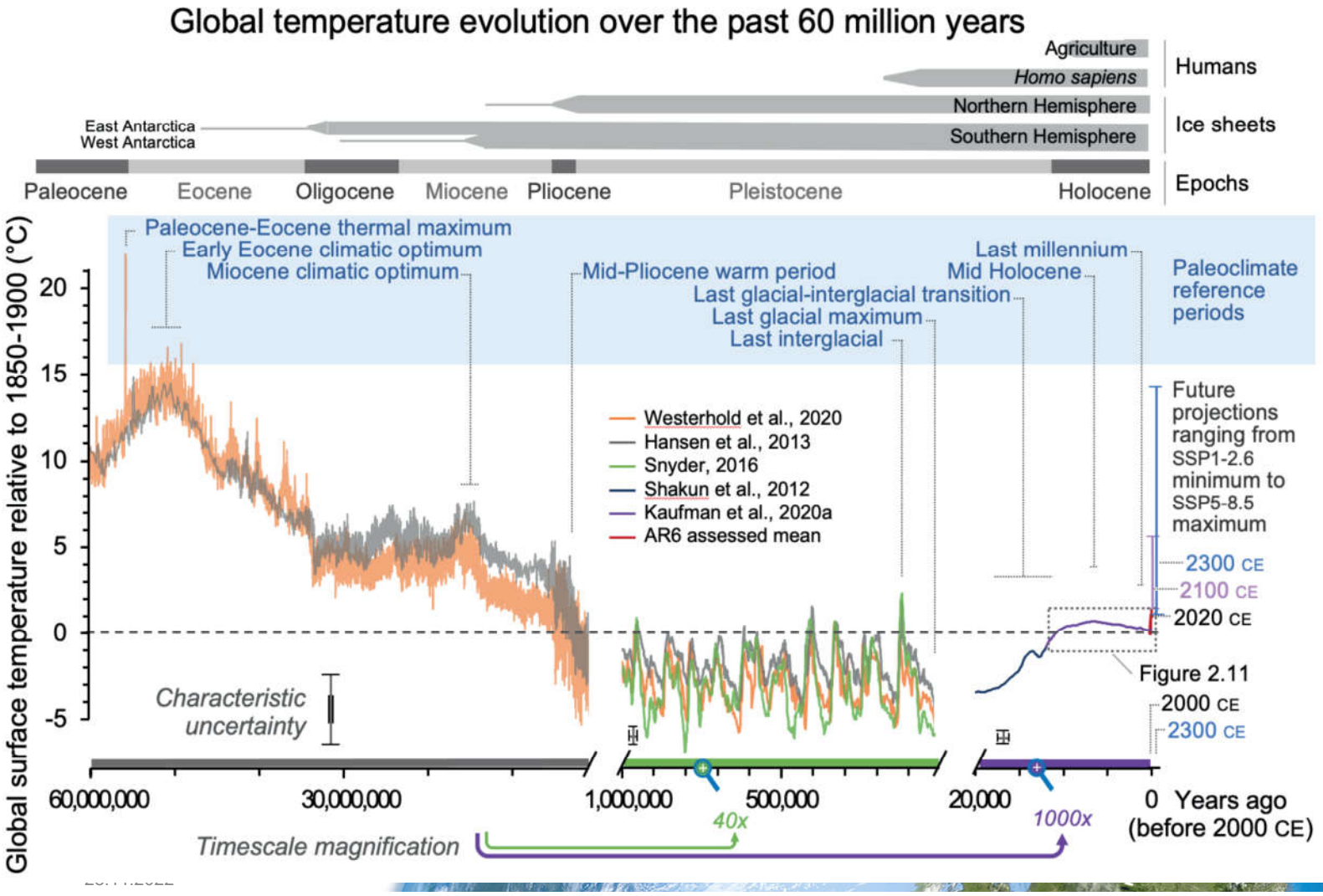

IPCC 2021, Chap. 2

Paleo reference periods

Period	Age/Year[a]	Sketch of the Climate State (Relative to 1850–1900), and *Model Experiment Protocols* (*italic*). Values for large-scale climate indicators including global temperature, sea level and atmospheric CO_2 are shown in Figure 2.34.	AR6 Sections (partial list)
Paleocene–Eocene Thermal Maximum (PETM)	55.9–55.7 Ma (million years ago)	A geologically rapid, large-magnitude warming event at the start of the Eocene when a large pulse of carbon was released to the ocean-atmosphere system, decreasing ocean pH and oxygen content. Terrestrial plant and animal communities changed composition, and species distributions shifted poleward. Many deep-sea species went extinct and tropical coral reefs diminished. *DeepMIP* (Lunt et al., 2017)	2.2.3.1 2.3.1.1.1 5.1.2.1 5.3.1.1 7.5.3.4
Early Eocene Climatic Optimum[b] (EECO)	53–49 Ma	Prolonged 'hothouse' period with atmospheric CO_2 concentration >1000 ppm, similar to SSP5-8.5 end-of-century values. Continental positions were somewhat different to present due to tectonic plate movements; polar ice was absent and there was more warming at high latitudes than in the equatorial regions. Near-tropical forests grew at 70°S, despite seasonal polar darkness. *DeepMIP*, about 50 Ma (Lunt et al., 2017, 2021)	2.2.3.1 2.3.1.1.1 7.4.4.1.2 7.5.3.4 7.5.6
Miocene Climatic Optimum[b] (MCO)	16.9–14.7 Ma	Prolonged warm period with atmospheric CO_2 concentrations 400–600 ppm, similar to SSP2-4.5 end-of-century values. Continental geography was broadly similar to modern. At times, Arctic sea ice may have been absent, and the AIS was much smaller or perhaps absent. Peak in Cenozoic reef development. *MioMIP1*, Early and Middle Miocene (Steinthorsdottir et al., 2021)	2.2.3.1 2.3.1.1.1
Mid-Pliocene Warm Period (MPWP)	3.3–3.0 Ma	Warm period when atmospheric CO_2 concentration was similar to present (Cross-Chapter Box 2.4). The Arctic was much warmer, but tropical temperatures were only slightly warmer. Sea level was higher than present. Treeline extended to the northern coastline of the NH continents. Also called, 'Piacenzian warm period.' *PMIP4 midPliocene-eoi400*, 3.2 Ma (Haywood et al., 2016, 2020)	CCB2.4 7.4.4.1.2 7.5.3.3 8.2.2.2 9.6.2
Last Interglacial (LIG)	129–116 ka (thousand years ago)	Most recent interglacial period, similar to mid-Holocene, but with more pronounced seasonal insolation cycle. Northern high latitudes were warmer, with reduced sea ice. Greenland and West Antarctic ice sheets were smaller and sea level was higher. Monsoon was enhanced. Boreal forests extended into Greenland and subtropical animals such as *Hippopotamus* occupied Britain. Coral reefs expanded latitudinally and contracted equatorially. *PMIP4 lig127k*, 127 ka (Otto-Bliesner et al., 2017, 2021)	2.2.3.2 2.3.1.1.1 2.3.3.3 9.2.2.1 9.6.2
Last Glacial Maximum (LGM)	23–19 ka	Most recent glaciation when global temperatures were lower, with greater cooling toward the poles. Ice sheets covered much of North America and north-west Eurasia, and sea level was commensurately lower. Atmospheric CO_2 was lower; more carbon was sequestered in the ocean interior. Precipitation was generally lower over most regions; the atmosphere was dustier, and ranges of many plant species contracted into glacial refugia; forest extent and coral reef distribution was reduced worldwide. *PMIP4lgm*, 21 ka (Kageyama et al., 2017, 2021a)	2.2.3.2 2.3.1.1.1 3.3.1.1 3.8.2.1 5.1.2.2 7.4.4.1.2 7.5.3.1 8.3.2.4 9.6.2
Last Deglacial Transition (LDT)	18–11 ka	Warming that followed the Last Glacial Maximum, with decreases in the extent of the cryosphere in both polar regions. Sea level, ocean meridional overturning circulation, and atmospheric CO_2 increased during two main steps. Temperate and boreal species ranges expanded northwards. Community turnover was large. Megafauna populations declined or went extinct.	2.2.3.2 5.1.2.2 5.3.1.2 8.6.1 9.6.2
Mid-Holocene (MH)	6.5–5.5 ka	Middle of the present interglacial when the CO_2 concentration was similar to the onset of the industrial era, but the orbital configuration led to warming and shifts in the hydrological cycle, especially NH monsoons. Approximate time during the current interglacial and before the onset of major industrial activities when GMST was highest. Biome-scale loss of North African grasslands caused by weakened monsoons and collapses of temperate tree populations linked to hydroclimate variability. *PMIP4 mid-Holocene*, 6 ka (Otto-Bliesner et al., 2017; Brierley et al., 2020)	2.3.1.1.2 2.3.2.4 2.3.3.3 3.3.1.1 3.8.2.1 8.3.2.4 8.6.2.2 9.6.2
Last millennium[c]	850–1850 CE	Climate variability during this period is better documented on annual to centennial scales than during previous reference periods. Climate changes were driven by solar, volcanic, land cover, and anthropogenic forcings, including strong increases in greenhouse gasses since 1750. *PMIP4 past1000*, 850–1849 CE (Jungclaus et al., 2017)	2.3.1.1.2 2.3.2.3 8.3.1.6 8.5.2.1 Box 11.3

IPCC 2021, Chap. 2

Paleo reference periods

Period	Age/Year[a]	Sketch of the Climate State (Relative to 1850–1900), and *Model Experiment Protocols* (*italic*). Values for large-scale climate indicators including global temperature, sea level and atmospheric CO_2 are shown in Figure 2.34.	AR6 Sections (partial list)
Paleocene–Eocene Thermal Maximum (PETM)	55.9–55.7 Ma (million years ago)	A geologically rapid, large-magnitude warming event at the start of the Eocene when a large pulse of carbon was released to the ocean-atmosphere system, decreasing ocean pH and oxygen content. Terrestrial plant and animal communities changed composition, and species distributions shifted poleward. Many deep-sea species went extinct and tropical coral reefs diminished. *DeepMIP* (Lunt et al., 2017)	2.2.3.1 2.3.1.1.1 5.1.2.1 5.3.1.1 7.5.3.4
Early Eocene Climatic Optimum[b] (EECO)	53–49 Ma	Prolonged 'hothouse' period with atmospheric CO_2 concentration >1000 ppm, similar to SSP5-8.5 end-of-century values. Continental positions were somewhat different to present due to tectonic plate movements; polar ice was absent and there was more warming at high latitudes than in the equatorial regions. Near-tropical forests grew at 70°S, despite seasonal polar darkness. *DeepMIP*, about 50 Ma (Lunt et al., 2017, 2021)	2.2.3.1 2.3.1.1.1 7.4.4.1.2 7.5.3.4 7.5.6
Miocene Climatic Optimum[b] (MCO)	16.9–14.7 Ma	Prolonged warm period with atmospheric CO_2 concentrations 400–600 ppm, similar to SSP2-4.5 end-of-century values. Continental geography was broadly similar to modern. At times, Arctic sea ice may have been absent, and the AIS was much smaller or perhaps absent. Peak in Cenozoic reef development. *MioMIP1*, Early and Middle Miocene (Steinthorsdottir et al., 2021)	2.2.3.1 2.3.1.1.1
Mid-Pliocene Warm Period (MPWP)	3.3–3.0 Ma	Warm period when atmospheric CO_2 concentration was similar to present (Cross-Chapter Box 2.4). The Arctic was much warmer, but tropical temperatures were only slightly warmer. Sea level was higher than present. Treeline extended to the northern coastline of the NH continents. Also called, 'Piacenzian warm period.' *PMIP4 midPliocene-eoi400*, 3.2 Ma (Haywood et al., 2016, 2020)	CCB2.4 7.4.4.1.2 7.5.3.3 8.2.2.2 9.6.2
Last Interglacial (LIG)	129–116 ka (thousand years ago)	Most recent interglacial period, similar to mid-Holocene, but with more pronounced seasonal insolation cycle. Northern high latitudes were warmer, with reduced sea ice. Greenland and West Antarctic ice sheets were smaller and sea level was higher. Monsoon was enhanced. Boreal forests extended into Greenland and subtropical animals such as *Hippopotamus* occupied Britain. Coral reefs expanded latitudinally and contracted equatorially. *PMIP4 lig127k*, 127 ka (Otto-Bliesner et al., 2017, 2021)	2.2.3.2 2.3.1.1.1 2.3.3.3 9.2.2.1 9.6.2

IPCC 2021, Chap. 2

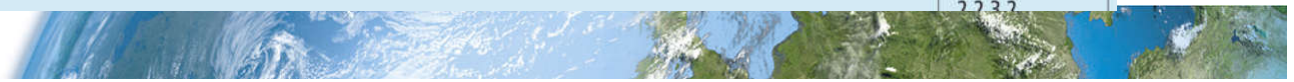

Paleo reference periods

		contracted equatorially. *PMIP4 lig127k*, 127 ka (Otto-Bliesner et al., 2017, 2021)	9.6.2
Last Glacial Maximum (LGM)	23–19 ka	Most recent glaciation when global temperatures were lower, with greater cooling toward the poles. Ice sheets covered much of North America and north-west Eurasia, and sea level was commensurately lower. Atmospheric CO_2 was lower; more carbon was sequestered in the ocean interior. Precipitation was generally lower over most regions; the atmosphere was dustier, and ranges of many plant species contracted into glacial refugia; forest extent and coral reef distribution was reduced worldwide. *PMIP4lgm*, 21 ka (Kageyama et al., 2017, 2021a)	2.2.3.2 2.3.1.1.1 3.3.1.1 3.8.2.1 5.1.2.2 7.4.4.1.2 7.5.3.1 8.3.2.4 9.6.2
Last Deglacial Transition (LDT)	18–11 ka	Warming that followed the Last Glacial Maximum, with decreases in the extent of the cryosphere in both polar regions. Sea level, ocean meridional overturning circulation, and atmospheric CO_2 increased during two main steps. Temperate and boreal species ranges expanded northwards. Community turnover was large. Megafauna populations declined or went extinct.	2.2.3.2 5.1.2.2 5.3.1.2 8.6.1 9.6.2
Mid-Holocene (MH)	6.5–5.5 ka	Middle of the present interglacial when the CO_2 concentration was similar to the onset of the industrial era, but the orbital configuration led to warming and shifts in the hydrological cycle, especially NH monsoons. Approximate time during the current interglacial and before the onset of major industrial activities when GMST was highest. Biome-scale loss of North African grasslands caused by weakened monsoons and collapses of temperate tree populations linked to hydroclimate variability. *PMIP4 mid-Holocene*, 6 ka (Otto-Bliesner et al., 2017; Brierley et al., 2020)	2.3.1.1.2 2.3.2.4 2.3.3.3 3.3.1.1 3.8.2.1 8.3.2.4 8.6.2.2 9.6.2
Last millennium[c]	850–1850 CE	Climate variability during this period is better documented on annual to centennial scales than during previous reference periods. Climate changes were driven by solar, volcanic, land cover, and anthropogenic forcings, including strong increases in greenhouse gasses since 1750. *PMIP4 past1000,* 850–1849 CE (Jungclaus et al., 2017)	2.3.1.1.2 2.3.2.3 8.3.1.6 8.5.2.1 Box 11.3

IPCC 2021, Chap. 2

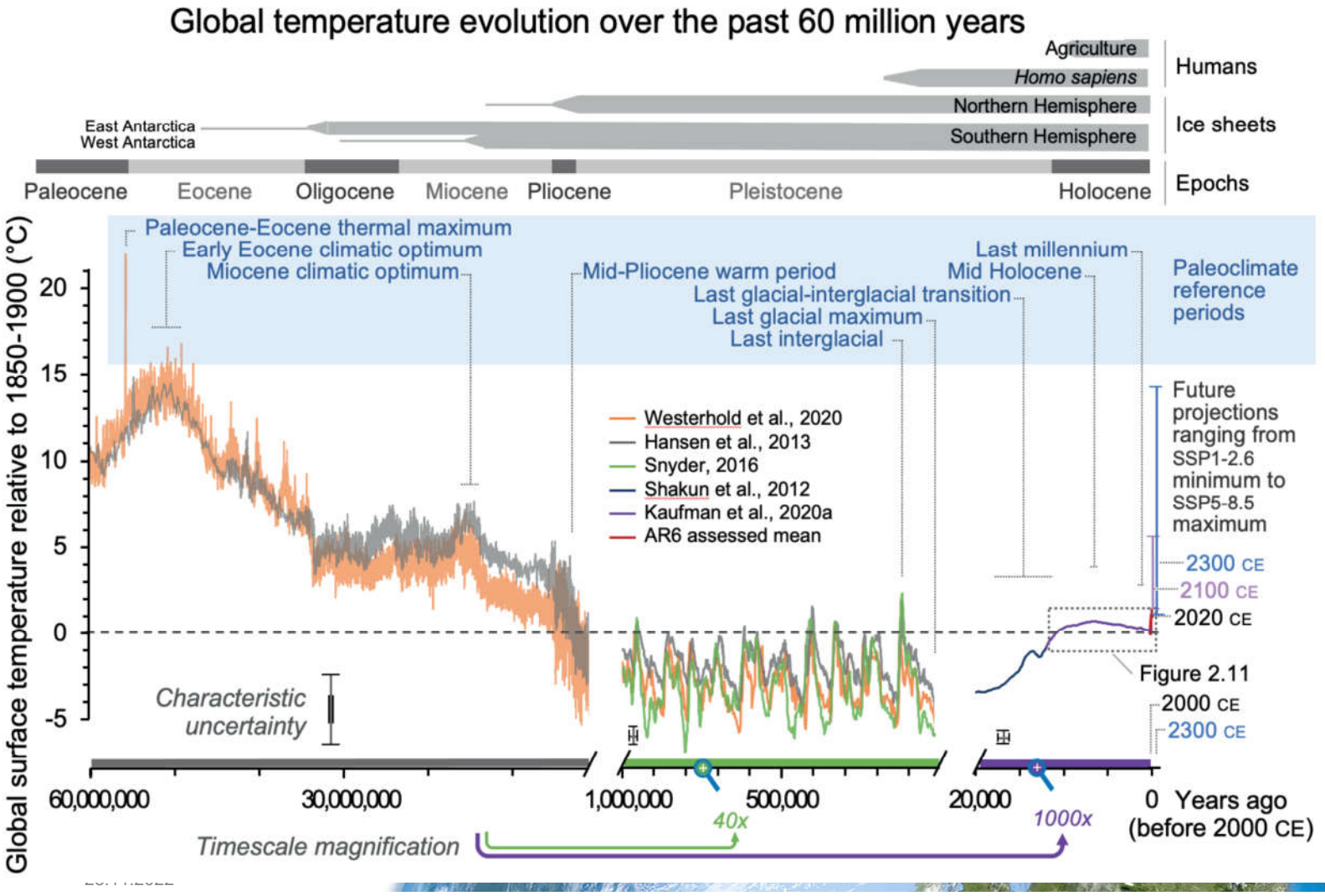
Global temperature evolution over the past 60 million years
Agriculture
Homo sapiens
Humans
Northern Hemisphere
East Antarctica
West Antarctica
Southern Hemisphere
Ice sheets
Paleocene
Eocene
Oligocene
Miocene
Pliocene
Pleistocene
Holocene
Epochs
Paleocene-Eocene thermal maximum
Early Eocene climatic optimum
Miocene climatic optimum
Mid-Pliocene warm period
Last glacial-interglacial transition
Last glacial maximum
Last interglacial
Last millennium
Mid Holocene
Paleoclimate reference periods
Global surface temperature relative to 1850-1900 (°C)
20
15
10
5
0
-5
Westerhold et al., 2020
Hansen et al., 2013
Snyder, 2016
Shakun et al., 2012
Kaufman et al., 2020a
AR6 assessed mean
Future projections ranging from SSP1-2.6 minimum to SSP5-8.5 maximum
2300 CE
2100 CE
2020 CE
Figure 2.11
2000 CE
2300 CE
Characteristic uncertainty
60,000,000
30,000,000
1,000,000
500,000
20,000
0 Years ago (before 2000 CE)
40x
1000x
Timescale magnification

Statements in the Executive Summary

Changes in Climate System Drivers (1)

Climate system drivers lead to climate change by altering the Earth's energy balance. The influence of a climate driver is described in terms of its effective radiative forcing (ERF), measured in W m^{-2}. Positive ERF values exert a warming influence and negative ERF values exert a cooling influence (Chapter 7).

Present-day global concentrations of atmospheric carbon dioxide (CO_2) are at higher levels than at any time in at least the past two million years (*high confidence*). Changes in ERF since the late 19th century are dominated by increases in concentrations of greenhouse gases and trends in aerosols; the net ERF is positive and changing at an increasing rate since the 1970s (*medium confidence*). {2.2, 7.2, 7.3}

IPCC 2021, Chap. 2

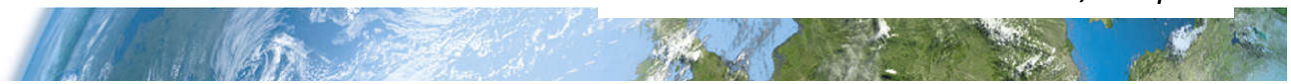

Evolution of atmospheric CO_2

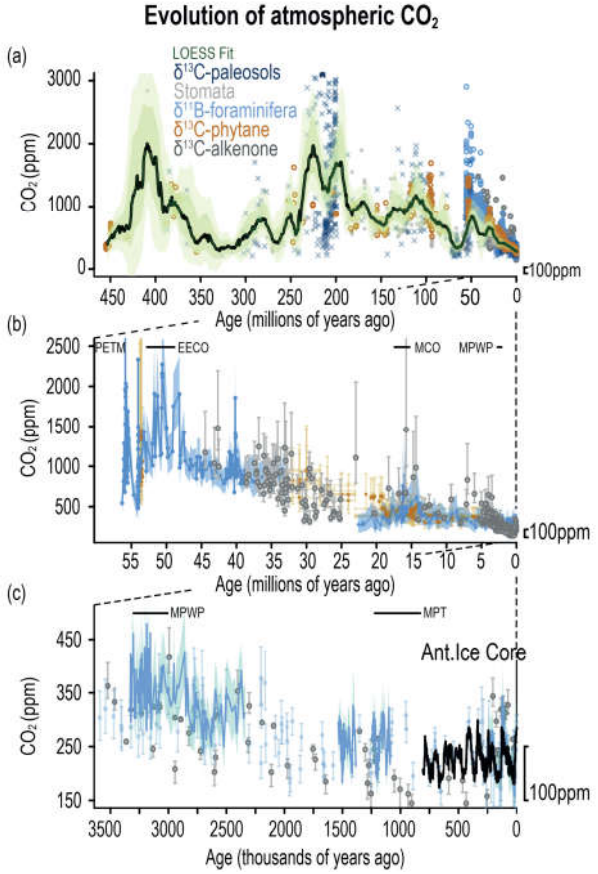

Figure 2.3 | The evolution of atmospheric CO_2 through the last 450 million years (450 Myr). The periods covered are 0–450 Ma **(a)**, 0–58 Ma **(b)**, and 0–3500 ka **(c)**, reconstructed from continental rock, marine sediment and ice core records. Note different time scales and axes ranges in panels (a), (b) and (c). Dark and light green bands in (a) are uncertainty envelopes at 68% and 95% uncertainty, respectively. 100 ppm in each panel is shown by the marker in the lower right-hand corner to aid comparison between panels. In panel (b) and (c) the major paleoclimate reference periods (CCB2.1) have been labelled, and in addition: MPT (Mid Pleistocene Transition), MCO (Miocene Climatic Optimum). Further details on data sources and processing are available in the chapter data table (Table 2.SM.1).

IPCC 2021, Chap. 2

Evolution of atmospheric CO_2

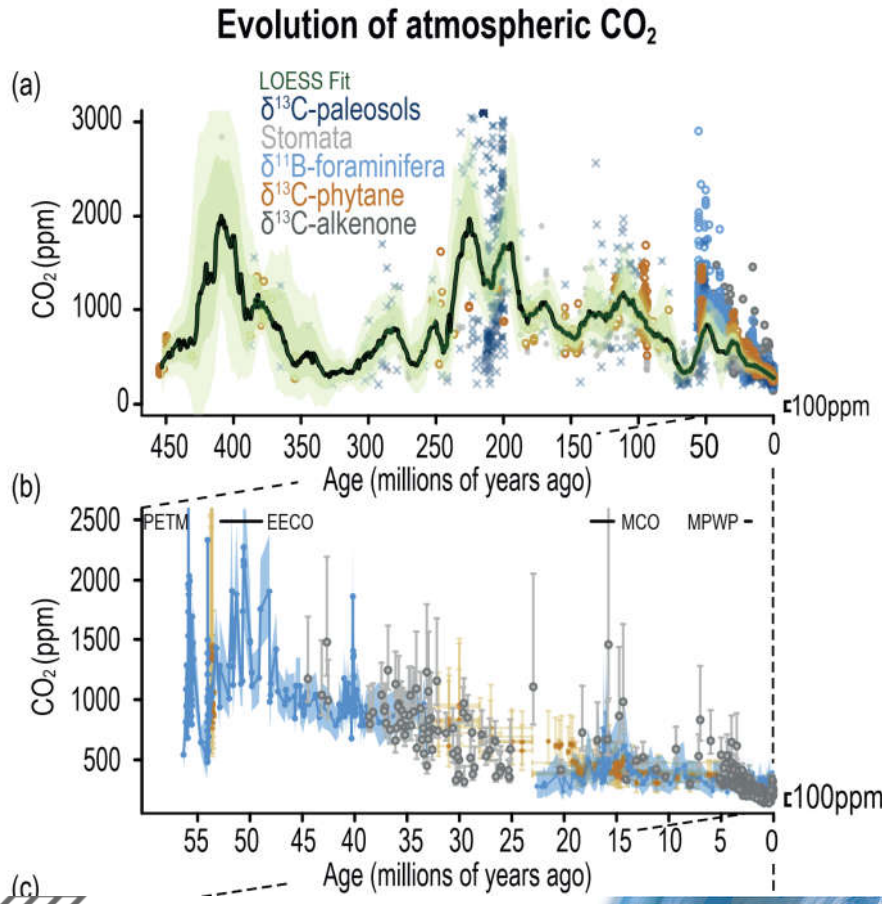

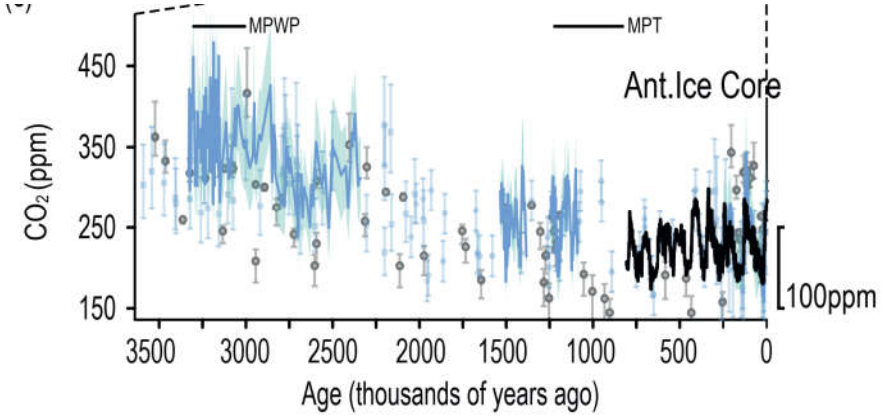

IPCC 2021, Chap. 2

Statements in the Executive Summary

Changes in Climate System Drivers (2)

Change in ERF from natural factors since 1750 is negligible in comparison to anthropogenic drivers (*very high confidence*). Solar activity since 1900 was high but not exceptional compared to the past 9000 years (*high confidence*). The average magnitude and variability of volcanic aerosol forcing since 1900 have not been unusual compared to the past 2500 years (*medium confidence*). {2.2.1, 2.2.2}

IPCC 2021, Chap. 2

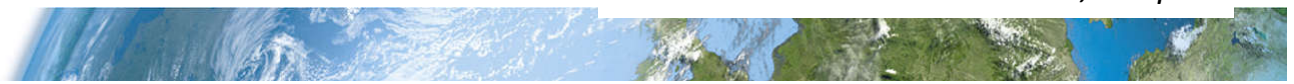

Time series of solar and volcanic forcing for the past 2500 years and since 1850

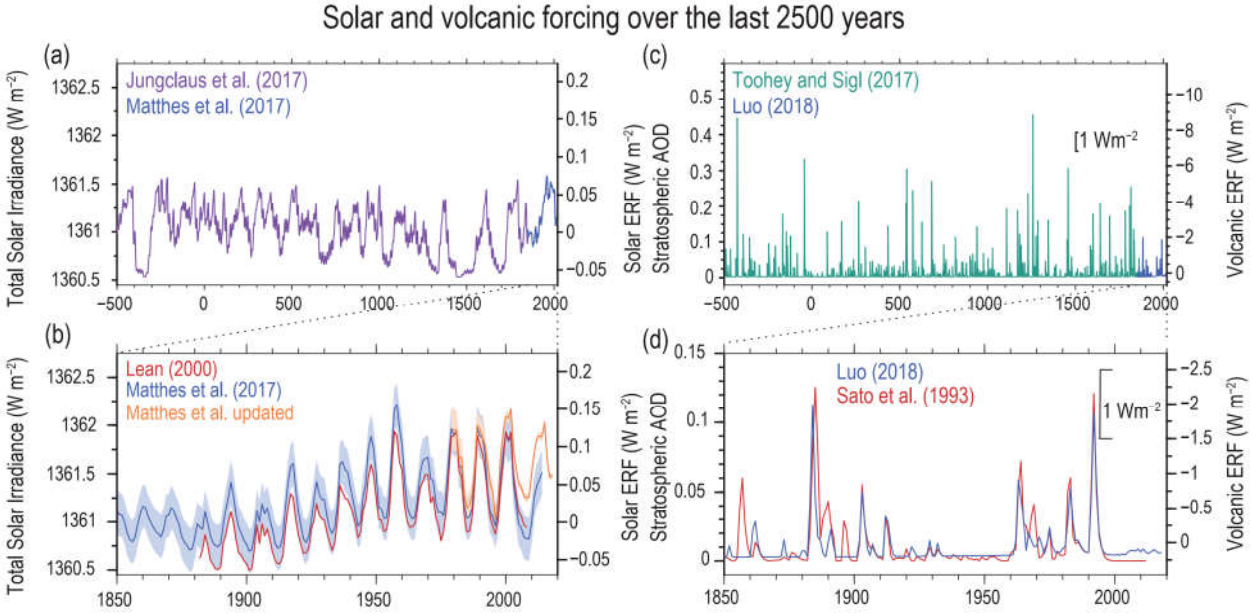

Figure 2.2 | Time series of solar and volcanic forcing for the past 2500 years (a, c) and since 1850 (b, d). (a) Total solar irradiance (TSI) reconstruction (10-year running averages) recommended for CMIP6/PMIP4 millennial experiments based on the radiocarbon dataset before 1850 (blue) scaled to the CMIP6 historical forcing after 1850 (purple). **(b)** TSI time series (six-month running averages) from CMIP6 historical forcing as inferred from sunspot numbers (blue), compared to CMIP5 forcing based on (red) and an update to CMIP6 by a TSI composite (orange). **(c)** Volcanic forcing represented as reconstructed stratospheric aerosol optical depth (SAOD; as presented in Section 7.3.4.6) at 550 nm. Estimates covering 500 BCE to 1900 CE (green) and 1850–2015 (blue). **(d)** SAOD reconstruction from CMIP6 (v 4) (blue), compared to CMIP5 forcing (red). Note the change in y-axis range between panels (c) and (d). Further details on data sources and processing are available in the chapter data table (Table 2.SM.1).

IPCC 2021, Chap. 2

Time series of solar and volcanic forcing for the past 2500 years and since 1850

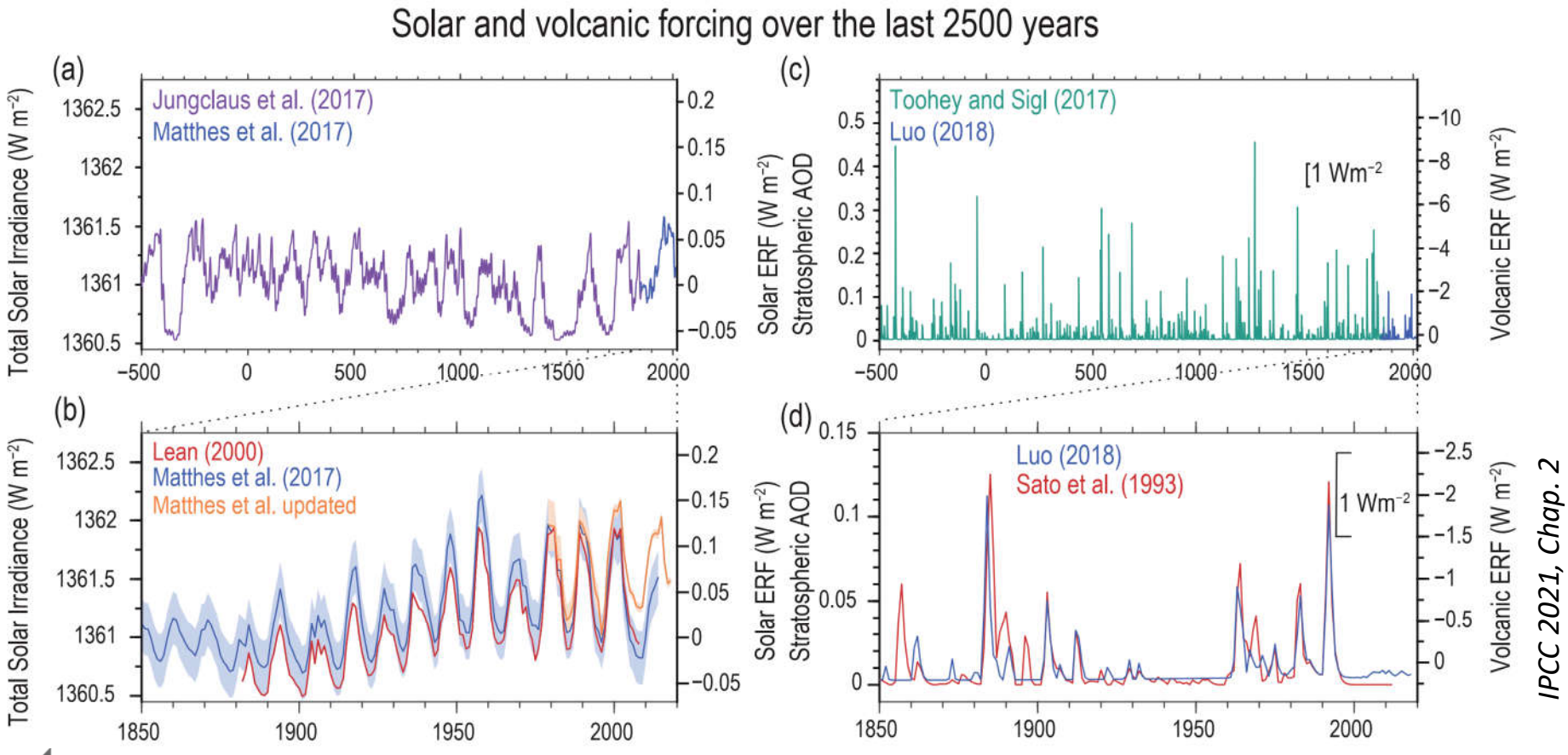

IPCC 2021, Chap. 2

Statements in the Executive Summary

Changes in Climate System Drivers (3)

In 2019, concentrations of CO_2, methane (CH_4) and nitrous oxide (N_2O) reached levels of 409.9 (±0.4) ppm, 1866.3 (±3.3) ppb and 332.1 (±0.4) ppb, respectively. Since 1850, these well-mixed greenhouse gases (GHGs) have increased at rates that have no precedent on centennial time scales in at least the past 800,000 years. Concentrations of CO_2, CH_4, and N_2O increased from 1750 to 2019 by 131.6 ± 2.9 ppm (47.3%), 1137 ± 10 ppb (156%), and 62 ± 6 ppb (23.0%) respectively. These changes are larger than those between glacial and interglacial periods over the last 800,000 years for CO_2 and CH_4 and of comparable magnitude for N_2O (*very high confidence*). The best estimate of the total ERF from CO_2, CH_4 and N_2O in 2019 relative to 1750 is 2.9 W m^{-2}, an increase of 12.5 % from 2011. ERF from halogenated components in 2019 was 0.4 W m^{v-2}, an increase of 3.5% since 2011.

IPCC 2021, Chap. 2

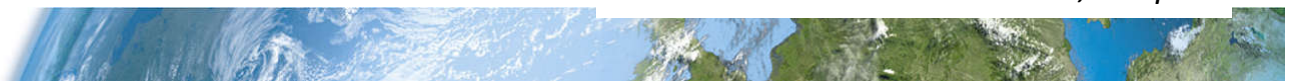

Atmospheric WMGHG concentrations from ice cores

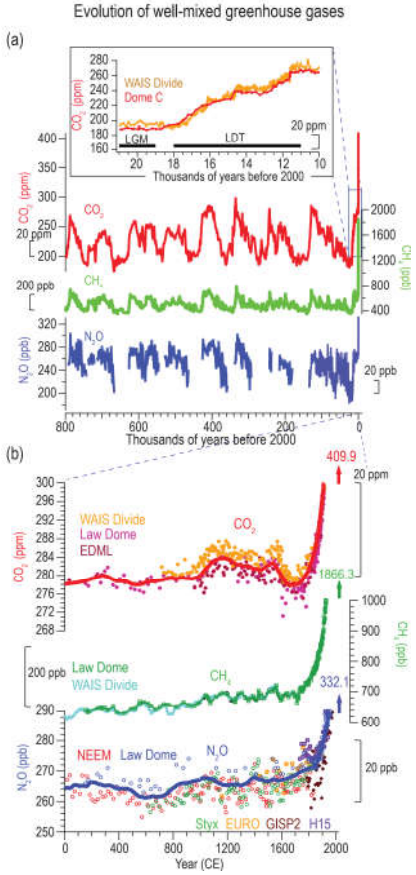

Figure 2.4 | Atmospheric well-mixed greenhouse gas (WMGHG) concentrations from ice cores. (a) Records during the last 800 kyr with the Last Glacial Maximum (LGM) to Holocene transition as inset. **(b)** Multiple high-resolution records over the CE. The horizontal black bars in panel (a) inset indicate LGM and Last Deglacial Termination (LDT) respectively. The red and blue lines in (b) are 100-year running averages for CO_2 and N_2O concentrations, respectively. The numbers with vertical arrows in (b) are instrumentally measured concentrations in 2019. Further details on data sources and processing are available in the chapter data table (Table 2.SM.1).

IPCC 2021, Chap. 2

Atmospheric WMGHG concentrations from ice cores

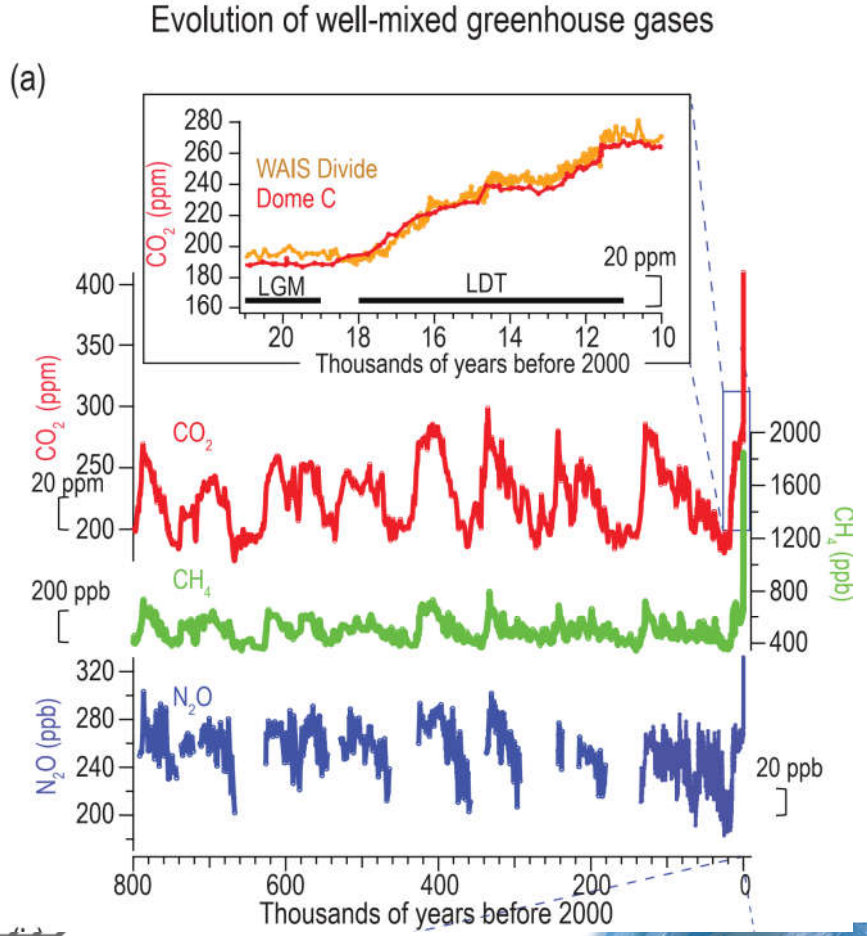

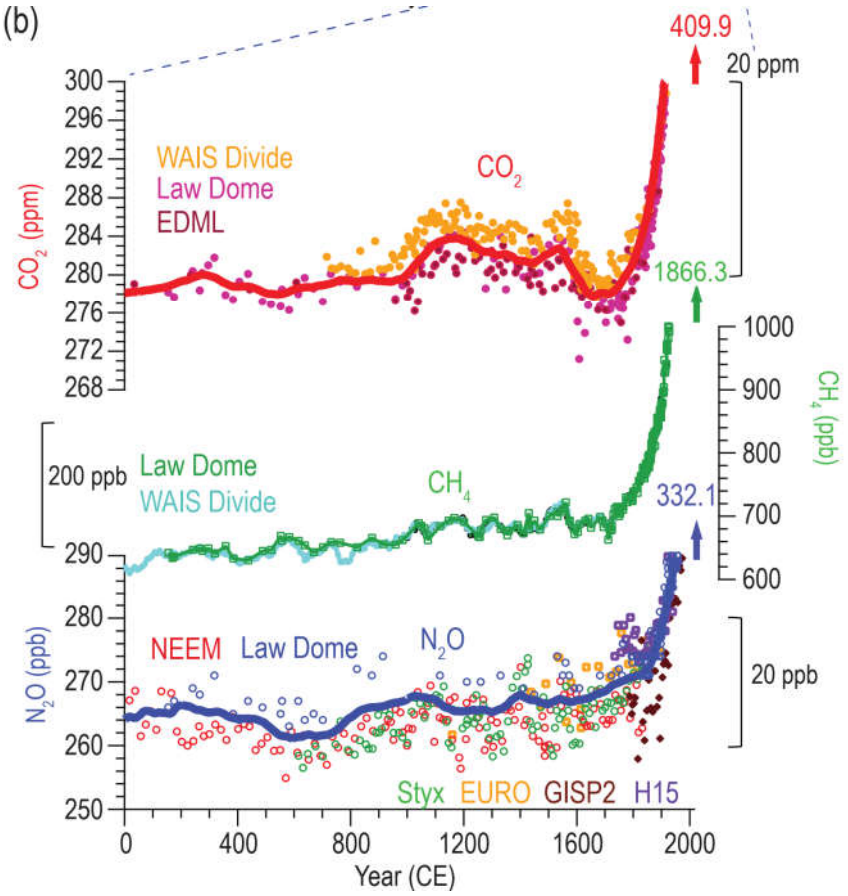

IPCC 2021, Chap. 2

Globally averaged dry-air mole fractions of greenhouse gases

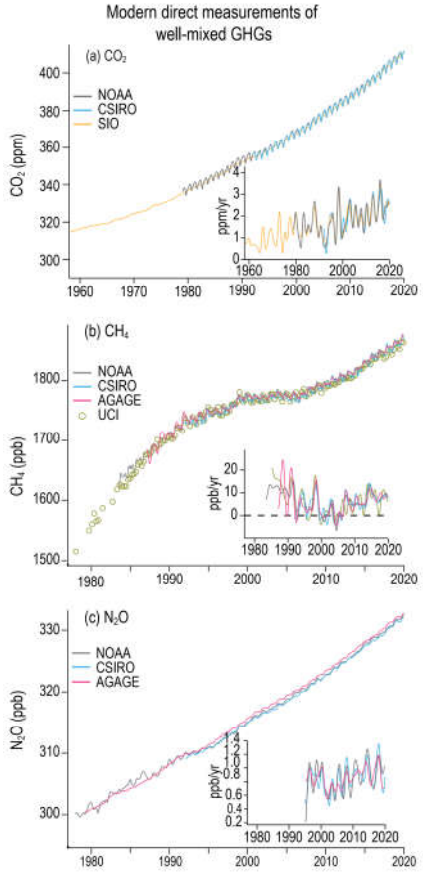

Figure 2.5 | Globally averaged dry-air mole fractions of greenhouse gases. **(a)** CO_2 from SIO, CSIRO, and NOAA/GML **(b)** CH_4 from NOAA, AGAGE, CSIRO, and UCI; and **(c)** N_2O from NOAA, AGAGE, and CSIRO (Table 2.2). Growth rates, calculated as the time derivative of the global means after removing seasonal cycle are shown as inset figures. Note that the CO_2 series is 1958–2019 whereas CH_4, and N_2O are 1979–2019. Units are parts per million (ppm) or parts per billion (ppb). Further details on data are in Annex III, and on data sources and processing are available in the chapter data table (Table 2.SM.1).

IPCC 2021, Chap. 2

Globally averaged dry-air mole fractions of greenhouse gases

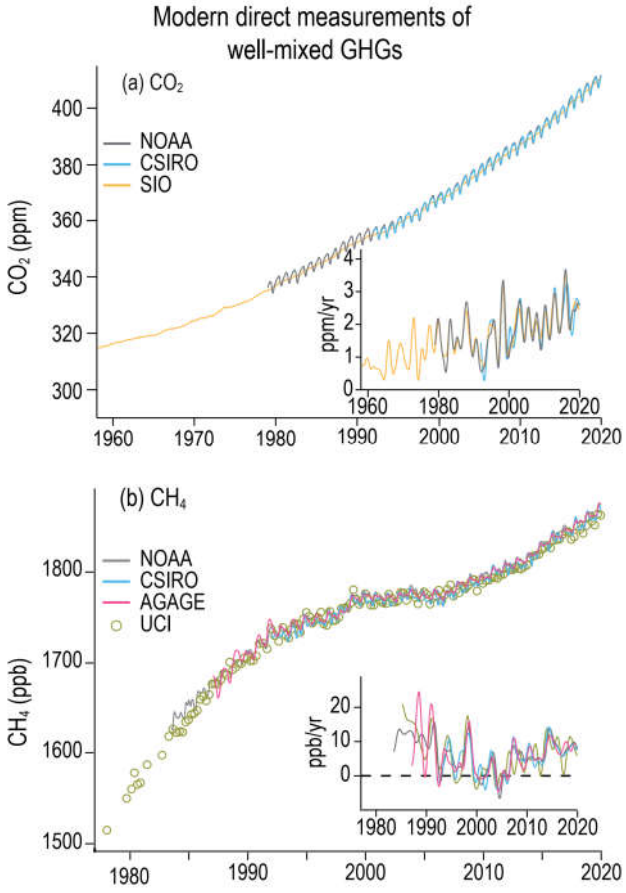

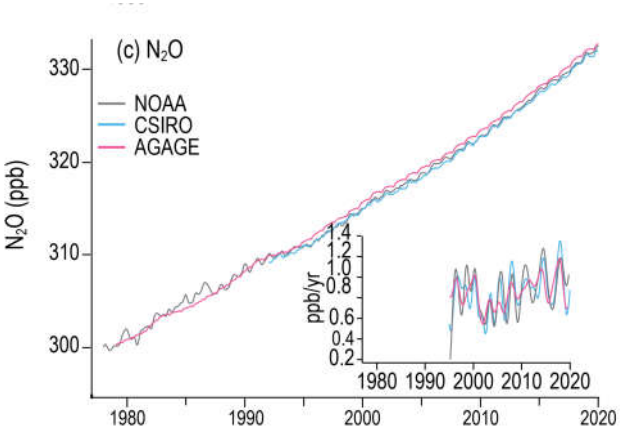

IPCC 2021, Chap. 2

Global mean atmospheric mixing ratios of select ozone-depleting substances and other greenhouse gases.

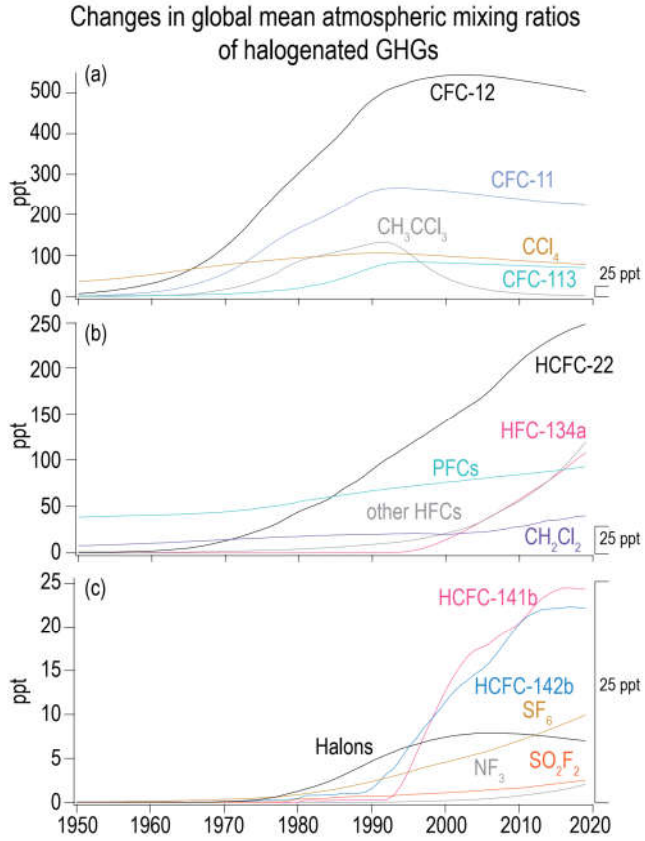

Figure 2.6 | Global mean atmospheric mixing ratios of select ozone-depleting substances and other greenhouse gases. Data shown are based on the CMIP6 historical dataset and data from NOAA and AGAGE global networks. PFCs include CF_4, C_2F_6, and C_3F_8, and *c*-C_4F_8; Halons include halon-1211, halon-1301, and halon-2402; other HFCs include HFC-23, HFC-32, HFC-125, HFC-143a, HFC-152a, HFC-227ea, HFC-236fa, HFC-245fa, and HFC-365mfc, and HFC-43-10mee. Note that the y-axis range is different for **(a)**, **(b)** and **(c)** and a 25 parts per trillion (ppt) yardstick is given next to each panel to aid interpretation. Further data are in Annex III and details on data sources and processing are available in the chapter data table (Table 2.SM.1).

IPCC 2021, Chap. 2

Global mean atmospheric mixing ratios of select ozone-depleting substances and other greenhouse gases.

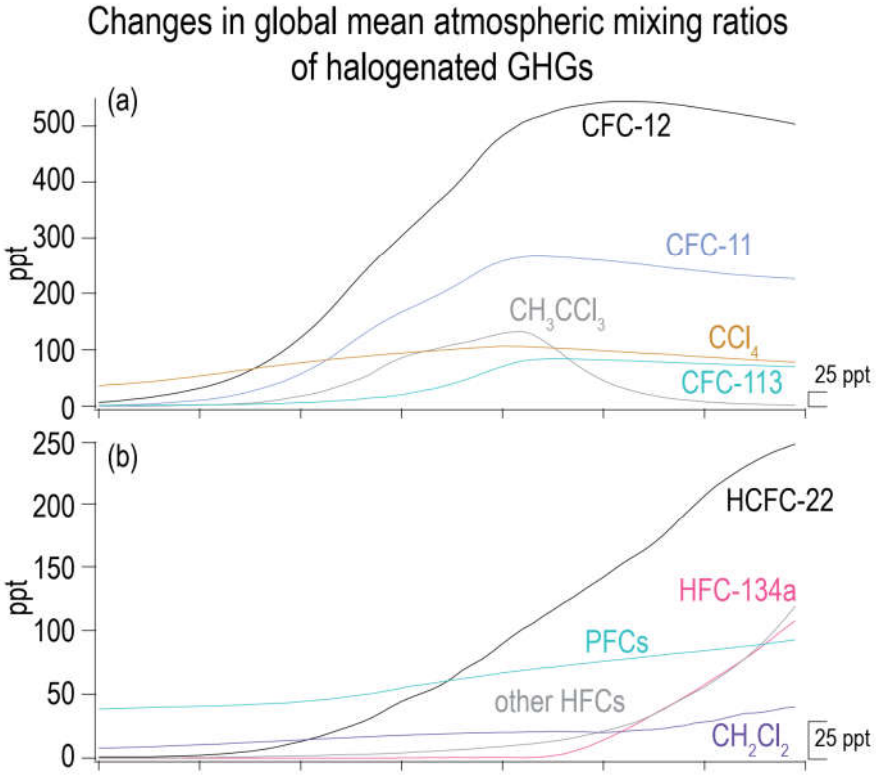

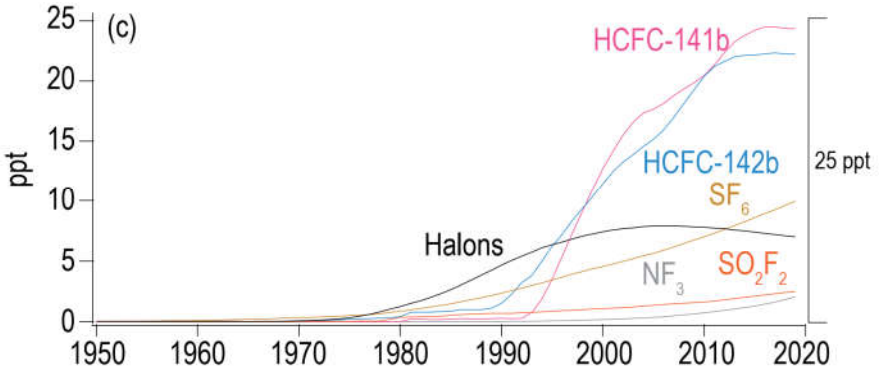

IPCC 2021, Chap. 2

Statements in the Executive Summary

Changes in Climate System Drivers (4)

Tropospheric aerosol concentrations across the Northern Hemisphere mid-latitudes increased from 1700 to the last quarter of the 20th century, but have subsequently declined (*high confidence*). Aerosol optical depth (AOD) has decreased since 2000 over Northern Hemisphere mid-latitudes and Southern Hemisphere mid-latitude continents, but increased over South Asia and East Africa (*high confidence*). These trends are even more pronounced in AOD from sub-micrometre aerosols for which the anthropogenic contribution is particularly large. The best-estimate of aerosol ERF in 2019 relative to 1750 is –1.1 W m^{-2}. {2.2.6, 7.3.3}

IPCC 2021, Chap. 2

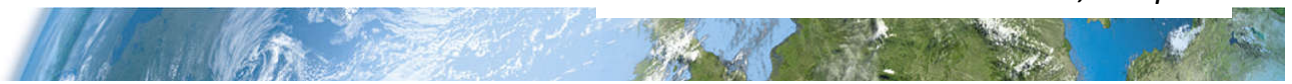

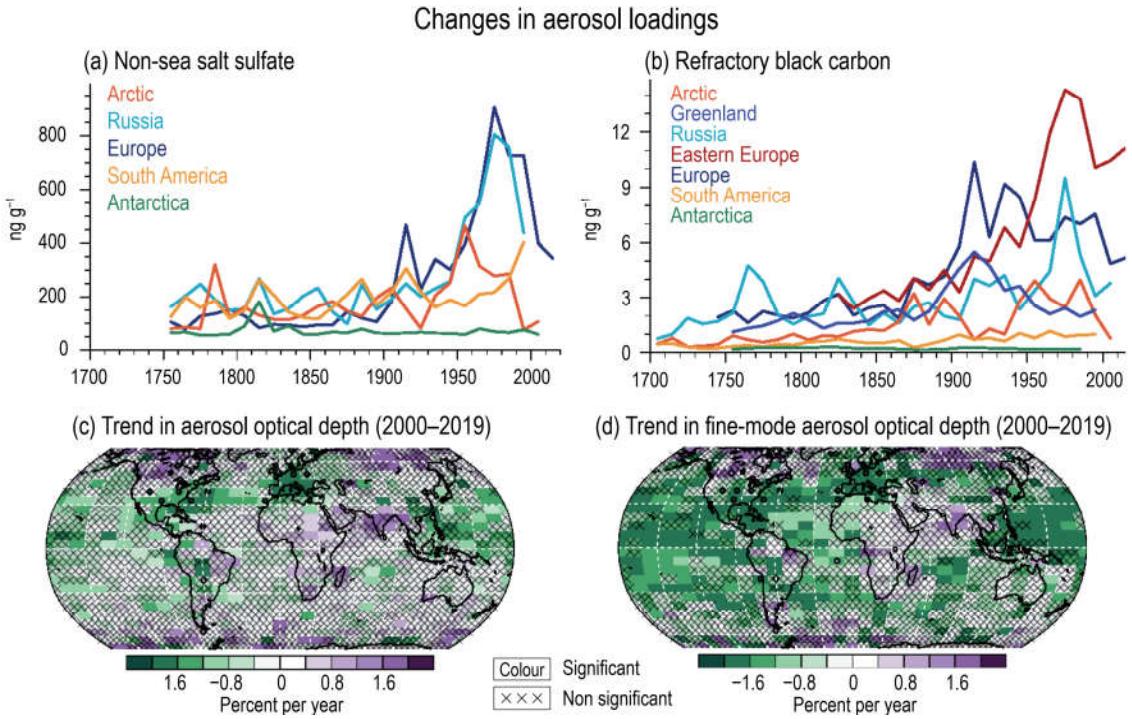

Figure 2.9 | Aerosol evolution from ice-core measurements. Changes are shown as 10-year averaged time series **(a, b)** and trends in remote-sensing aerosol optical depth (AOD) and AODf **(c, d). (a)** Concentrations of non-sea salt (nss) sulphate (ng g^{-1}). **(b)** Black carbon (BC) in glacier ice from the Arctic (Lomonosovfonna), Russia (Belukha), Europe (Colle Gnifetti), South America (Illimani), Antarctica (stacked sulphate record, and BC from the B40 core), and BC from Greenland (stacked rBC record from Greenland and eastern Europe (Elbrus)). **(c)** Linear trend in annual mean AOD retrieved from satellite data for the 2000–2019 period (% yr^{-1}). The average trend from MODerate Resolution Imaging Spectroradiometer (MODIS) and Multi-Angle Imaging Spectroradiometer (MISR) is shown. Trends are calculated using OLS regression with significance assessed following AR(1) adjustment after Santer et al. (2008). Superimposed are the trends in annual-mean AOD from the AERONET surface sunphotometer network for 2000–2019. **(d)** Linear trend in 2000–2019 as in (c), but for fine-mode AOD, AODf, and using only MISR over land. '×' marks denote non-significant trends. Further details on data sources and processing are available in the chapter data table (Table 2.SM.1).

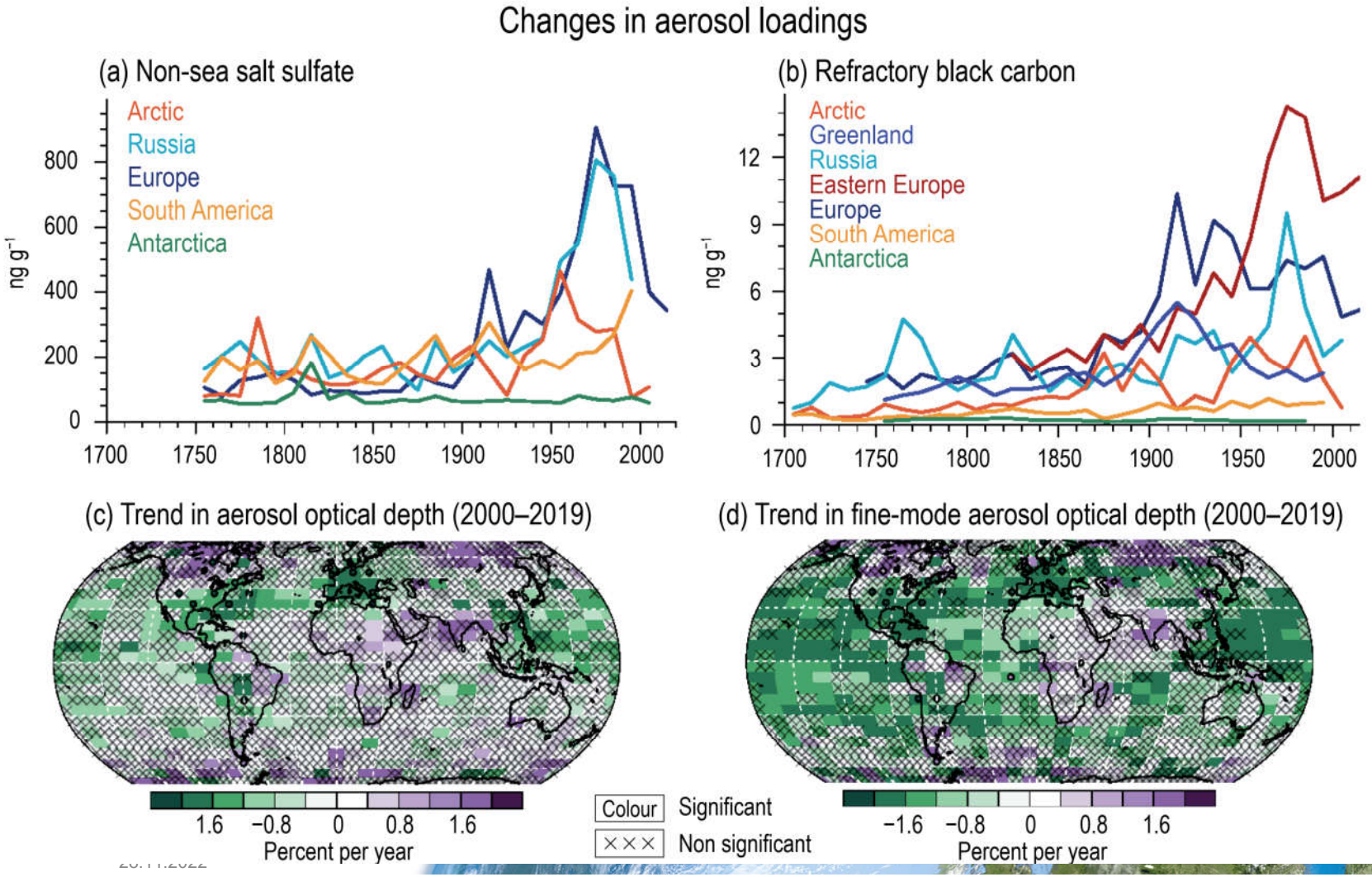
Changes in aerosol loadings
(a) Non-sea salt sulfate
Arctic
Russia
Europe
South America
Antarctica
ng g⁻¹
0
200
400
600
800
1700
1750
1800
1850
1900
1950
2000
(b) Refractory black carbon
Arctic
Greenland
Russia
Eastern Europe
Europe
South America
Antarctica
ng g⁻¹
0
3
6
9
12
1700
1750
1800
1850
1900
1950
2000
(c) Trend in aerosol optical depth (2000–2019)
1.6
−0.8
0
0.8
1.6
Percent per year
(d) Trend in fine-mode aerosol optical depth (2000–2019)
−1.6
−0.8
0
0.8
1.6
Percent per year
Colour
Significant
×××
Non significant

Statements in the Executive Summary

Changes in Climate System Drivers (5)

Changes in other short-lived gases are associated with an overall positive ERF (*medium confidence*). Stratospheric ozone has declined between 60˚S and 60˚N by 2.2% from the 1980s to 2014–2017 (*high confidence*). Since the mid-20th century, tropospheric ozone has increased by 30–70% across the Northern Hemisphere (*medium confidence*). Since the mid-1990s, free tropospheric ozone increases were 2–7% per decade in the northern mid-latitudes (*high confidence*), 2–12% per decade in the tropics *(high confidence*) and <5% per decade in southern mid-latitudes (medium confidence). The best estimate of ozone column ERF (0.5 W m^{-2} relative to 1750) is dominated by changes in tropospheric ozone. Due to discrepancies in satellite and in situ records, there is low confidence in estimates of stratospheric water vapour change. {2.2.5, 7.3.2}

IPCC 2021, Chap. 2

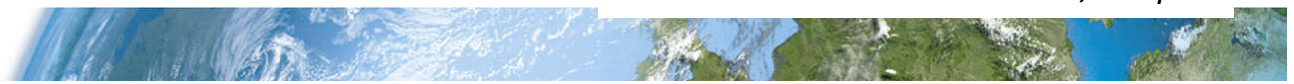

Time series of annual mean total column ozone from 1964-2019

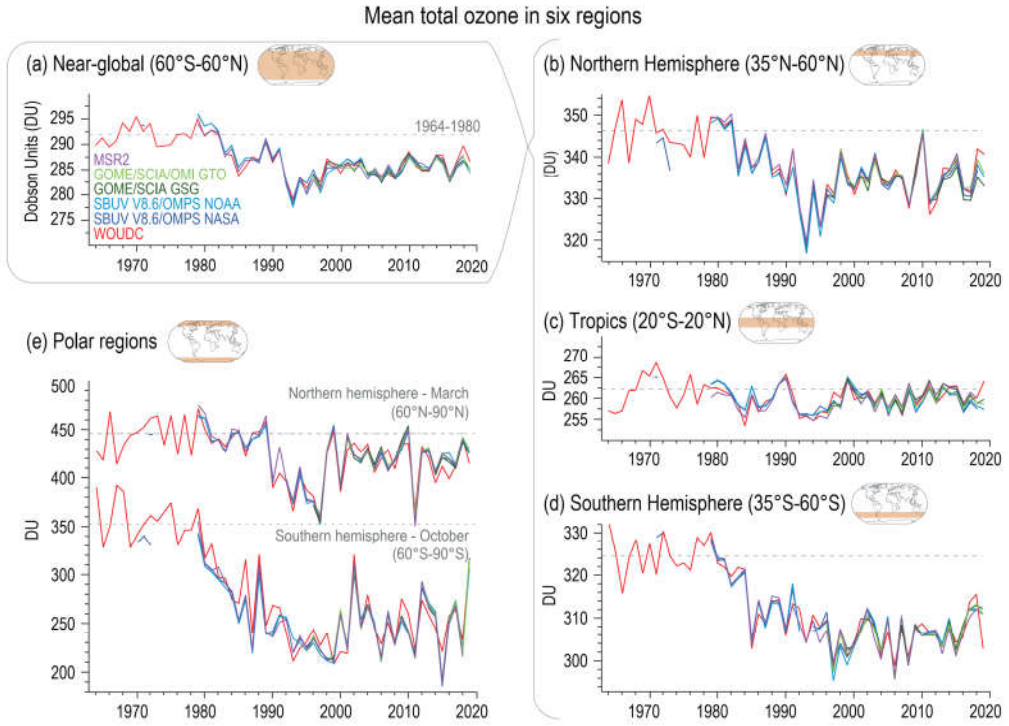

Figure 2.7 | Time series of annual mean total column ozone from 1964–2019. Values are in Dobson Units (DU), a good proxy for vertically integrated stratospheric ozone. Time series are shown for **(a)** near-global domain; **(b–d)** three zonal bands; and **(e)** polar (60°–90°) total ozone in March (Northern Hemisphere) and October (Southern Hemisphere): the months when polar ozone losses usually are largest. Further details on data sources and processing are available in the chapter data table (Table 2.SM.1).

IPCC 2021, Chap. 2

Time series of annual mean total column ozone from 1964-2019

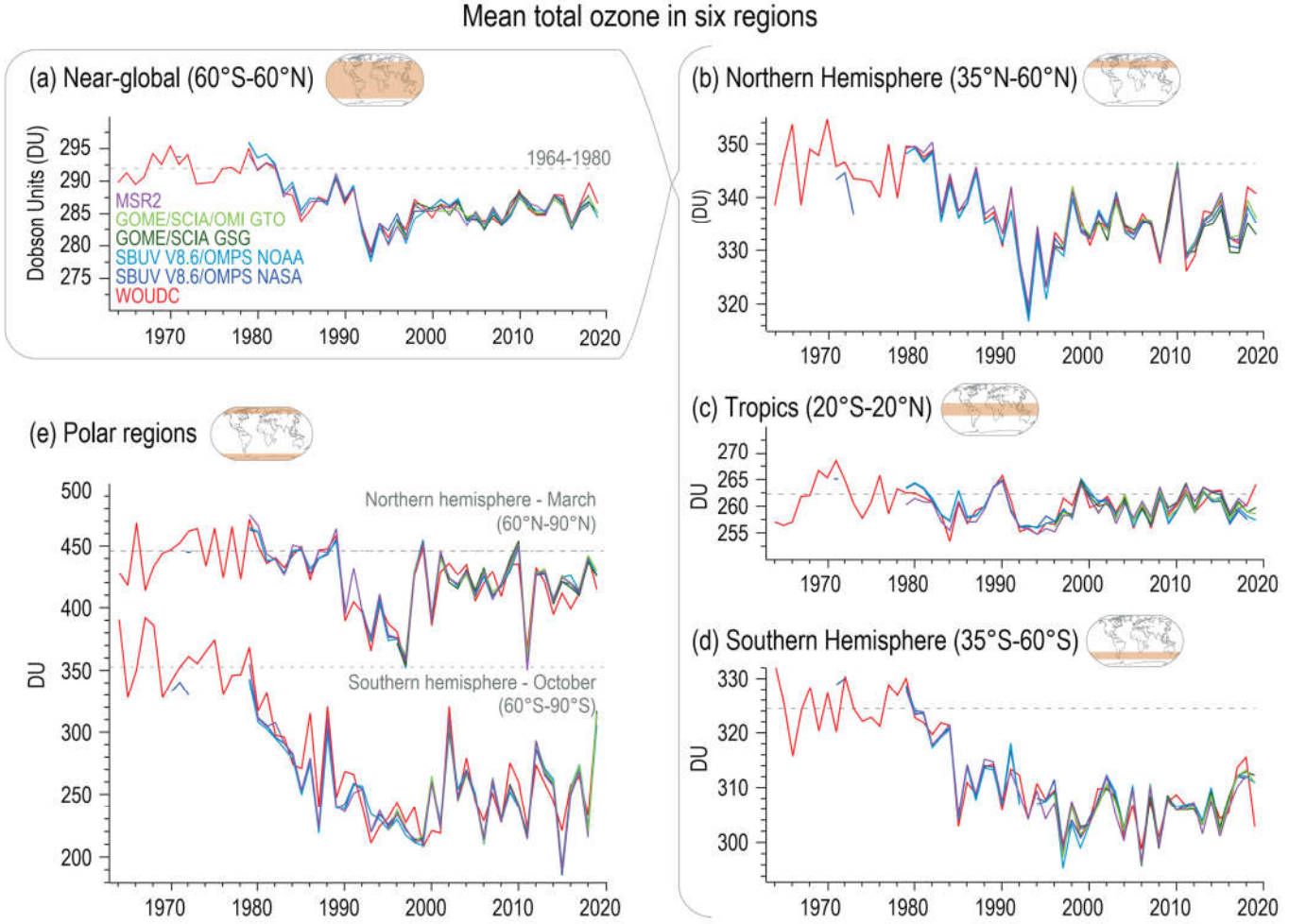

IPCC 2021, Chap. 2

Surface and tropospheric ozone trends

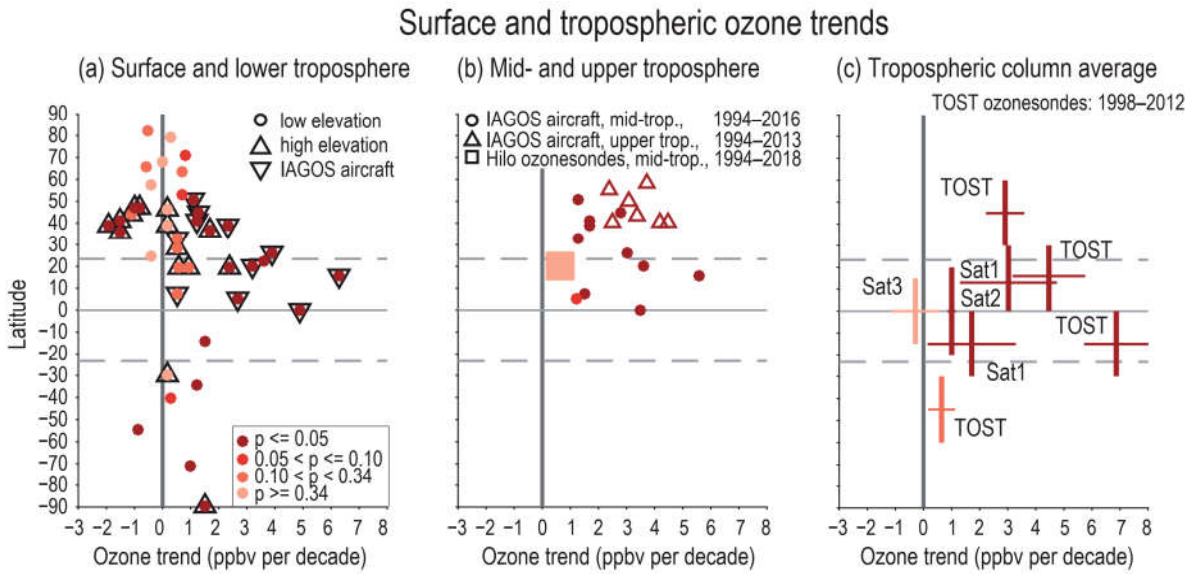

Satellite products:
Sat1 1979–2016 (TOMS, OMI/MLS)
Sat2 1995–2015 (GOME, SCIAMACHY, OMI, GOME-2A, GOME-2B)
Sat3 1995–2015 (GOME, SCIAMACHY, GOME-II)

Figure 2.8 | Surface and tropospheric ozone trends. (a) Decadal ozone trends by latitude at 28 remote surface sites and in the lower free troposphere (650 hPa, about 3.5 km) as measured by IAGOS aircraft above 11 regions. All trends are estimated for the time series up to the most recently available year, but begin in 1995 or 1994. Colours indicate significance (p-value) as denoted in the in-line key. See Figure 6.5 for a depiction of these trends globally. **(b)** Trends of ozone since 1994 as measured by IAGOS aircraft in 11 regions in the mid-troposphere (700–300 hPa; about 3–9 km) and upper troposphere (about 10–12 km), as measured by IAGOS aircraft and ozonesondes. **(c)** Trends of average tropospheric column ozone mixing ratios from the TOST composite ozonesonde product and three composite satellite products based on TOMS, OMI/MLS (Sat1), GOME, SCIAMACHY, OMI, GOME-2A, GOME-2B (Sat2), and GOME, SCIAMACHY, GOME-II (Sat3). Vertical bars indicate the latitude range of each product, while horizontal lines indicate the *very likely* uncertainty range. Further details on data sources and processing are available in the chapter data table (Table 2.SM.1).

IPCC 2021, Chap. 2

Surface and tropospheric ozone trends

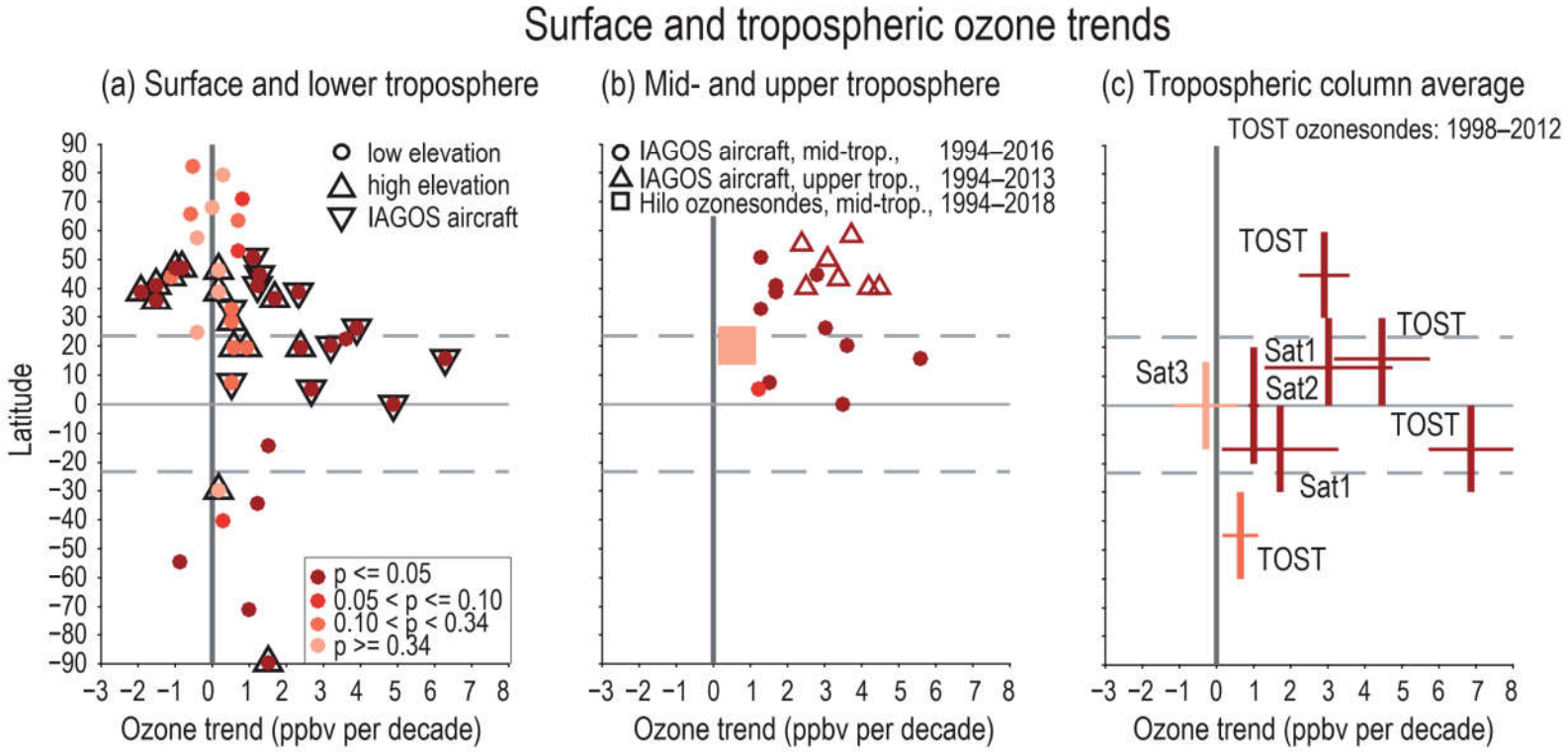

Satellite products:
Sat1 1979–2016 (TOMS, OMI/MLS)
Sat2 1995–2015 (GOME, SCIAMACHY, OMI, GOME-2A, GOME-2B)
Sat3 1995–2015 (GOME, SCIAMACHY, GOME-II)

IPCC 2021, Chap. 2

Statements in the Executive Summary

Changes in Climate System Drivers (6)

Biophysical effects from historical changes in land use have an overall negative ERF (*medium confidence*). The best-estimate ERF from the increase in global albedo is –0.15 W m^{-2} since 1700 and –0.12 W m^{-2} since 1850 (*medium confidence*). {2.2.7, 7.3.4}

IPCC 2021, Chap. 2

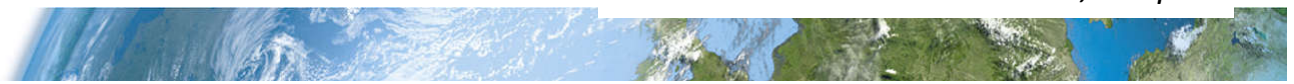

Temporal evolution of effective radiative forcing (ERF)

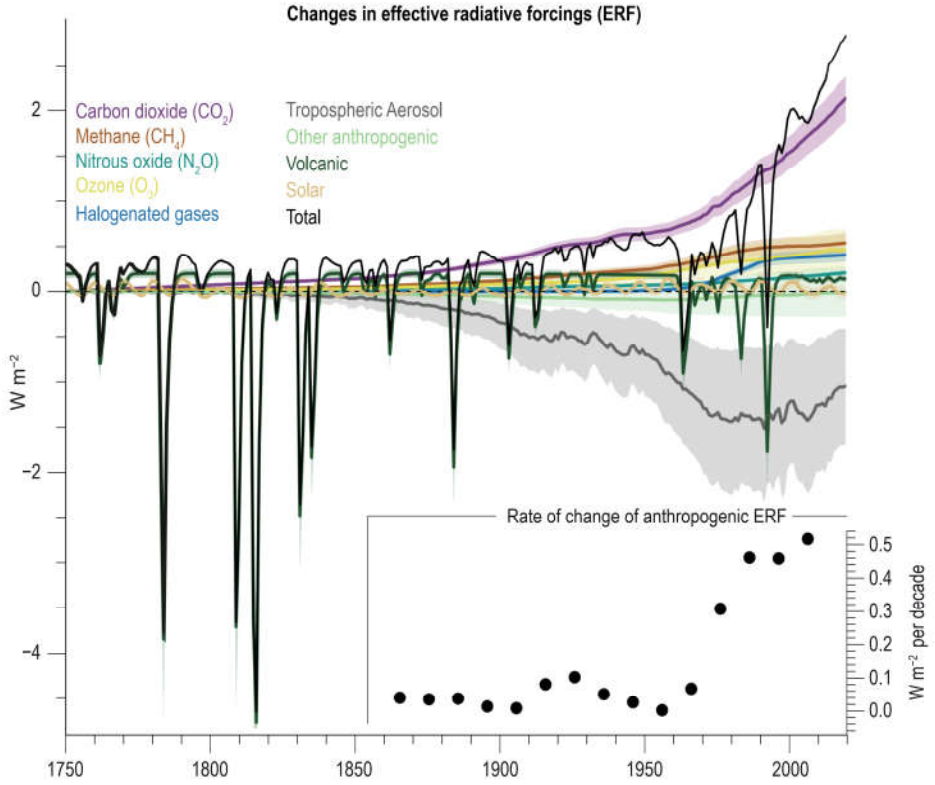

Figure 2.10 | Temporal evolution of effective radiative forcing (ERF) related to the drivers assessed in Section 2.2. ERFs are based upon the calculations described in Chapter 7, of which the global annual mean, central assessment values are shown as lines and the 5 to 95% uncertainty range as shading (Section 7.3, see Figures 7.6 to 7.8 for more detail on uncertainties). The inset plot shows the rate of change (linear trend) in total anthropogenic ERF (total without TSI and volcanic ERF) for 30-year periods centred at each dot. Further details on data sources and processing are available in the chapter data table (Table 2.SM.1).

IPCC 2021, Chap. 2

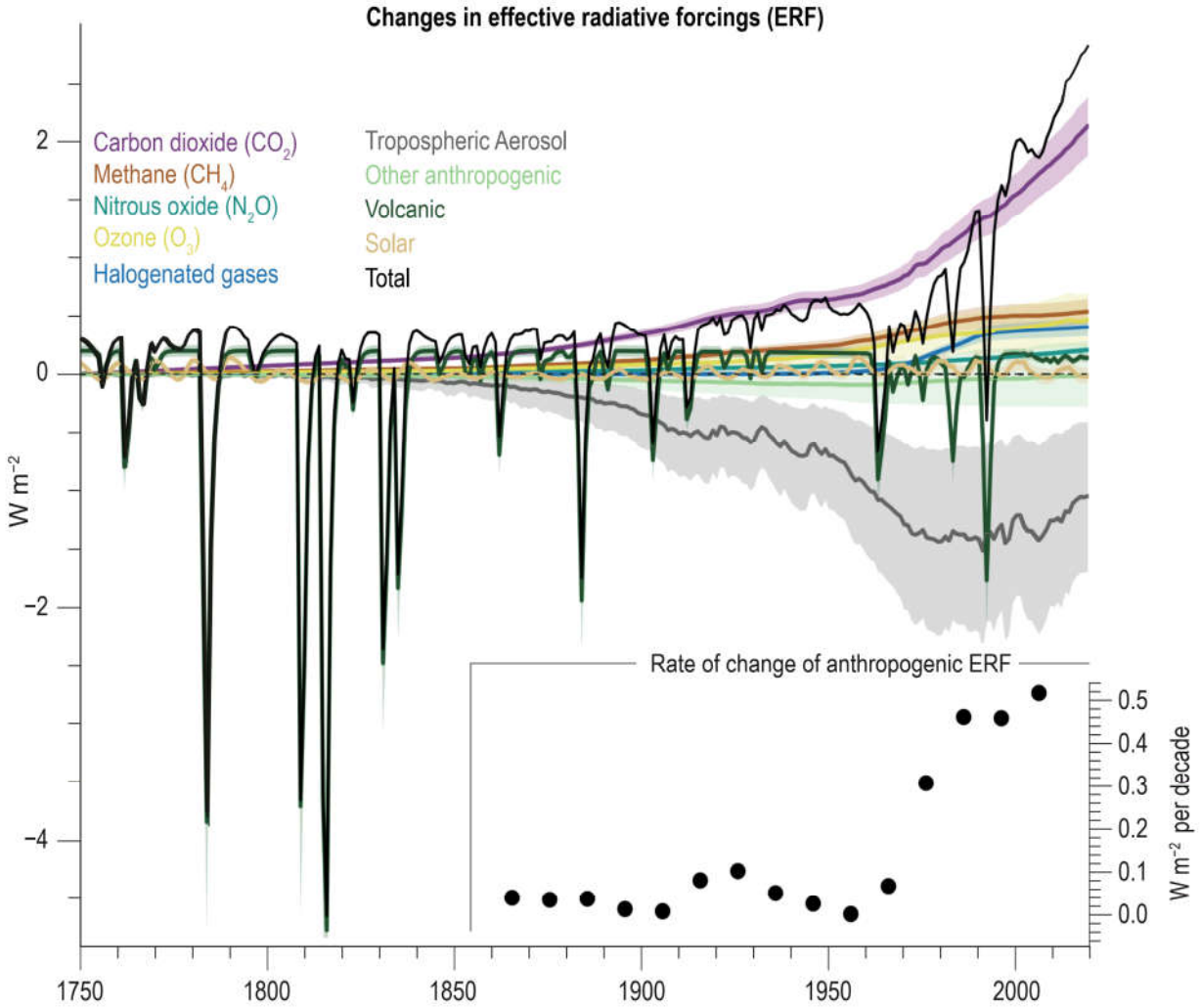

IPCC 2021, Chap. 2

Statements in the Executive Summary

Changes in Key Indicators of Global Climate Change (1)

Observed changes in the atmosphere, oceans, cryosphere and biosphere provide unequivocal evidence a world that has warmed. Over the past several decades, key indicators of the climate system are increasingly at levels unseen in centuries to millennia, and are changing at rates unprecedented in at least the last 2000 years (*high confidence*). In the last decade, global mean surface temperature (GMST) was *more likely than not* higher than for any multi-century average during the Holocene (past 11,700 years) and was comparable to temperatures of the Last Interglacial period (roughly 125,000 years ago). {2.3}

IPCC 2021, Chap. 2

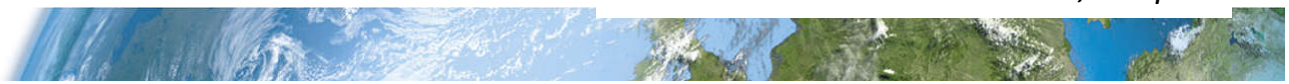

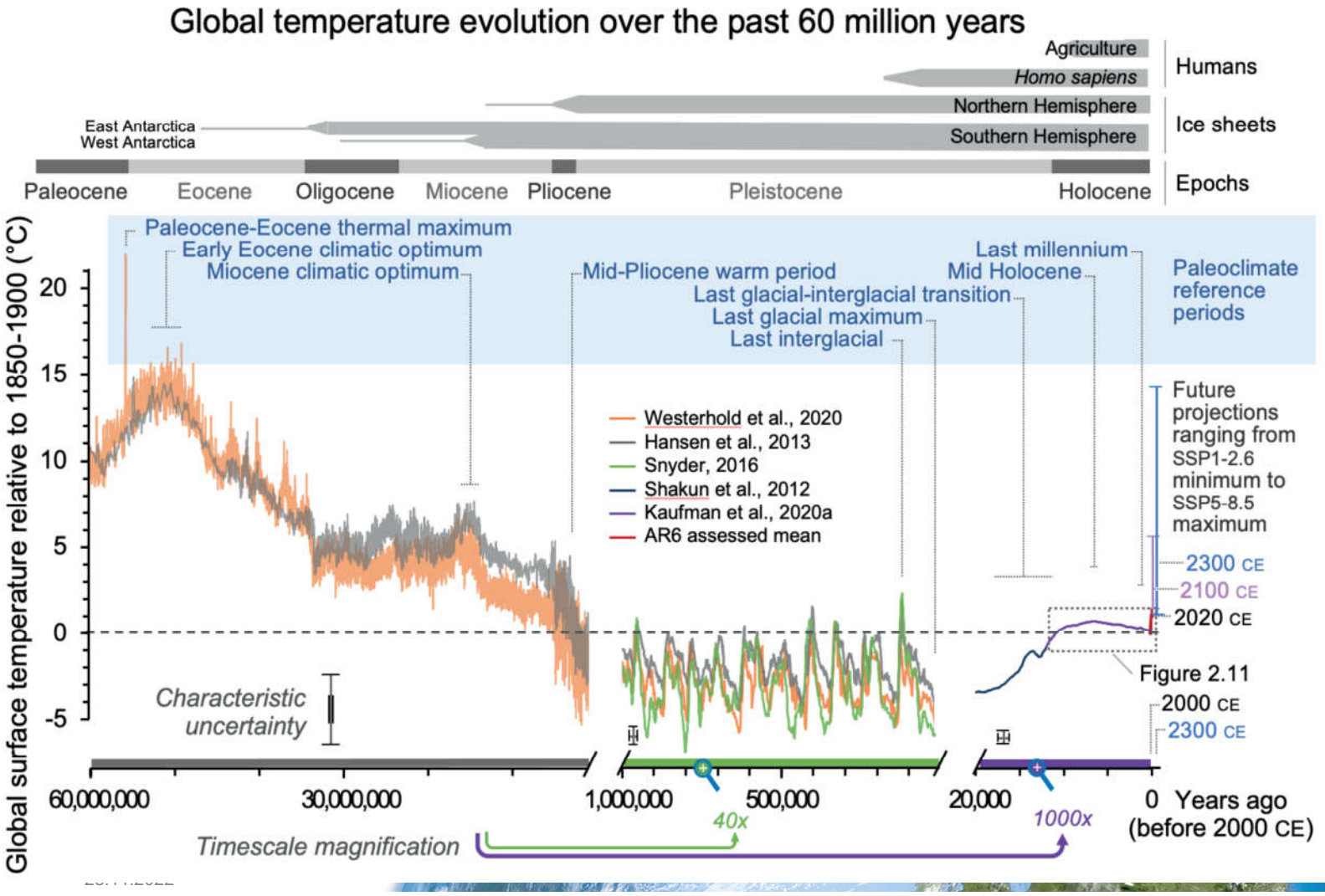

IPCC 2021, Chap. 2

Statements in the Executive Summary

Changes in Key Indicators of Global Climate Change (2)

GMST increased by 0.85 [0.69 to 0.95] °C between 1850–1900 and 1995–2014 and by 1.09 [0.95 to 1.20] °C between 1850–1900 and 2011–2020. From 1850–1900 to 2011–2020, the temperature increase over land (1.59 [1.34 to 1.83] °C) has been faster than over the oceans (0.88 [0.68 to 1.01] °C). Over the last 50 years, observed GMST has increased at a rate unprecedented in at least the last 2000 years (*medium confidence*). The increase in GMST since the mid-19th century was preceded by a slow decrease that began in the mid-Holocene (around 6500 years ago) (*medium confidence*). {2.3.1.1, Cross-Chapter Box 2.1}

IPCC 2021, Chap. 2

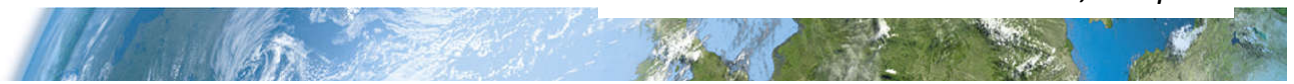

Earth's surface temperature history

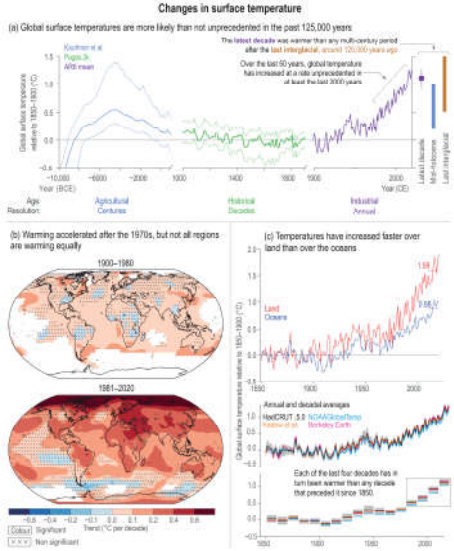

Figure 2.11 | Earth's surface temperature history with key findings annotated within each panel. (a) GMST over the Holocene divided into three time scales: (i) 12 kyr–1 kyr in 100-year time steps; (ii) 1000–1900 CE, 10-year smooth; and (iii) 1900–2020 CE (from panel (c)). Median of the multi-method reconstruction (bold lines), with 5th and 95th percentiles of the ensemble members (thin lines). Vertical bars are the assessed *medium confidence* ranges of GMST for the Last Interglacial and mid-Holocene (Section 2.3.1.1). The last decade value and *very likely* range arises from Section 2.3.1.1.3. **(b)** Spatially resolved trends (°C per decade) for HadCRUTv5 over (upper map) 1900–1980, and (lower map) 1981–2020. Significance is assessed following AR(1) adjustment after Santer et al. (2008), '×' marks denote non-significant trends. **(c)** Temperature from instrumental data for 1850–2020, including (upper panel) multi-product mean annual time series assessed in Section 2.3.1.1.3 for temperature over the oceans (blue line) and temperature over the land (red line) and indicating the warming to the most recent 10 years; and annually (middle panel) and decadally (bottom panel) resolved averages for the GMST datasets assessed in Section 2.3.1.1.3. The grey shading in each panel shows the uncertainty associated with the HadCRUT5 estimate (Morice et al., 2021). All temperatures relative to the 1850–1900 reference period. Further details on data sources and processing are available in the chapter data table (Table 2.SM.1).

IPCC 2021, Chap. 2

Earth's surface temperature history

Changes in surface temperature

(a) Global surface temperatures are more likely than not unprecedented in the past 125,000 years

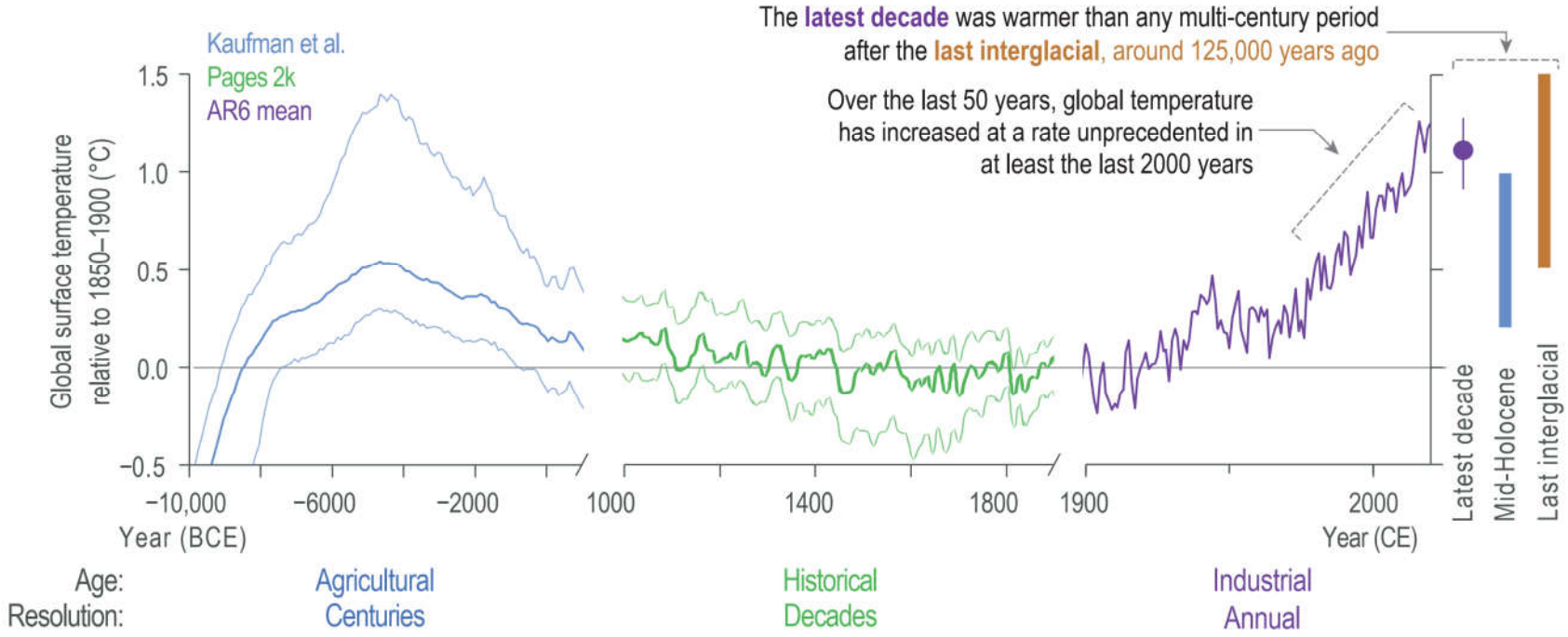

IPCC 2021, Chap. 2

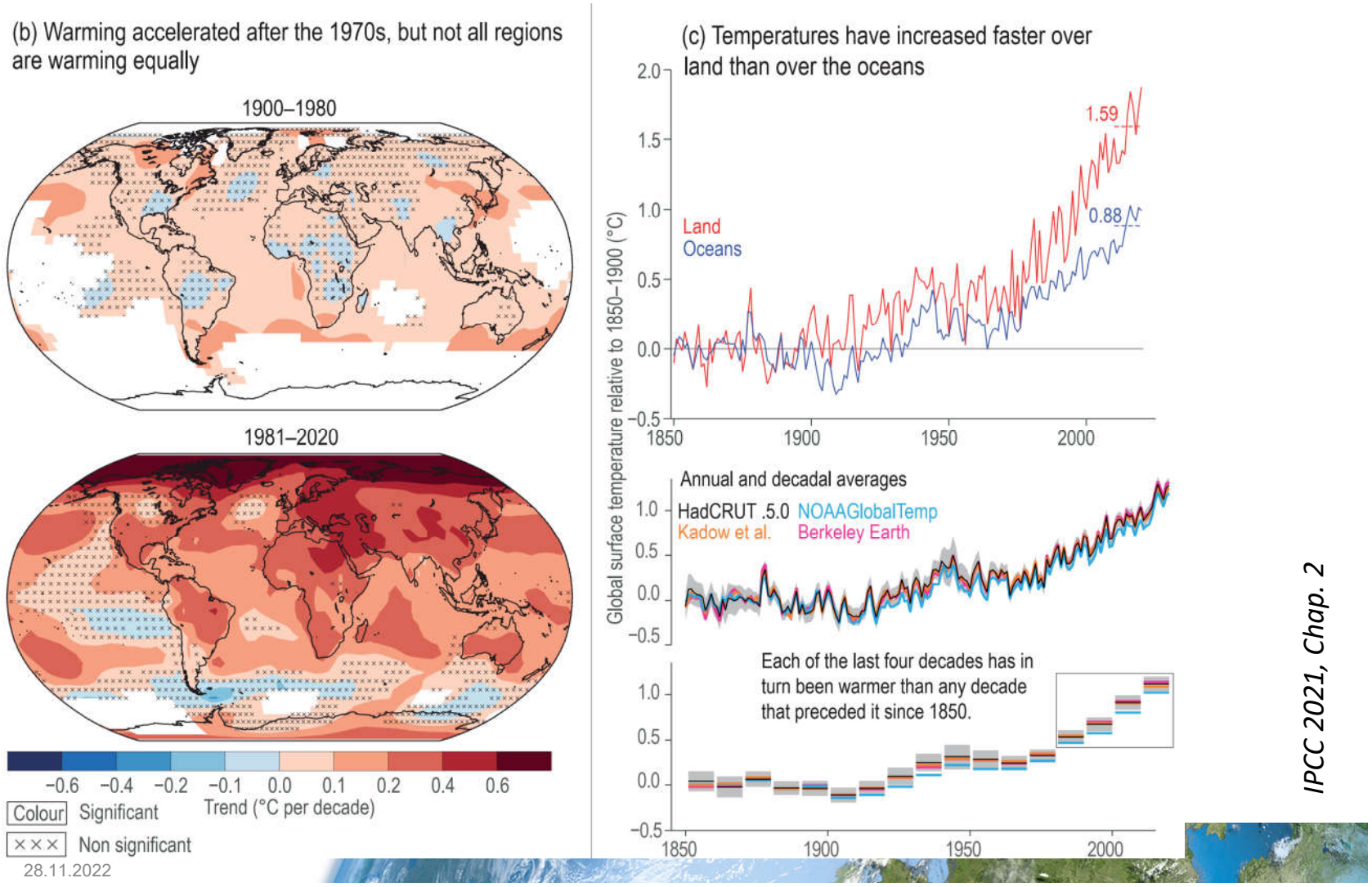

IPCC 2021, Chap. 2

Statements in the Executive Summary

Changes in Key Indicators of Global Climate Change (3)

Changes in GMST and global surface air temperature (GSAT) over time differ by at most 10% in either direction (high confidence), and the long-term changes in GMST and GSAT are presently assessed to be identical. There is expanded uncertainty in GSAT estimates, with the assessed change from 1850–1900 to 1995–2014 being 0.85 [0.67 to 0.98] ^{o}C. {Cross-Chapter box 2.3}

IPCC 2021, Chap. 2

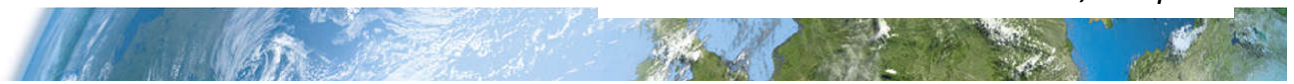

Changes in assessed historical surface temperature changes since AR5

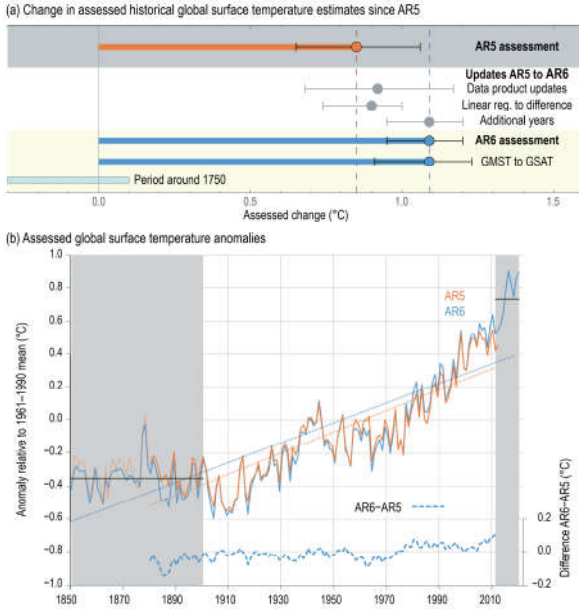

Cross-chapter Box 2.3, Figure 1 | Changes in assessed historical surface temperature changes since AR5. (a) Summary of the impact of various steps from AR5 assessment warming-to-date number for 1880–2012 using a linear trend fit to the AR6 assessment based upon the difference between 1850–1900 and 2011–2020. Whiskers provide 90% (*very likely*) ranges. AR6 assessment in addition denotes additional warming since the period around 1750 (Cross-Chapter Box 1.2). **(b)** Time series of the average of assessed AR5 series (orange, faint prior to 1880 when only HadCRUT4 was available) and AR6 assessed series (blue) and their differences (offset) including an illustration of the two trend fitting metrics used in AR5 and AR6. Further details on data sources and processing are available in the chapter data table (Table 2.SM.1).

IPCC 2021, Chap. 2

Changes in assessed historical surface temperature changes since AR5

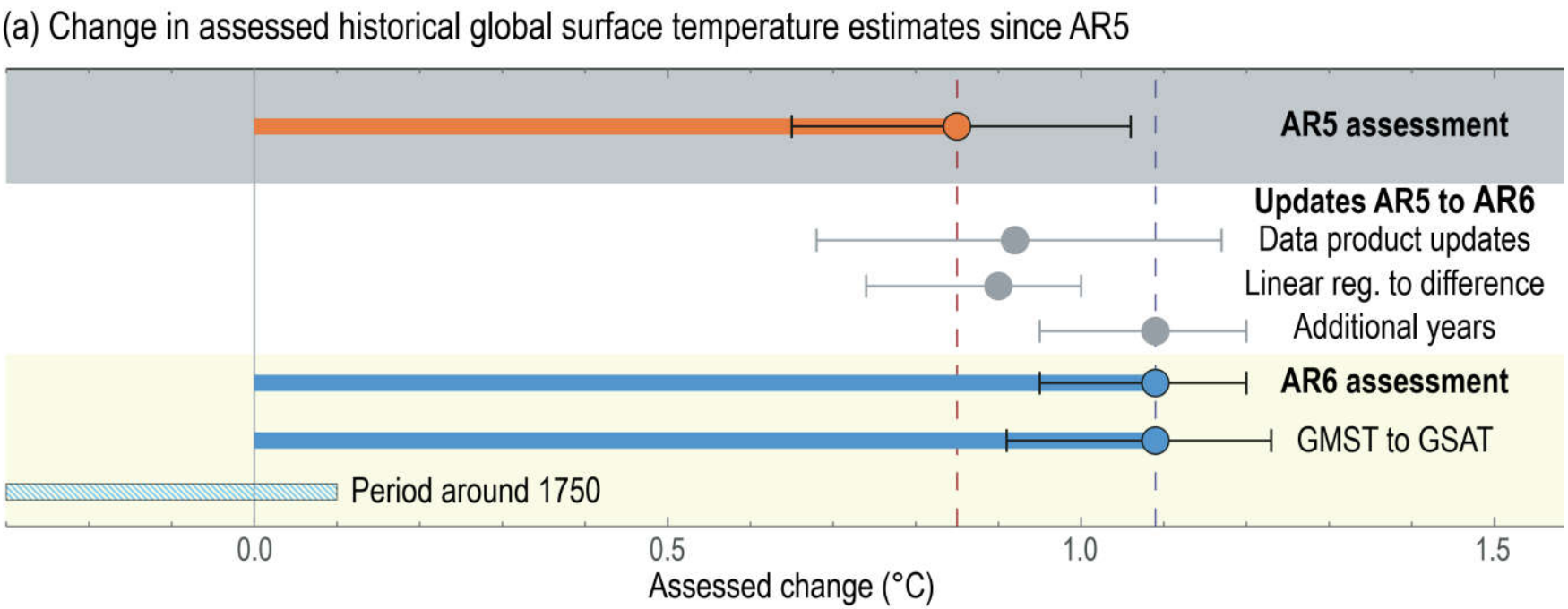

IPCC 2021, Chap. 2

Changes in assessed historical surface temperature changes since AR5

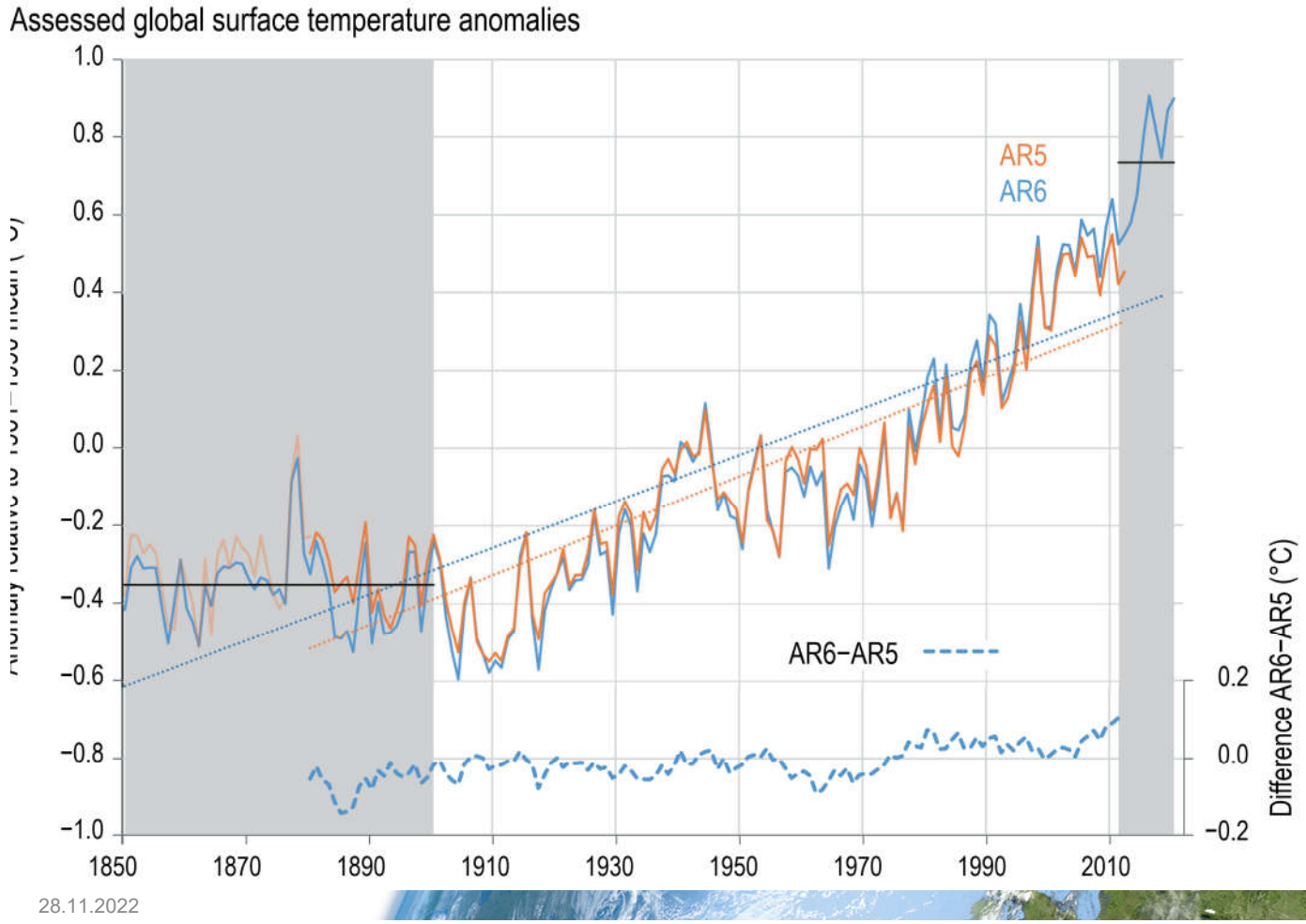

IPCC 2021, Chap. 2

Statements in the Executive Summary

Changes in Key Indicators of Global Climate Change (3)

Changes in GMST and global surface air temperature (GSAT) over time differ by at most 10% in either direction (high confidence), and the long-term changes in GMST and GSAT are presently assessed to be identical. There is expanded uncertainty in GSAT estimates, with the assessed change from 1850–1900 to 1995–2014 being 0.85 [0.67 to 0.98] ^{o}C. {Cross-Chapter box 2.3}

The troposphere has warmed since at least the 1950s, and it is *virtually certain* that the stratosphere has cooled. In the Tropics, the upper troposphere has warmed faster than the near-surface since at least 2001, the period over which new observation techniques permit more robust quantification (*medium confidence*). It is *virtually certain* that the tropopause height has risen globally over 1980–2018, but there is *low confidence* in the magnitude. {2.3.1.2}

IPCC 2021, Chap. 2

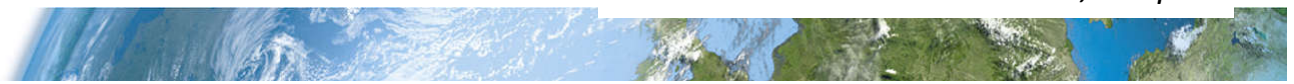

Temperature trends in the upper air

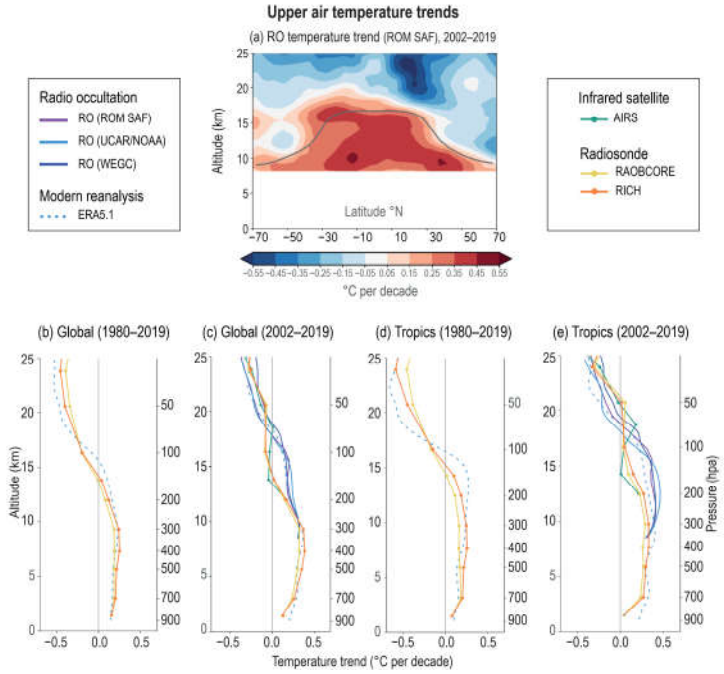

Figure 2.12 | Temperature trends in the upper air. (a) Zonal cross-section of temperature anomaly trends (2007–2016 baseline) for 2002–2019 in the upper troposphere and lower stratosphere region. The climatological tropopause altitude is marked by a grey line. Significance is not indicated due to the short period over which trends are shown, and because the assessment findings associated to this figure relate to difference between trends at different heights, not the absolute trends. **(b, c)** Trends in temperature at various atmospheric heights for 1980–2019 and 2002–2019 for the near-global (70°N–70°S) domain. **(d, e)** as for (b, c) but for the tropical (20°N–20°S) region. Further details on data sources and processing are available in the chapter data table (Table 2.SM.1).

IPCC 2021, Chap. 2

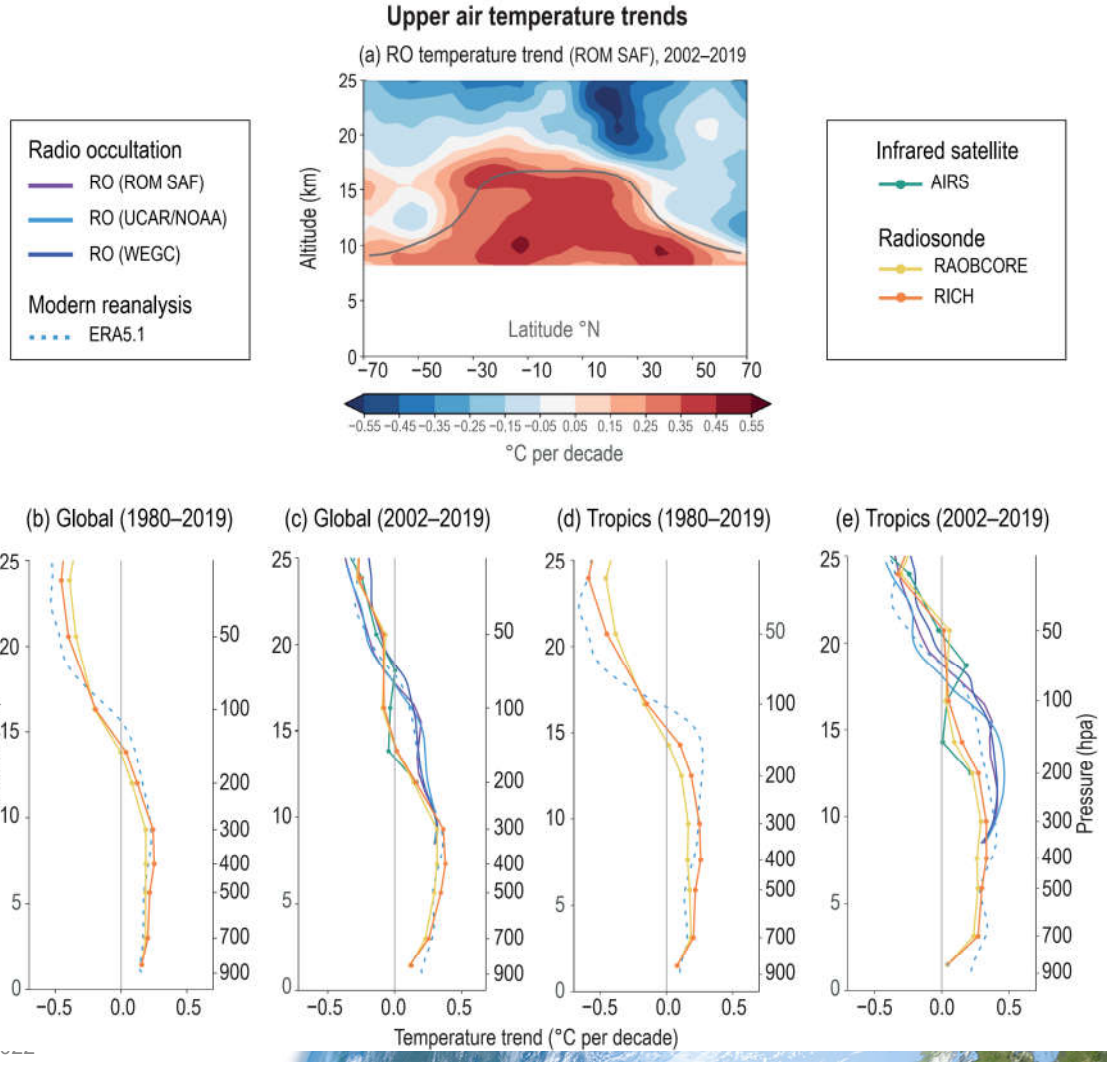

IPCC 2021, Chap. 2

Statements in the Executive Summary

Changes in Key Indicators of Global Climate Change (4)

Changes in several components of the global hydrological cycle provide evidence for overall strengthening since at least 1980 (*high confidence*). However, there is *low confidence* in comparing recent changes with past variations due to limitations in paleoclimate records at continental and global scales. Global land precipitation has *likely* increased since 1950, with a faster increase since the 1980s (medium confidence). Near-surface specific humidity has increased over both land (*very likely*) and the oceans (*likely*) since at least the 1970s. Relative humidity has *very likely* decreased over land areas since 2000. Global total column water vapour content has *very likely* increased during the satellite era. Observational uncertainty leads to *low confidence* in global trends in precipitation minus evaporation and river runoff. {2.3.1.3}

IPCC 2021, Chap. 2

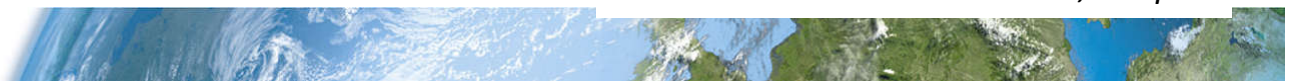

Changes in surface humidity

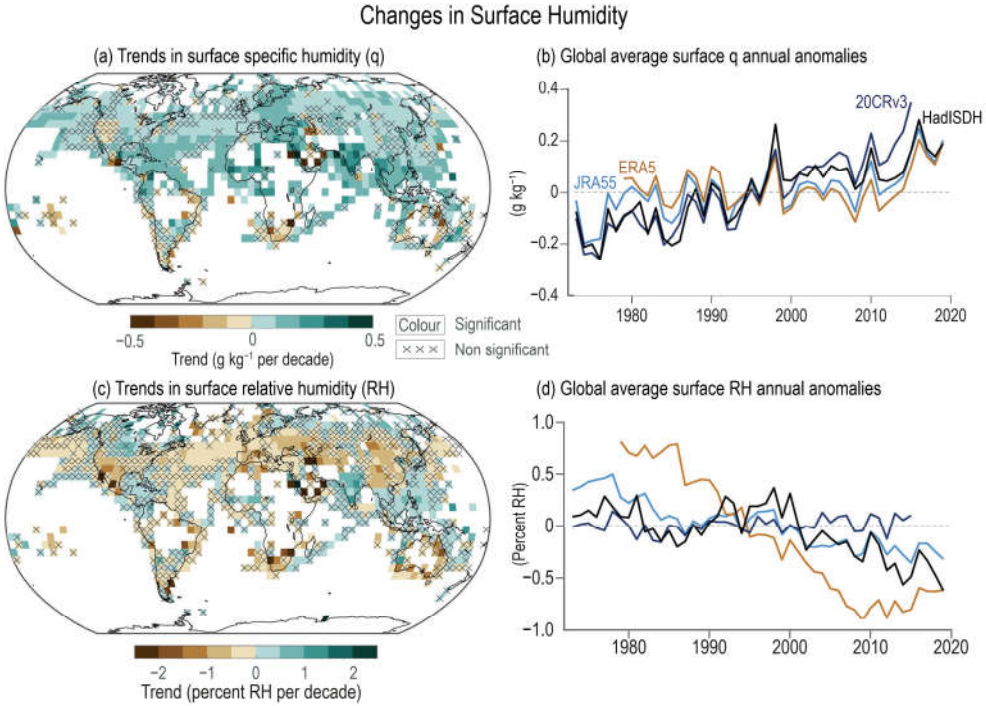

Figure 2.13 | Changes in surface humidity. (a) Trends in surface specific humidity over 1973–2019. Trends are calculated using OLS regression with significance assessed following AR(1) adjustment after Santer et al. (2008); '×' marks denote non-significant trends). **(b)** Global average surface specific humidity annual anomalies (1981–2010 base period). **(c)** as (a) but for the relative humidity. **(d)** as (b) but for the global average surface relative humidity annual anomalies. Further details on data sources and processing are available in the chapter data table (Table 2.SM.1).

IPCC 2021, Chap. 2

Changes in Surface Humidity

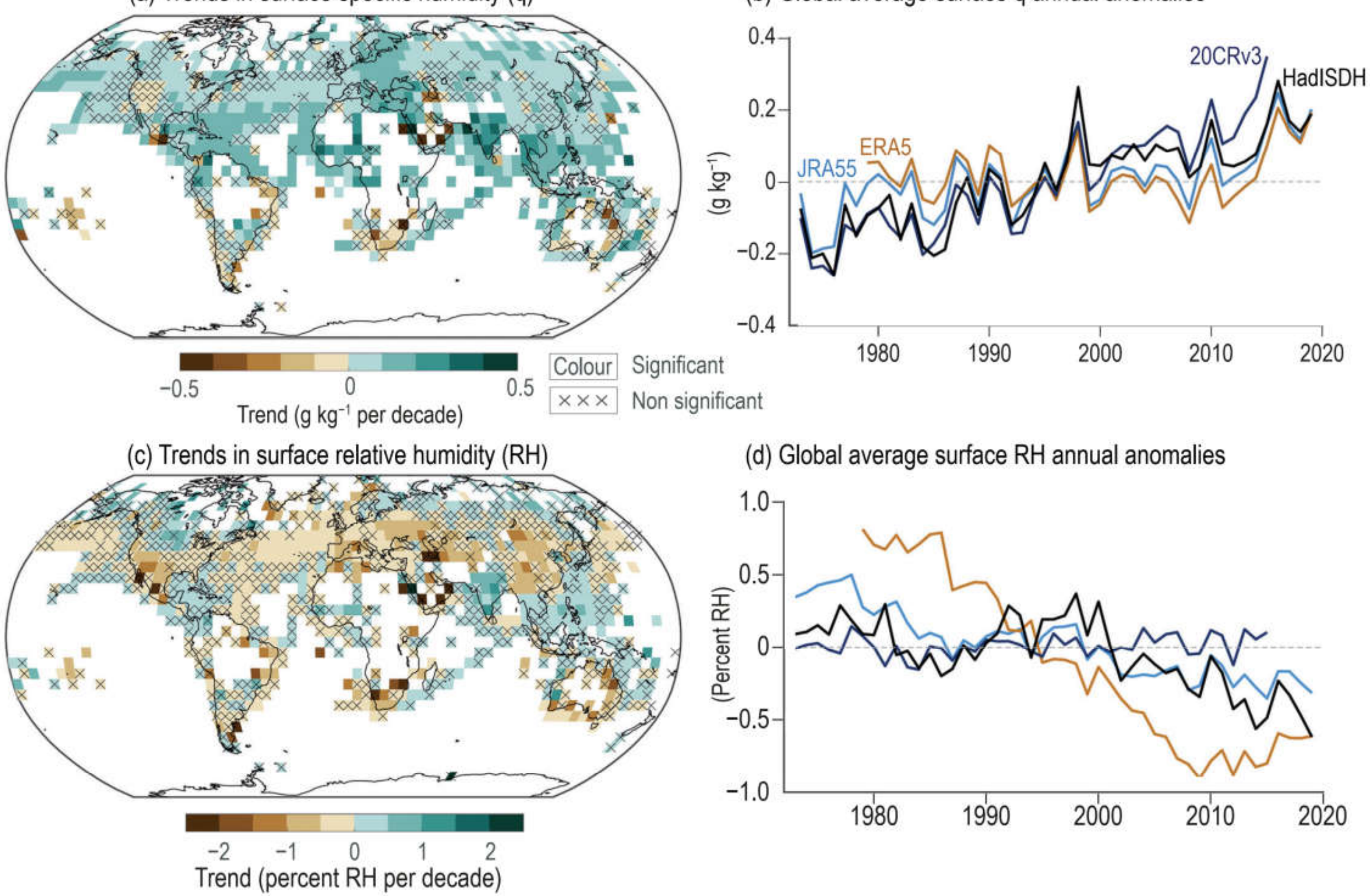

IPCC 2021, Chap. 2

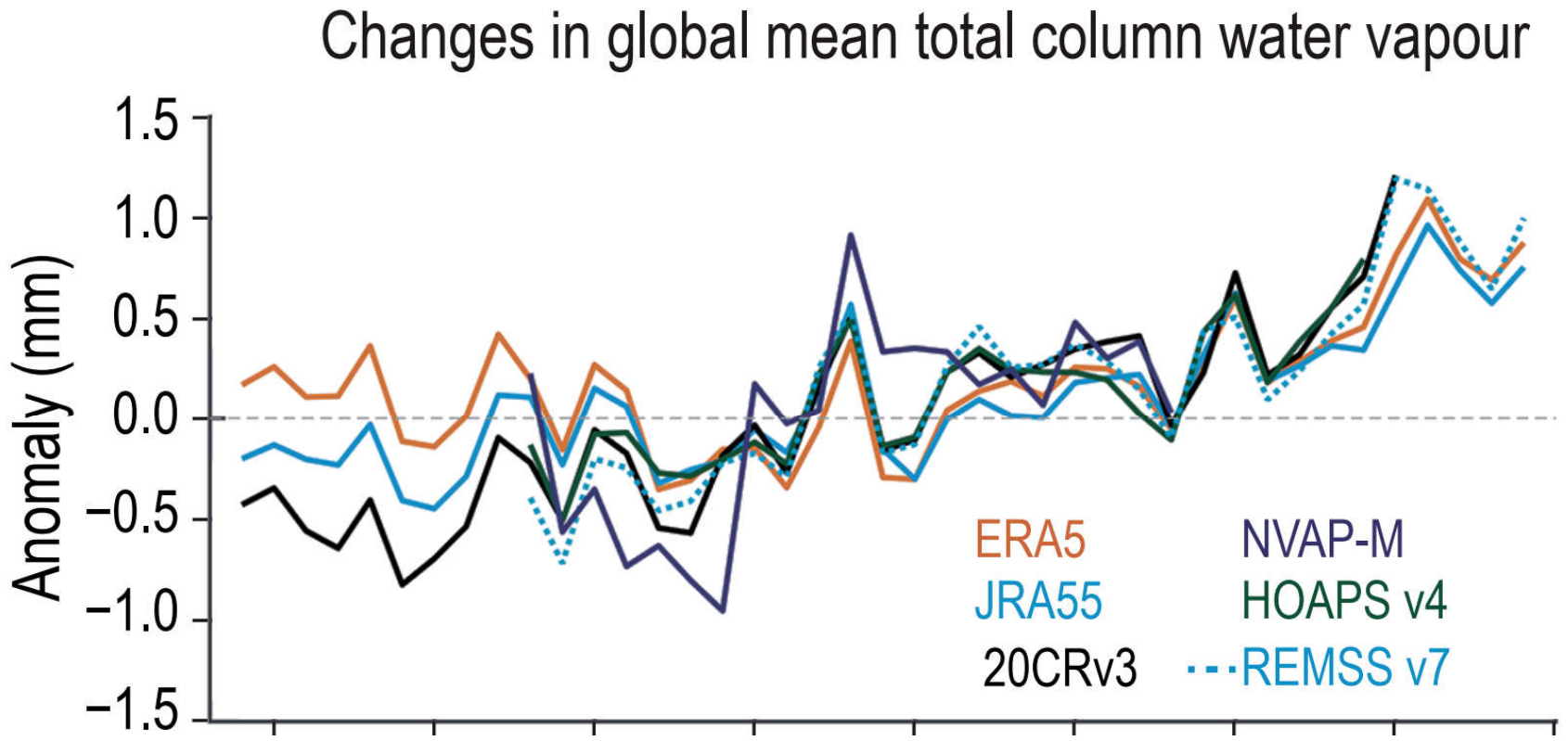

Figure 2.14 | Time series of global mean total column water vapour annual anomalies (mm) relative to a 1988–2008 base period. Further details on data sources and processing are available in the chapter data table (Table 2.SM.1).

IPCC 2021, Chap. 2

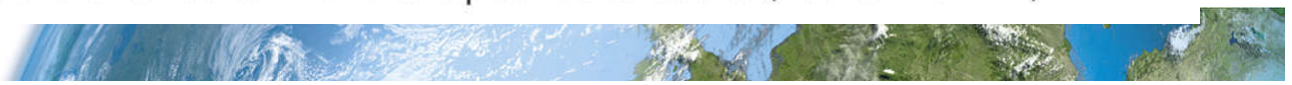

Changes in observed precipitation

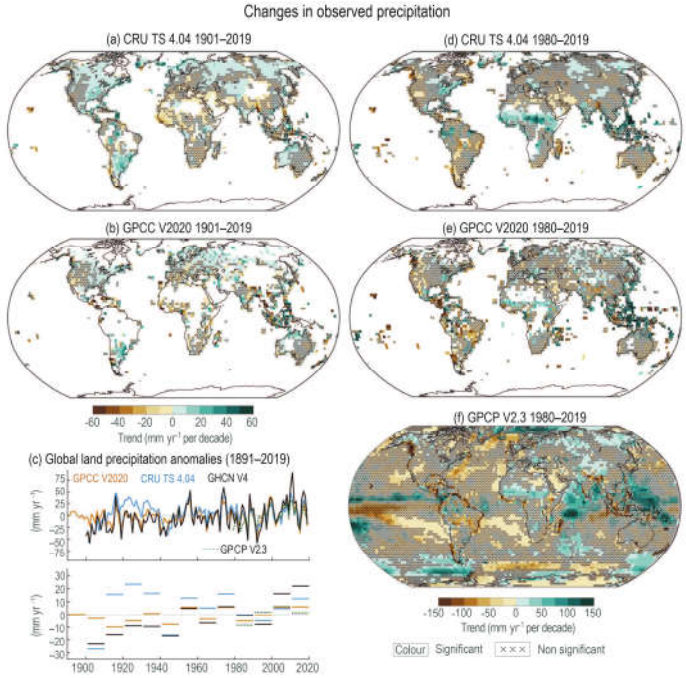

Figure 2.15 | Changes in observed precipitation. (a, b) Spatial variability of observed precipitation trends over land for 1901–2019 for two global in-situ products. Trends are calculated using OLS regression with significance assessed following AR(1) adjustment after Santer et al. (2008) ('×' marks denote non-significant trends). **(c)** Annual time series and decadal means from 1891 to date relative to a 1981–2010 climatology (note that different products commence at distinct times). **(d, e)** as (a, b), but for the periods starting in 1980. **(f)** is for the same period for the globally complete merged GPCP v2.3 product. Further details on data sources and processing are available in the chapter data table (Table 2.SM.1).

IPCC 2021, Chap. 2

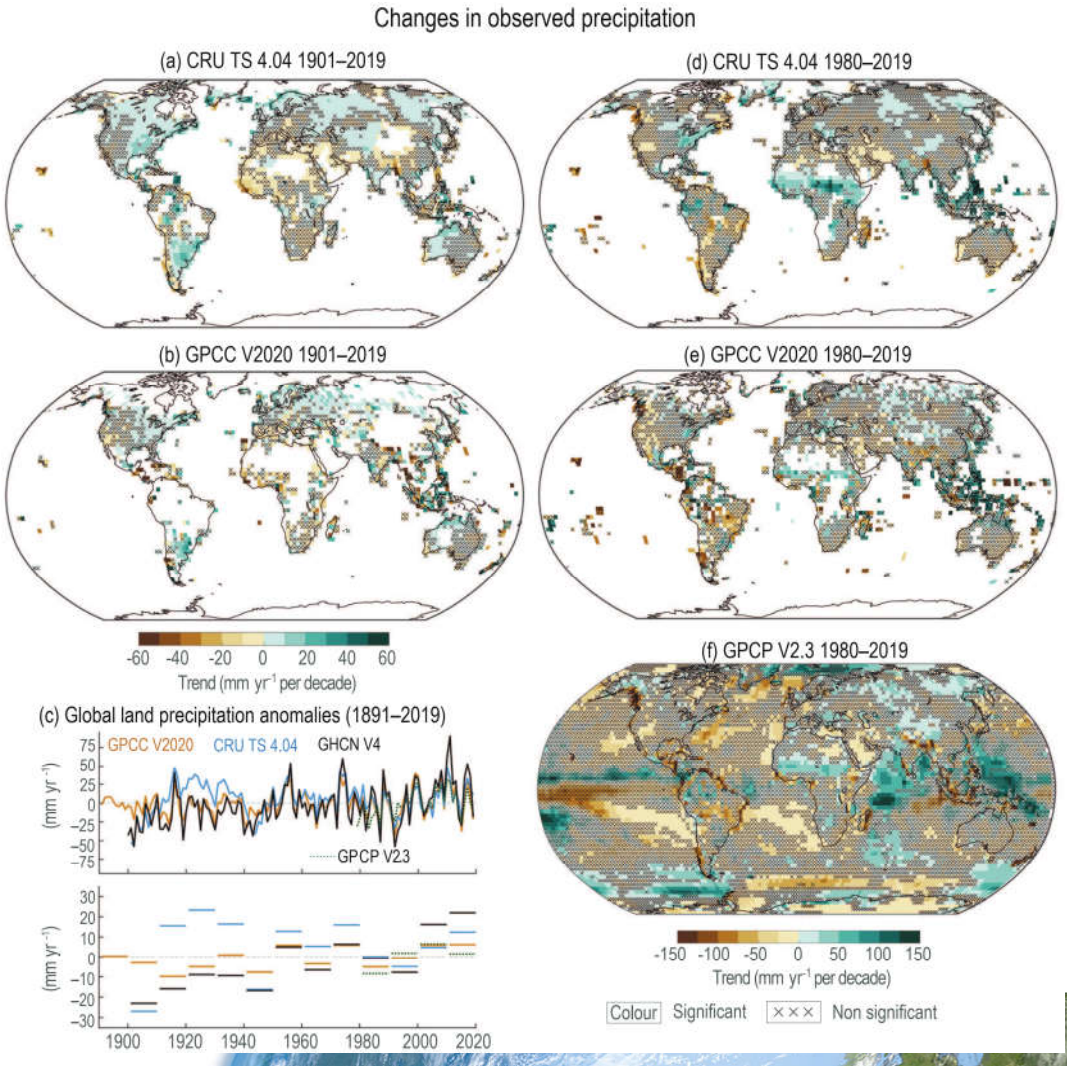

IPCC 2021, Chap. 2

Changes in precipitation minus evaporation

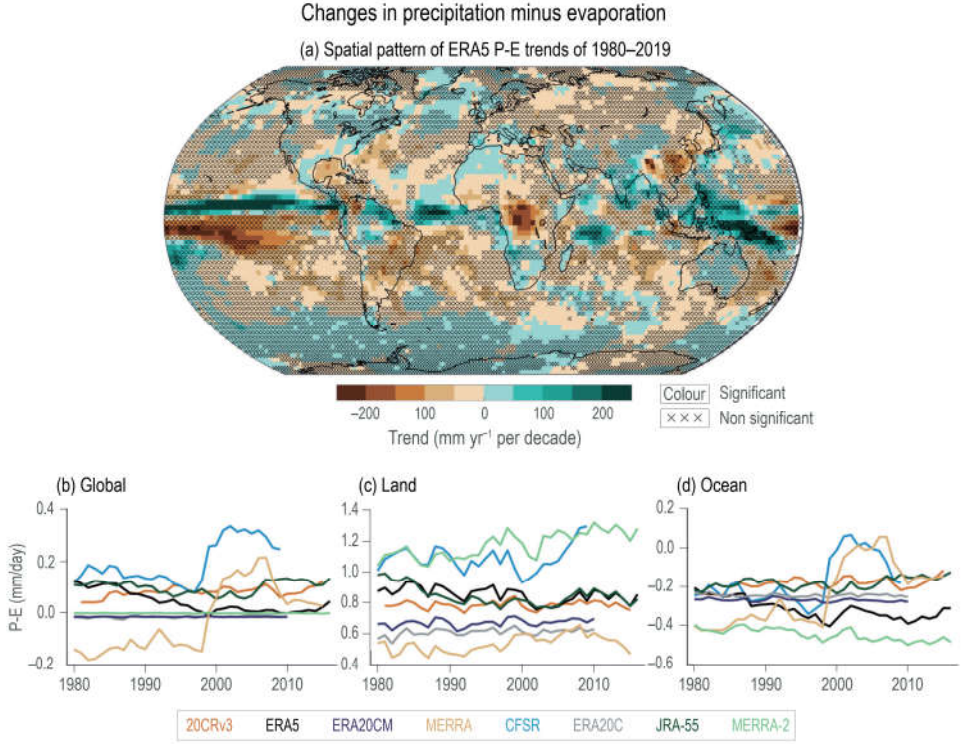

Figure 2.16 | Changes in precipitation minus evaporation. (a) Trends in precipitation minus evaporation (P–E) between 1980 and 2019. Trends are calculated using OLS regression with significance assessed following AR(1) adjustment after Santer et al. (2008) ('×' marks denote non-significant trends). Time series of **(b)** global, **(c)** land-only and **(d)** ocean-only average annual P–E (mm day^{-1}). Further details on data sources and processing are available in the chapter data table (Table 2.SM.1).

IPCC 2021, Chap. 2

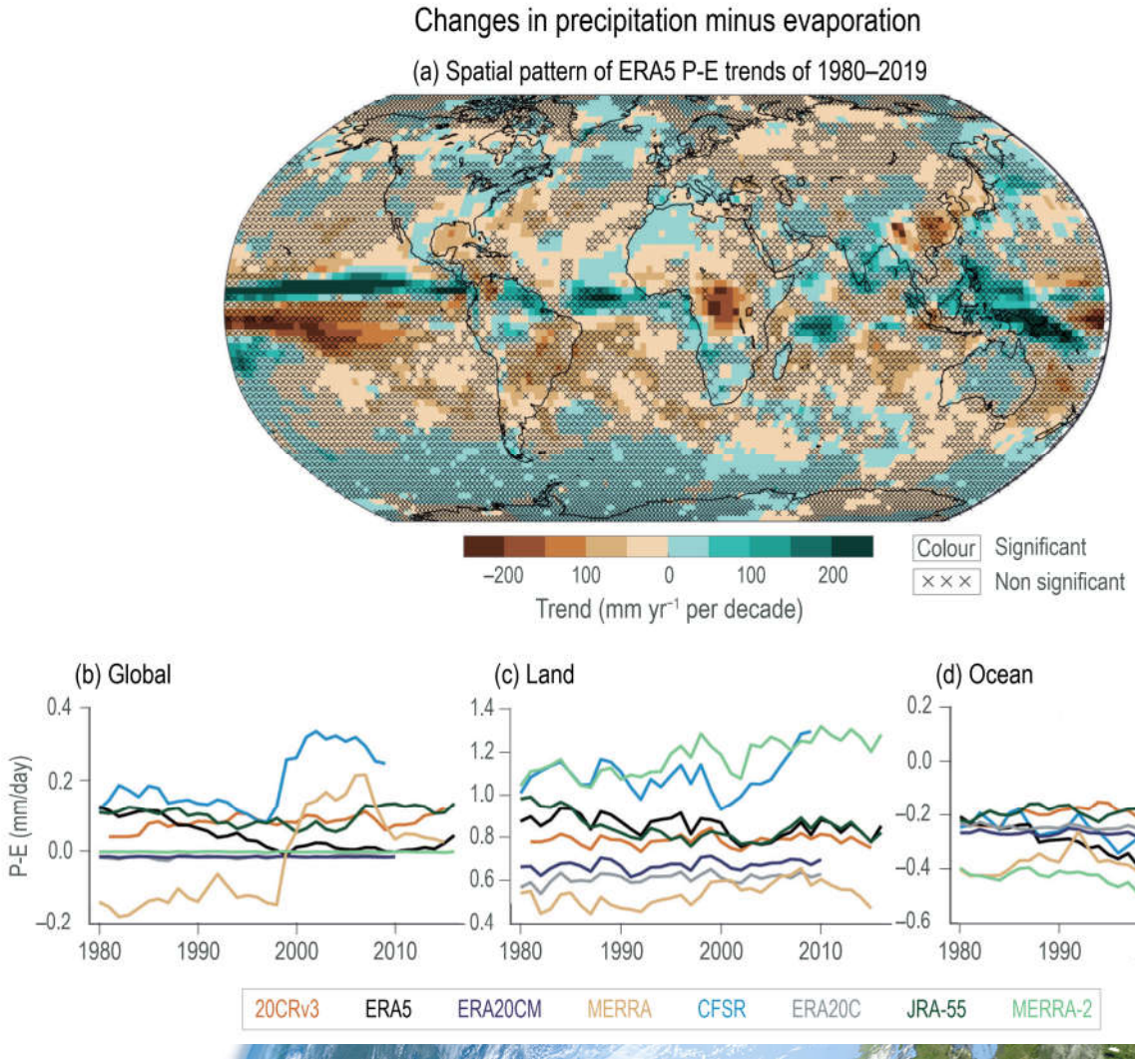
Changes in precipitation minus evaporation
(a) Spatial pattern of ERA5 P-E trends of 1980–2019
–200
100
0
100
200
Trend (mm yr⁻¹ per decade)
Colour
Significant
×××
Non significant
(b) Global
(c) Land
(d) Ocean
P-E (mm/day)
0.4
0.2
0.0
–0.2
1.4
1.2
1.0
0.8
0.6
0.4
0.2
0.0
–0.2
–0.4
–0.6
1980
1990
2000
2010
20CRv3
ERA5
ERA20CM
MERRA
CFSR
ERA20C
JRA-55
MERRA-2

Statements in the Executive Summary

Changes in Key Indicators of Global Climate Change (5)

Several aspects of the large-scale atmospheric circulation have *likely* changed since the mid-20th century, but limited proxy evidence yields *low confidence* in how these changes compare to longer-term climate. The Hadley circulation has *very likely* widened since at least the 1980s, and extratropical storm tracks have *likely* shifted poleward in both hemispheres. Global monsoon precipitation has *likely* increased since the 1980s, mainly in the Northern Hemisphere (*medium confidence*). Since the 1970s, near-surface winds have *likely* weakened over land. Over the oceans, near-surface winds *likely* strengthened over 1980–2000, but divergent estimates lead to *low confidence* in the sign of change thereafter. It is *likely* that the northern stratospheric polar vortex has weakened since the 1980s and experienced more frequent excursions toward Eurasia. {2.3.1.4}

IPCC 2021, Chap. 2

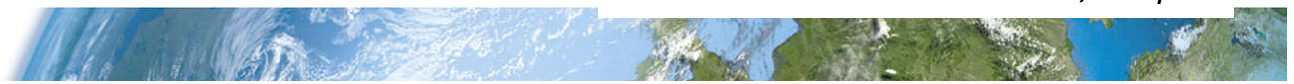

Hadley Cell extent and Hadley Cell intensity

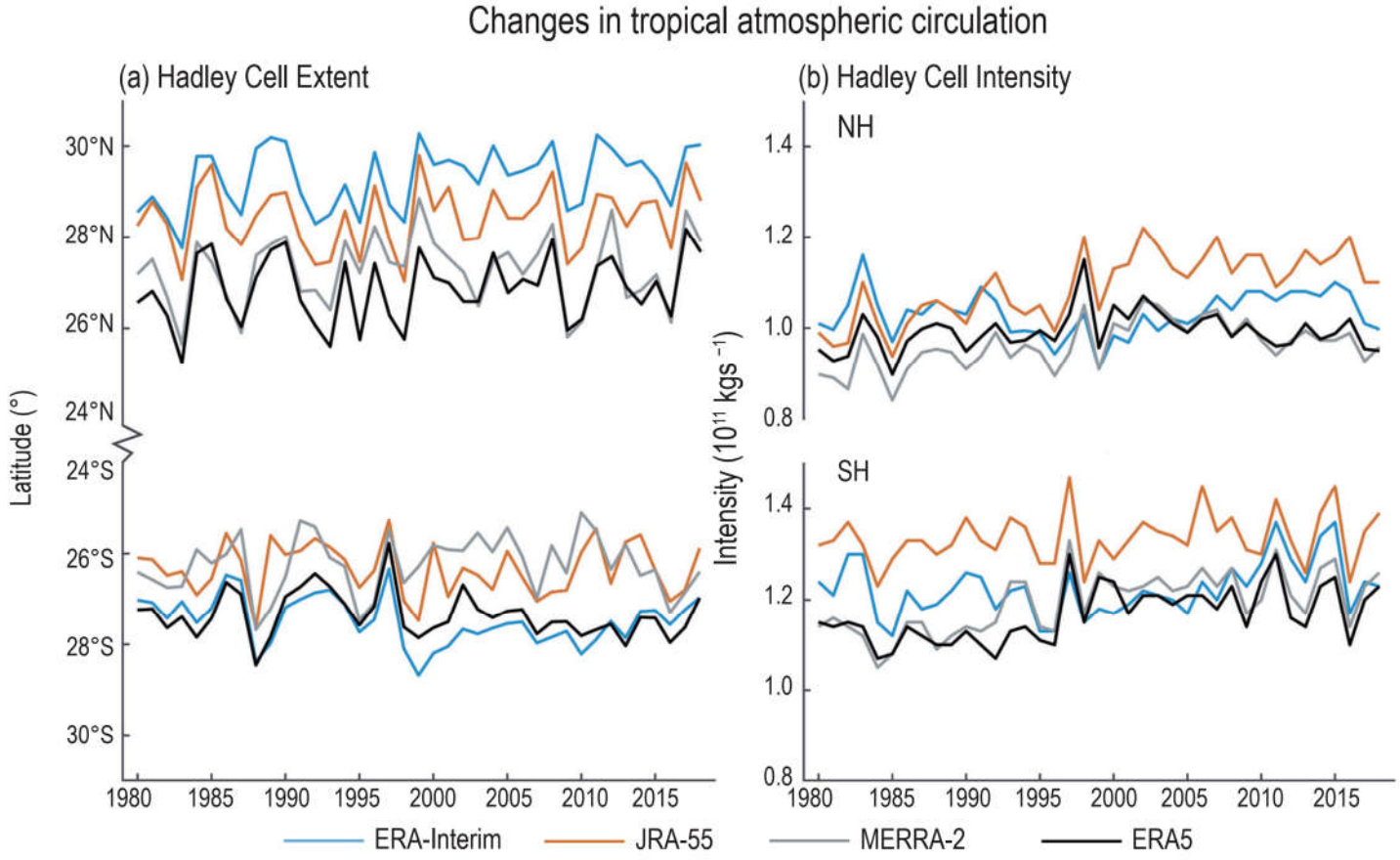

Figure 2.17 | Time series of the annual mean Northern Hemisphere (NH, top curves) and Southern Hemisphere (SH, bottom curves) Hadley cell extent (a) and Hadley cell intensity (b) since 1979. Further details on data sources and processing are available in the chapter data table (Table 2.SM.1).

IPCC 2021, Chap. 2

Trends in ERA5 zonal-mean zonal wind speed

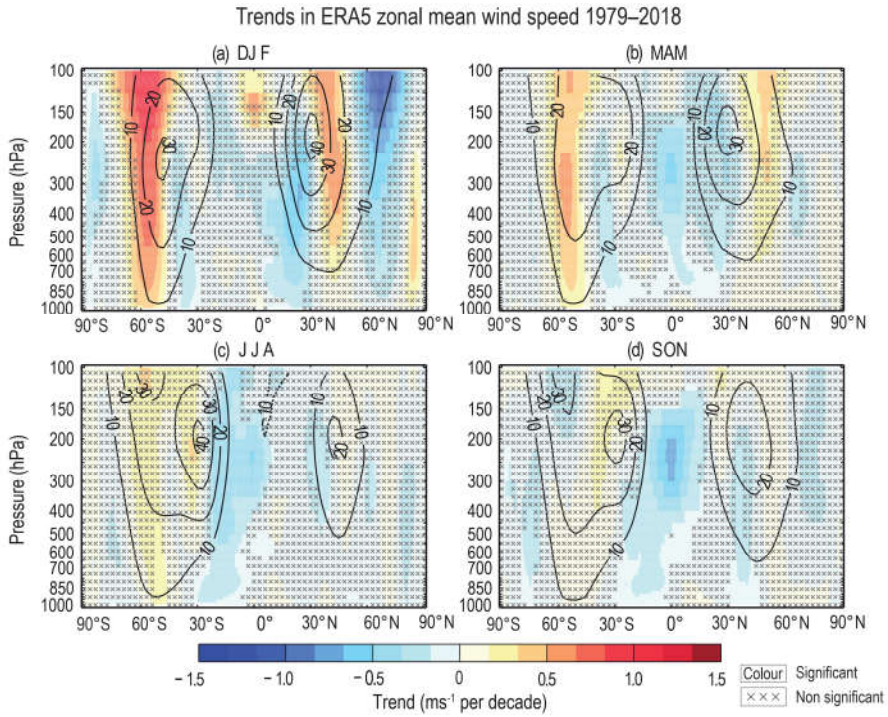

Figure 2.18 | Trends in ERA5 zonal-mean zonal wind speed. Shown are **(a)** DJF (December–January–February); **(b)** MAM (March–April–May); **(c)** JJA (June–July–August); and **(d)** SON (September–October–November). Climatological zonal winds during the data period are shown in solid contour lines for westerly winds and in dashed lines for easterly. Trends are calculated using OLS regression with significance assessed following AR(1) adjustment after Santer et al. (2008) ('×' marks denote non-significant trends). Further details on data sources and processing are available in the chapter data table (Table 2.SM.1).

IPCC 2021, Chap. 2

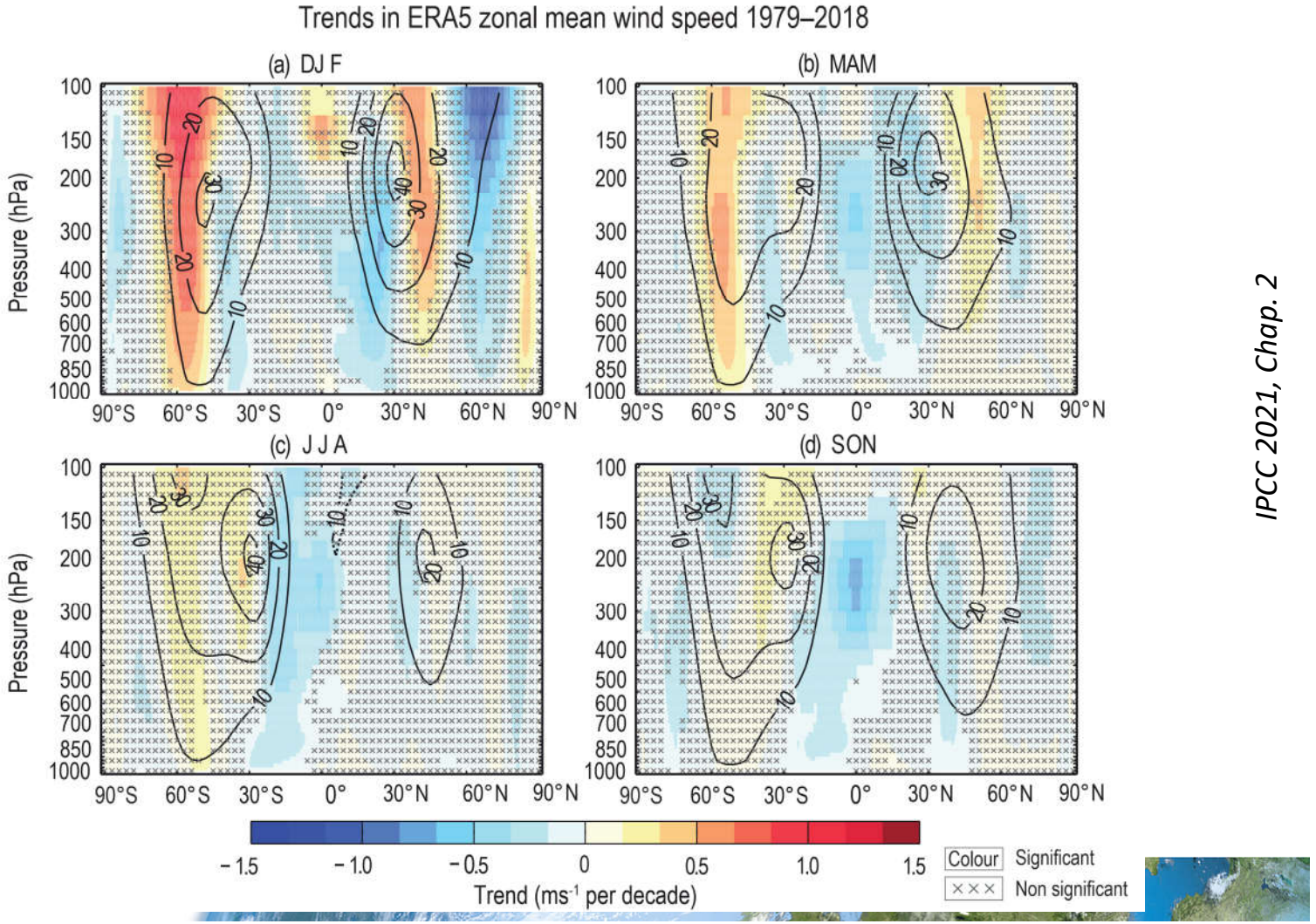

IPCC 2021, Chap. 2

Trends in surface wind speed

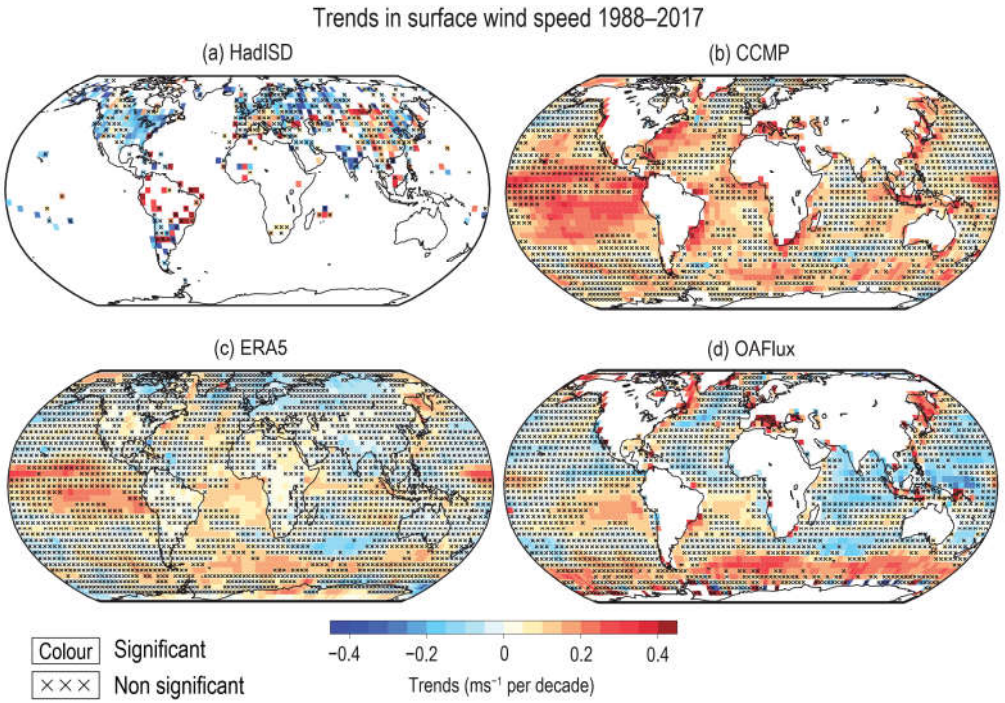

Figure 2.19 | Trends in surface wind speed. (a) Station observed winds from the integrated surface database (HadISD v2.0.2.2017f); **(b)** Cross-Calibrated Multi-Platform wind product; **(c)** ERA5; and **(d)** wind speed from the Objectively Analyzed Air-Sea Heat Fluxes dataset, release 3 (OAFLUX, release 3). White areas indicate incomplete or missing data. Trends are calculated using OLS regression with significance assessed following AR(1) adjustment after Santer et al. (2008); '×' marks denote non-significant trends. Further details on data sources and processing are available in the chapter data table (Table 2.SM.1).

IPCC 2021, Chap. 2

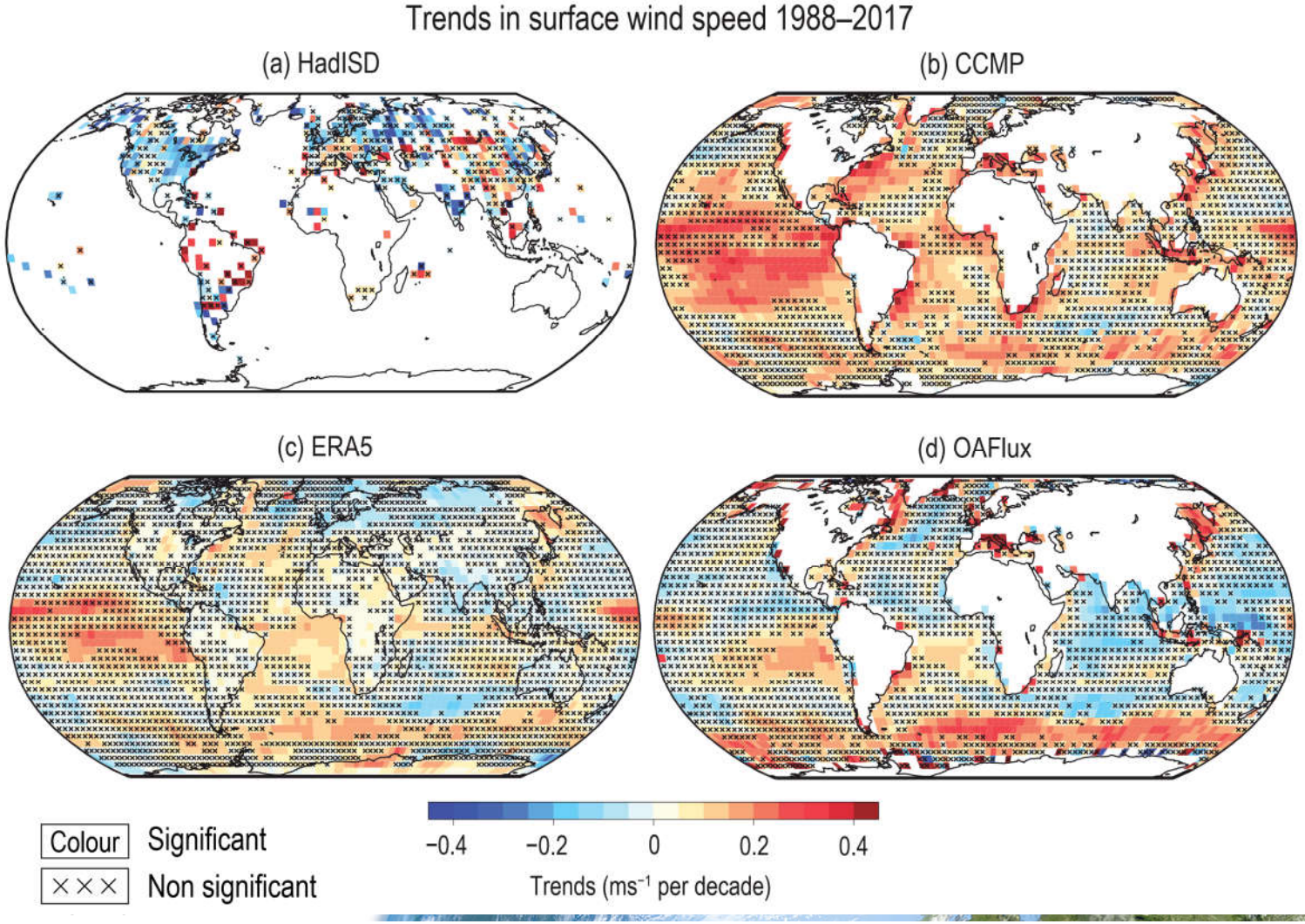
Trends in surface wind speed 1988–2017
(a) HadISD
(b) CCMP
(c) ERA5
(d) OAFlux
Colour Significant
××× Non significant
−0.4
−0.2
0
0.2
0.4
Trends (ms⁻¹ per decade)

Statements in the Executive Summary

Changes in Key Indicators of Global Climate Change (6)

Current Arctic sea ice coverage levels are the lowest since at least 1850 for both annual mean and late-summer values (*high confidence*) and for the past 1000 years for late-summer values (*medium confidence*). Between 1979 and 2019, Arctic sea ice area has decreased in both summer and winter, with sea ice becoming younger, thinner and more dynamic (*very high confidence*). Decadal means for Arctic sea ice area decreased from 6.23 million km^2 in 1979–1988 to 3.76 million km^2 in 2010–2019 for September and from 14.52 to 13.42 million km^2 for March. Antarctic sea ice area has experienced little net change since 1979 (*high confidence*), with only minor differences between sea ice area decadal means for 1979–1988 (2.04 million km^2 for February, 15.39 million km^2 for September) and 2010–2019 (2.17 million km^2 for February, 15.75 million km^2 for September). {2.3.2.1}

IPCC 2021, Chap. 2

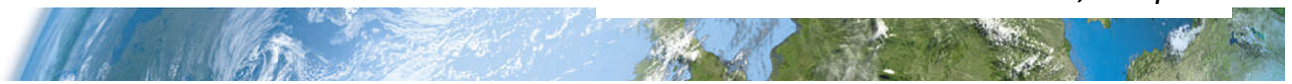

Changes in Arctic and Antarctic sea ice area

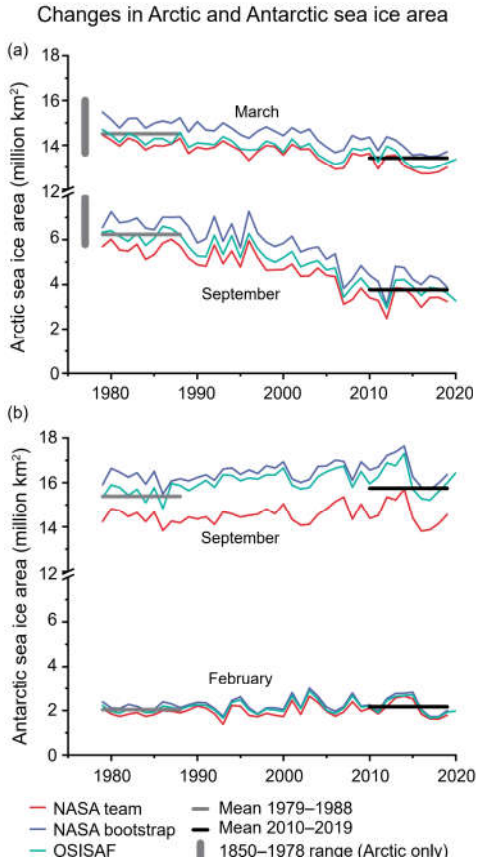

Figure 2.20 | Changes in Arctic and Antarctic sea ice area. (a) Three time series of Arctic sea-ice area (SIA) for March and September from 1979 to 2020 (passive microwave satellite era). In addition, the range of SIA from 1850–1978 is indicated by the vertical bar to the left. **(b)** Three time series of Antarctic sea ice area for September and February (1979–2020). In both (a) and (b), decadal means for the three series for the first and most recent decades of observations are shown by horizontal lines in grey (1979–1988) and black (2010–2019). SIA values have been calculated from sea ice concentration fields. Available data for 2020 (OSISAF) is shown in both (a) and (b). Further details on data sources and processing are available in the chapter data table (Table 2.SM.1).

IPCC 2021, Chap. 2

Changes in Arctic and Antarctic sea ice area

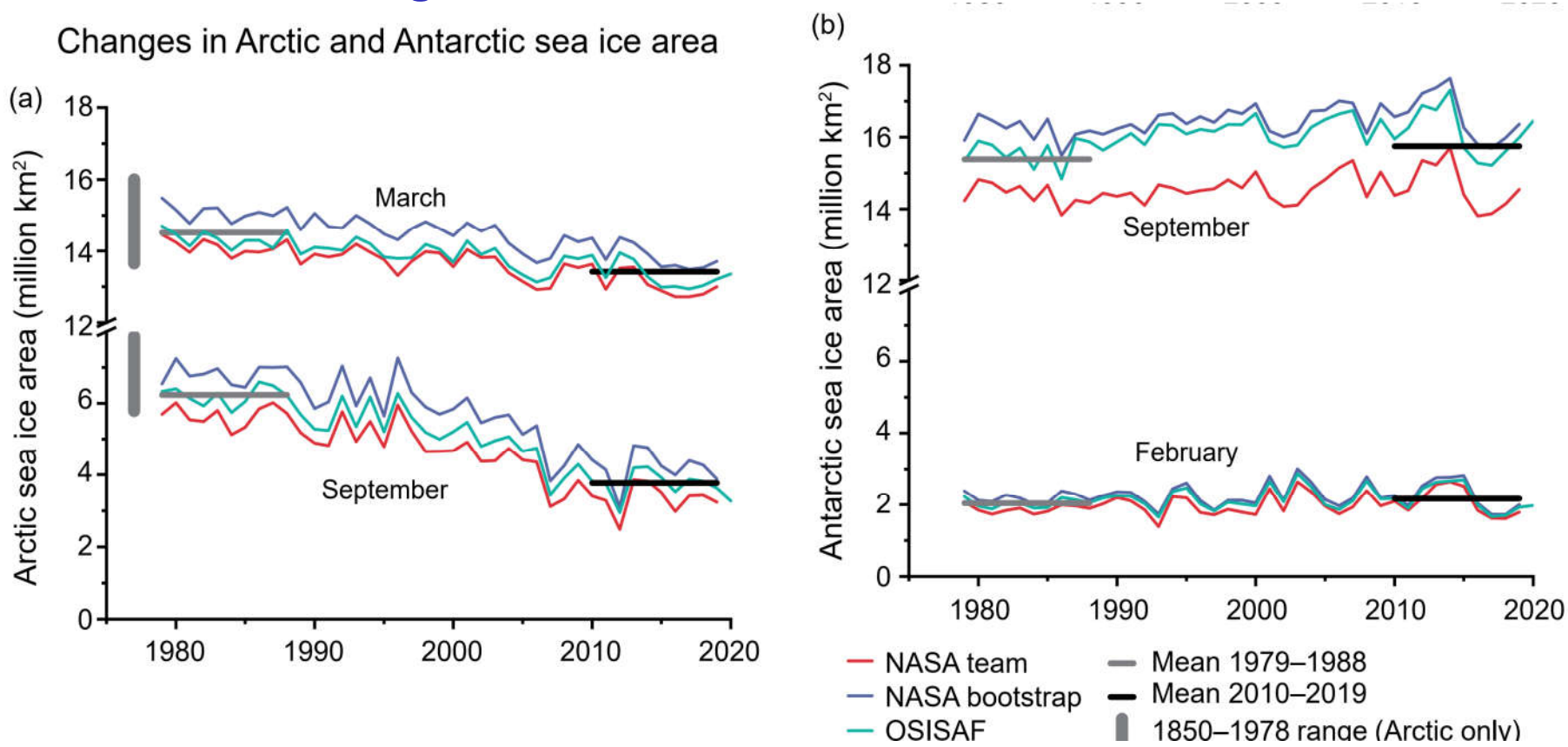

IPCC 2021, Chap. 2

Arctic sea ice thickness changes

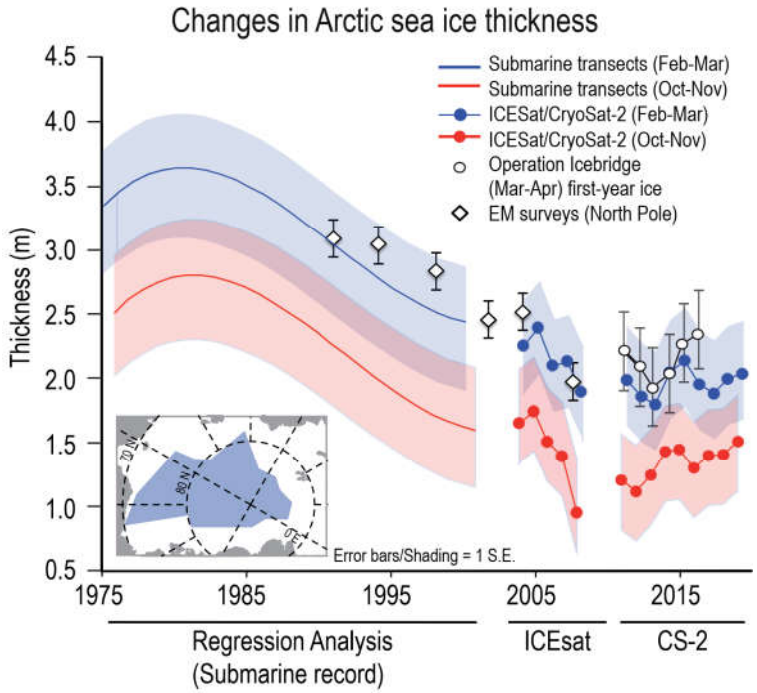

Figure 2.21 | Arctic sea ice thickness changes (means) for autumn (red/dotted red) and winter (blue/dotted blue). Shadings (blue and red) show 1 standard error (S.E.) ranges from the regression analysis of submarine ice thickness and expected uncertainties in satellite ice thickness estimates. Data release area of submarine data ice thickness data is shown in inset. Satellite ice thickness estimates are for the Arctic south of 88°N. Thickness estimates from more localized airborne/ground electromagnetic surveys near the North Pole (diamonds) and from Operation IceBridge (circles) are shown within the context of the larger scale changes in the submarine and satellite records. Further details on data sources and processing are available in the chapter data table (Table 2.SM.1).

IPCC 2021, Chap. 2

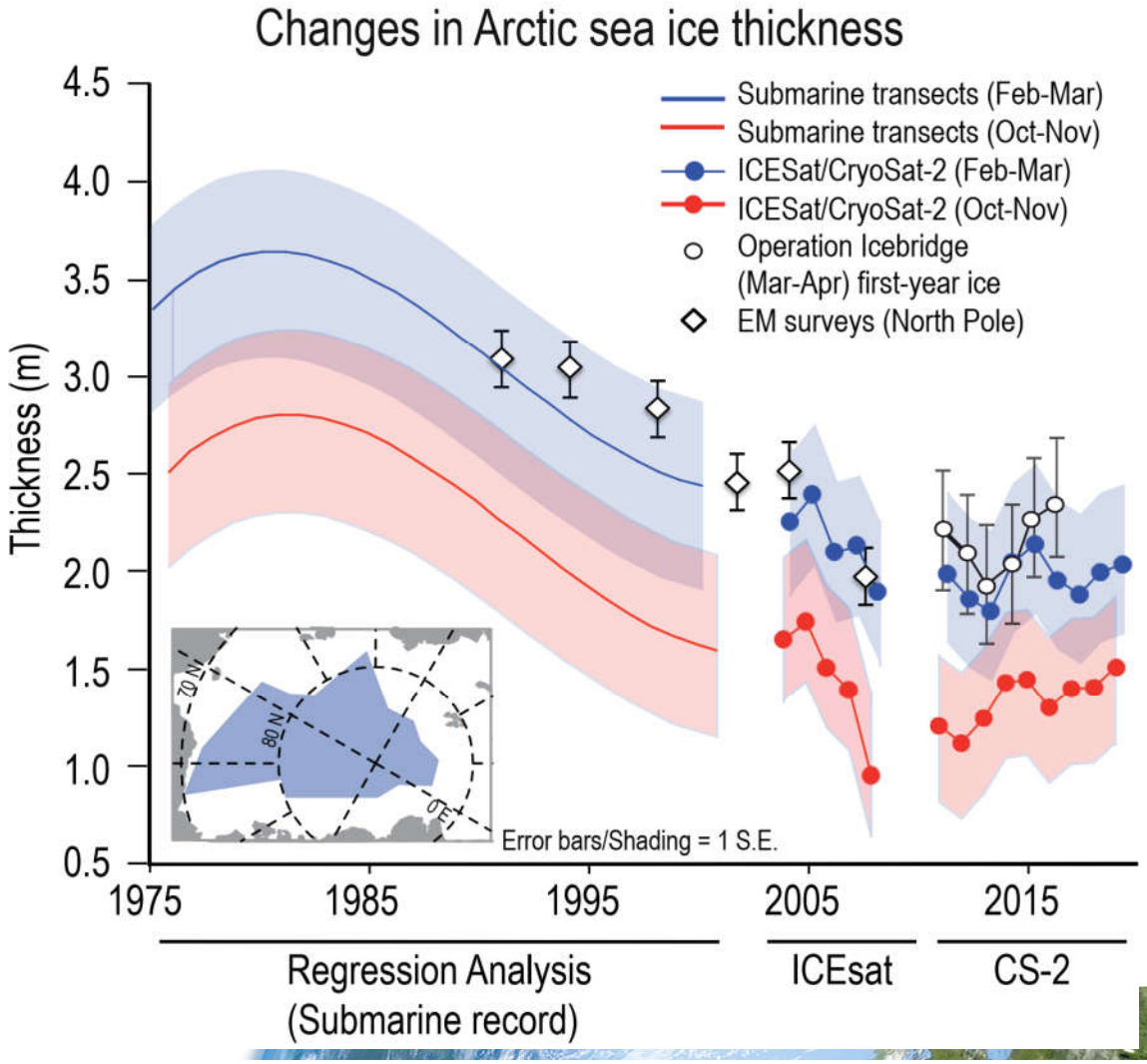

IPCC 2021, Chap. 2

Statements in the Executive Summary

Changes in Key Indicators of Global Climate Change (7)

Changes across the terrestrial cryosphere are widespread, with several indicators now in states unprecedented in centuries to millennia (*high con*fidence). Reductions in spring snow cover extent have occurred across the Northern Hemisphere since at least 1978 (*very high confidence*). With few exceptions, glaciers have retreated since the second half of the 19th century and continued to retreat with increased rates since the 1990s (*very high confidence*); this behaviour is unprecedented in at least the last 2000 years (*medium confidence*). Greenland Ice Sheet mass loss has increased substantially since 2000 (*high confidence*). The Greenland Ice Sheet was smaller than at present during the Last Interglacial period (*high confidence*) and the mid-Holocene (*high confidence*). The Antarctic Ice Sheet (AIS) lost mass between 1992 and 2020 (*very high confidence*), with an increasing rate of mass loss over this period (*medium confidence*). Although permafrost persists in areas of the Northern Hemisphere where it was absent prior to 3000 years ago, increases in temperatures in the upper 30 m over the past three to four decades have been widespread (*high confidence*). {2.3.2}

IPCC 2021, Chap. 2

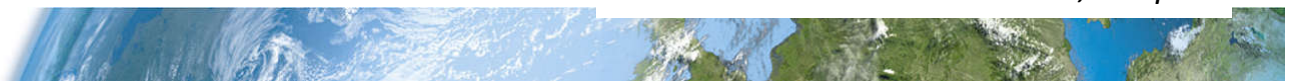

April snow cover extent for the Northern Hemisphere (1922–2018)

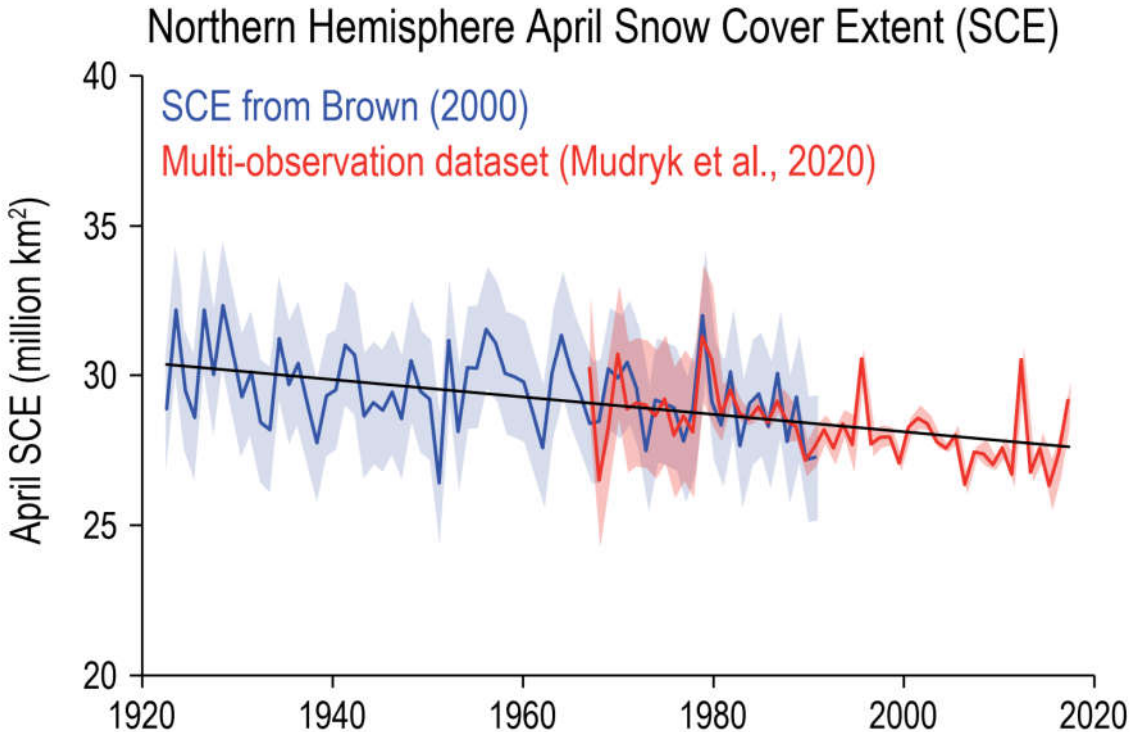

IPCC 2021, Chap. 2

Figure 2.22 | April snow cover extent (SCE) for the Northern Hemisphere (1922–2018). Shading shows *very likely* range. The trend over the entire 1922–2018 period (black line) is –0.29 (± 0.07) million km² per decade. Further details on data sources and processing are available in the chapter data table (Table 2.SM.1).

Glacier advance and annual mass change

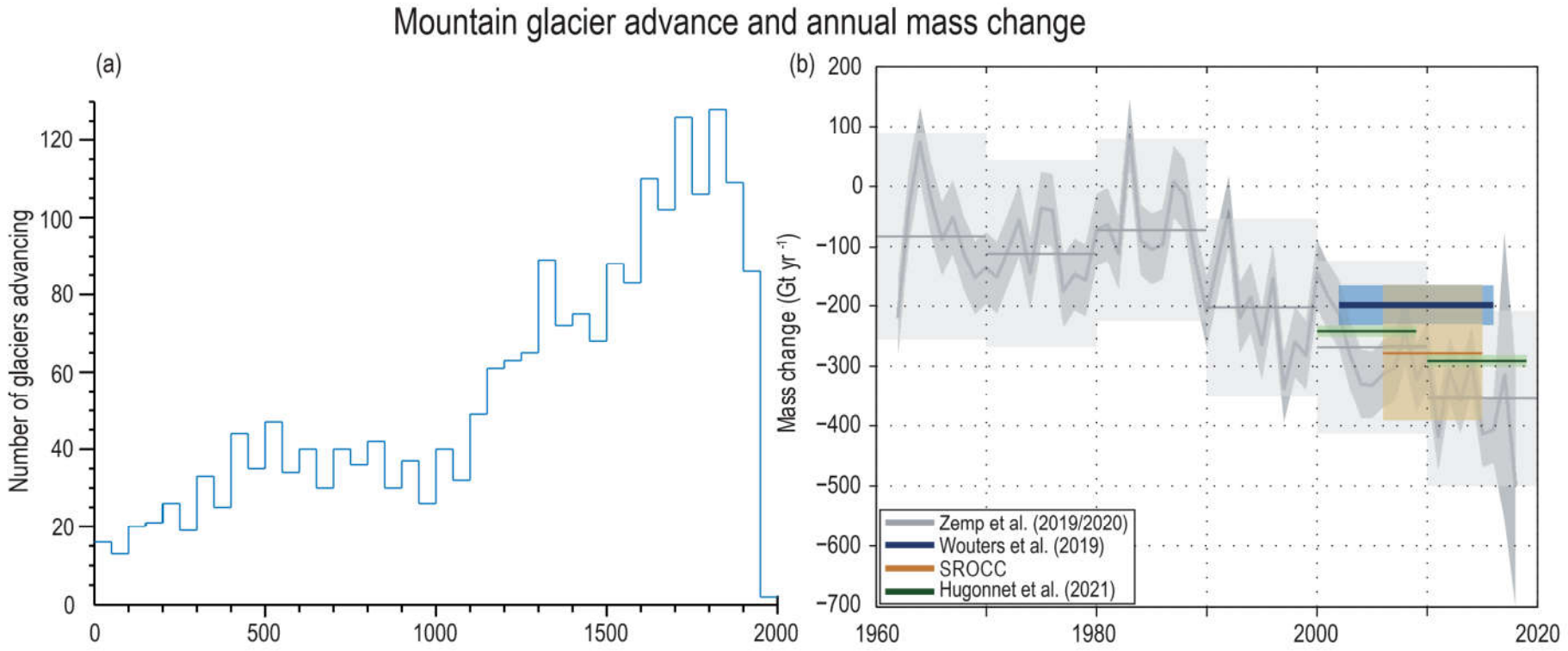

Figure 2.23 | Mountain glacier advance and annual mass change. (a) Number of a finite selection of surveyed glaciers that advanced during the past 2000 years. **(b)** Annual and decadal global glacier mass change (Gt yr^{-1}) from 1961 until 2018. In addition, mass change mean estimates are shown. Ranges show the 90% confidence interval. Further details on data sources and processing are available in the chapter data table (Table 2.SM.1).

IPCC 2021, Chap. 2

Cumulative Antarctic Ice Sheet and Greenland Ice Sheet mass changes

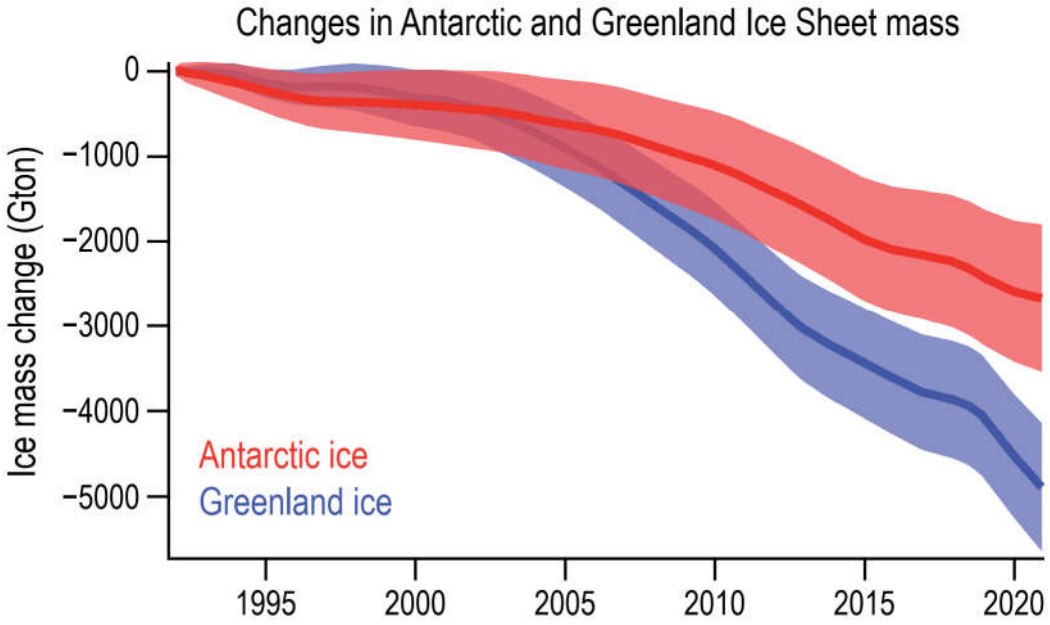

Figure 2.24 | Cumulative Antarctic Ice Sheet (AIS) and Greenland Ice Sheet (GrIS) mass changes. Values shown are in gigatons and come from satellite-based measurements (IMBIE Consortium, 2018, 2020) for the period 1992–2020. The estimated uncertainties, *very likely* range, for the respective cumulative changes are shaded. Further details on data sources and processing are available in the chapter data table (Table 2.SM.1).

IPCC 2021, Chap. 2

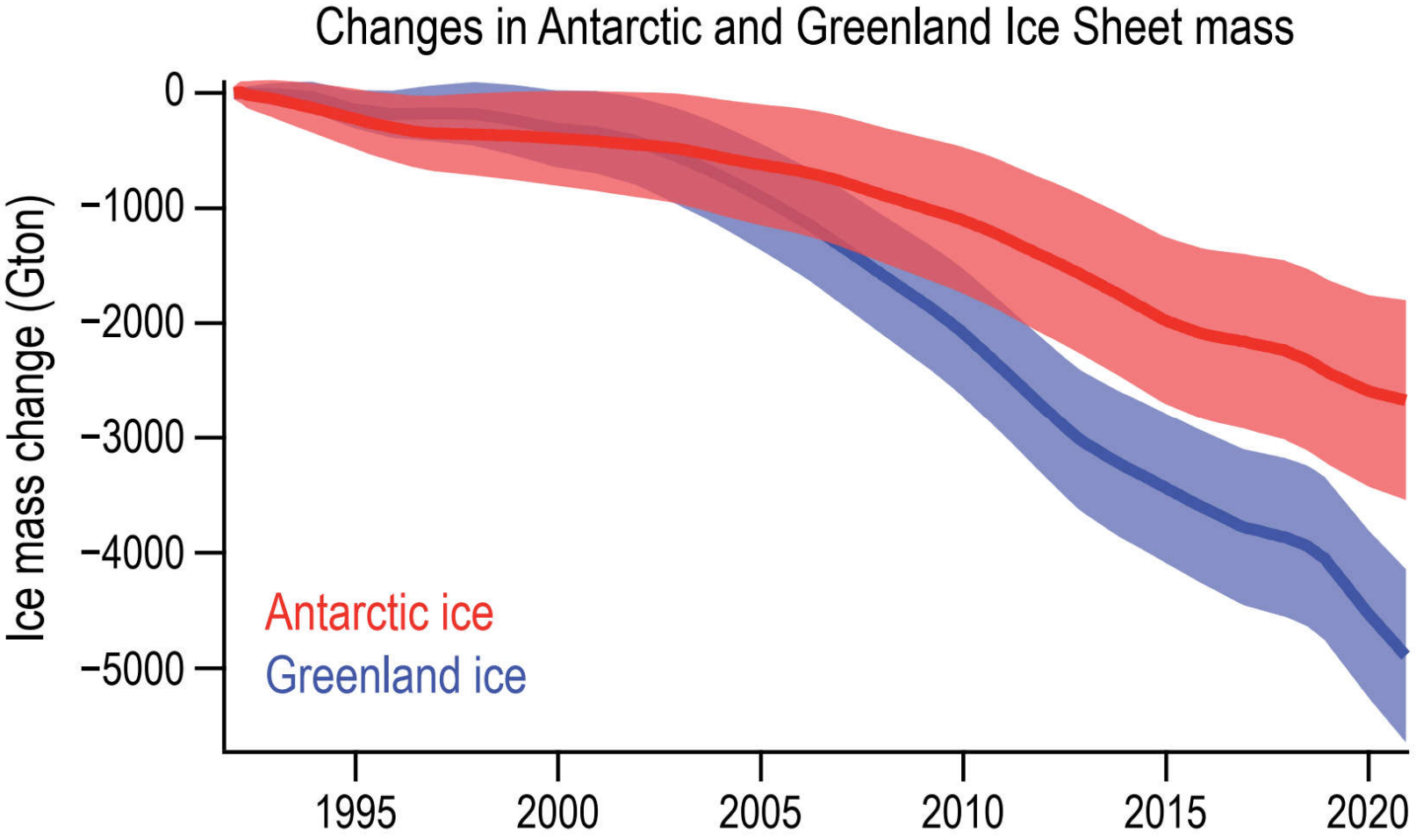

IPCC 2021, Chap. 2

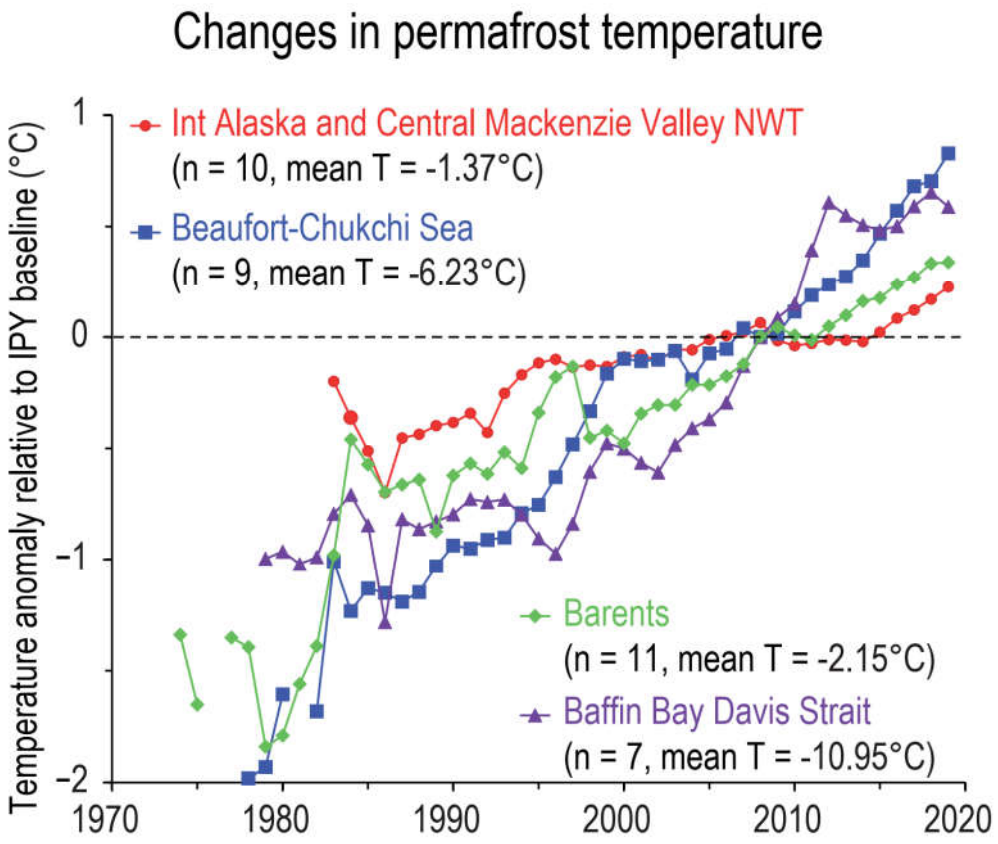

Figure 2.25 | Changes in permafrost temperature. Average departures of permafrost temperature (measured in the upper 20–30 m) from a baseline established during International Polar Year (2007–2009) for Arctic regions. Further details on data sources and processing are available in the chapter data table (Table 2.SM.1).

Statements in the Executive Summary

Changes in Key Indicators of Global Climate Change (8)

Global mean sea level (GMSL) is rising, and the rate of GMSL rise since the 20th century is faster than over any preceding century in at least the last three millennia (*high confidence*). Since 1901, GMSL has risen by 0.20 [0.15–0.25] m, and the rate of rise is accelerating. Further back in time, there is *medium confidence* that GMSL was within –3.5 to 0.5 m (*very likely*) of present during the mid-Holocene (6000 years ago), 5 to 10 m (*likely*) higher during the Last Interglacial (125,000 years ago), and 5 to 25 m (*very likely*) higher during the mid-Pliocene Warm Period (MPWP) (3.3 million years ago). {2.3.3.3}

IPCC 2021, Chap. 2

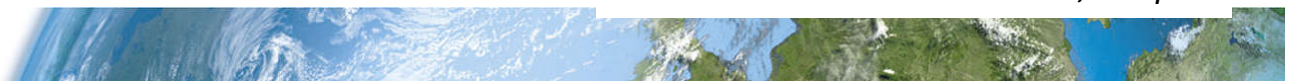

Changes in global mean sea level

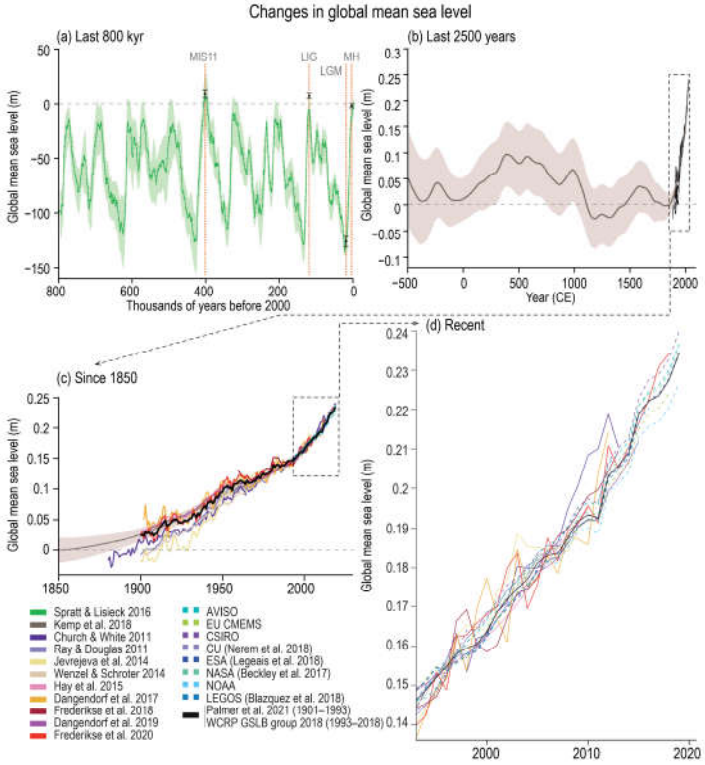

Figure 2.28 | Changes in global mean sea level. (a) Reconstruction of sea-level from ice core oxygen isotope analysis for the last 800 kyr. For target paleo periods (CCB2.1) and MIS11 the estimates based upon a broader range of sources are given as box whiskers. Note the much broader axis range (200 m) than for later panels (tenths of metres). **(b)** Reconstructions for the last 2500 years based upon a range of proxy sources with direct instrumental records superposed since the late 19th century. **(c)** Tide-gauge and, more latterly, altimeter-based estimates since 1850. The consensus estimate used in various calculations in Chapters 7 and 9 is shown in black. **(d)** The most recent period of record from tide-gauge and altimeter-based records. Further details on data sources and processing are available in the chapter data table (Table 2.SM.1).

IPCC 2021, Chap. 2

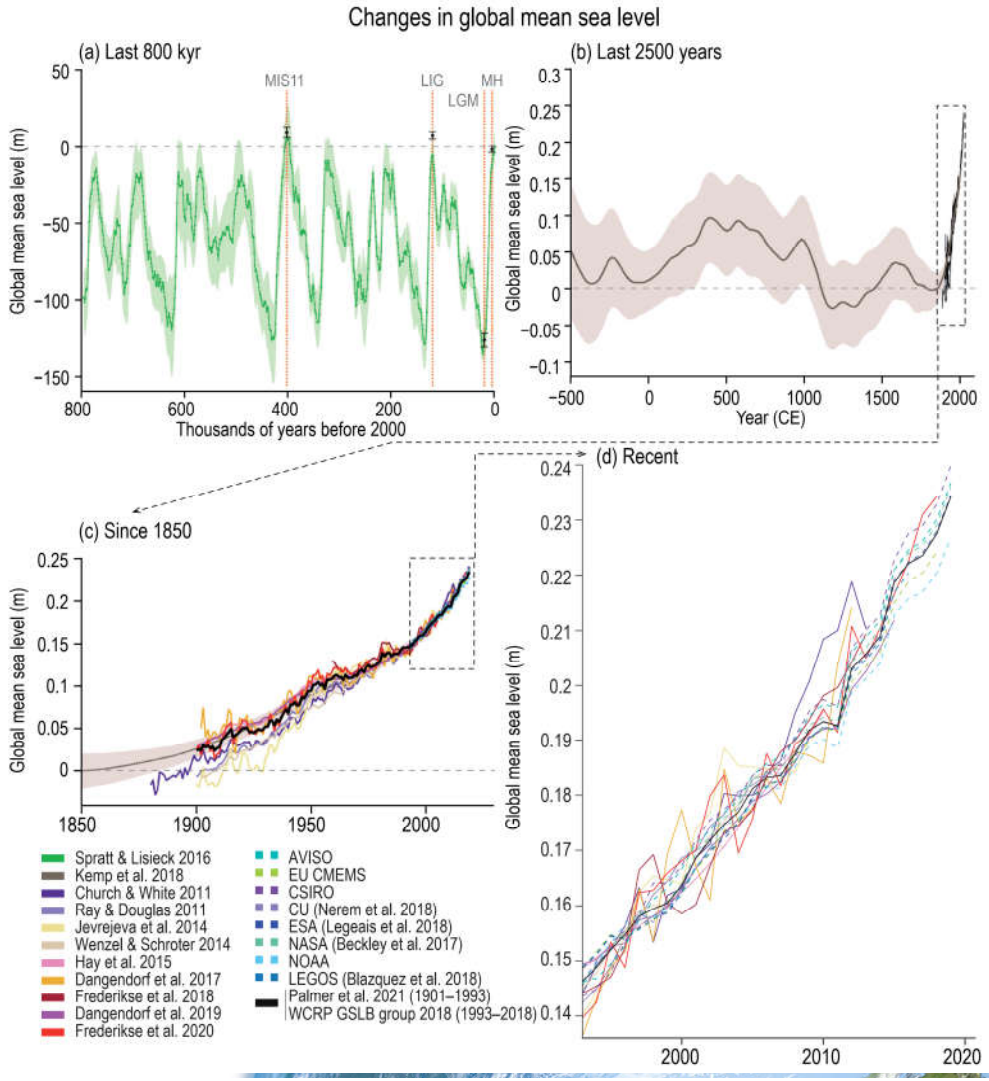

IPCC 2021, Chap. 2

Statements in the Executive Summary

Changes in Key Indicators of Global Climate Change (9)

Recent ocean changes are widespread, and key ocean indicators are in states unprecedented for centuries to millennia (*high confidence*). Since 1971, it is *virtually certain* that global ocean heat content has increased for the upper (0–700 m) layer, *very likely* for the intermediate (700–2000 m) layer and *likely* below 2000 m, and is currently increasing faster than at any point since at least the last deglacial transition (18-11 thousand years ago) (*medium confidence*). It is *virtually certain* that large-scale near-surface salinity contrasts have intensified since at least 1950. The Atlantic Meridional Overturning Circulation (AMOC) was relatively stable during the past 8000 years (*medium confidence*) but declined during the 20th century (*low confidence*). Ocean pH has declined globally at the surface over the past four decades (*virtually certain*) and in all ocean basins in the ocean interior (*high confidence*) over the past 2–3 decades. Deoxygenation has occurred in most open ocean regions during the mid 20th to early 21st centuries (*high confidence*), with decadal variability (*medium confidence*). Oxygen minimum zones are expanding at many locations (*high confidence*). {2.3.3}

IPCC 2021, Chap. 2

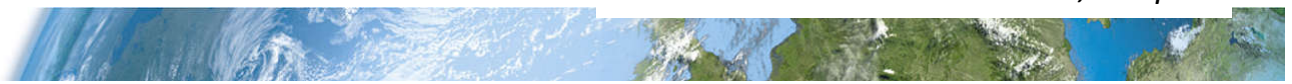

Changes in ocean heat content

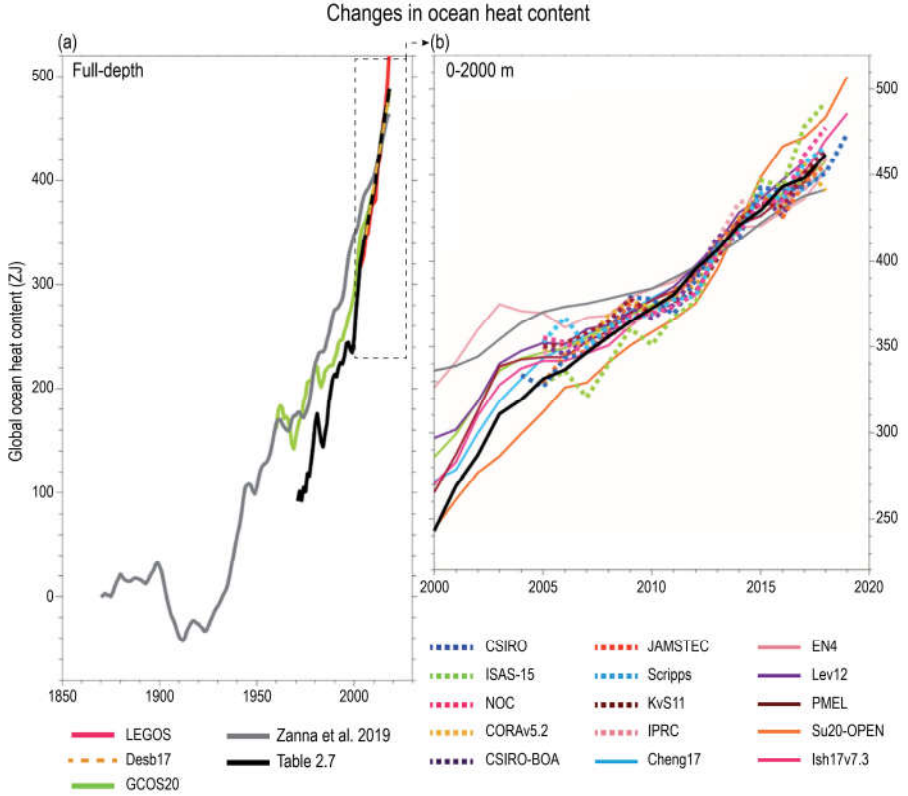

Figure 2.26 | Changes in ocean heat content (OHC). Changes are shown over **(a)** full depth of the ocean from 1871–2019 from a selection of indirect and direct measurement methods. The series from Table 2.7 is shown in solid black in both (a) and (b) (see Table 2.7 caption for details). **(b)** as (a) but for 0–2000 m depths only and reflecting the broad range of available estimates over this period. For further details see chapter data table (Table 2.SM.1).

IPCC 2021, Chap. 2

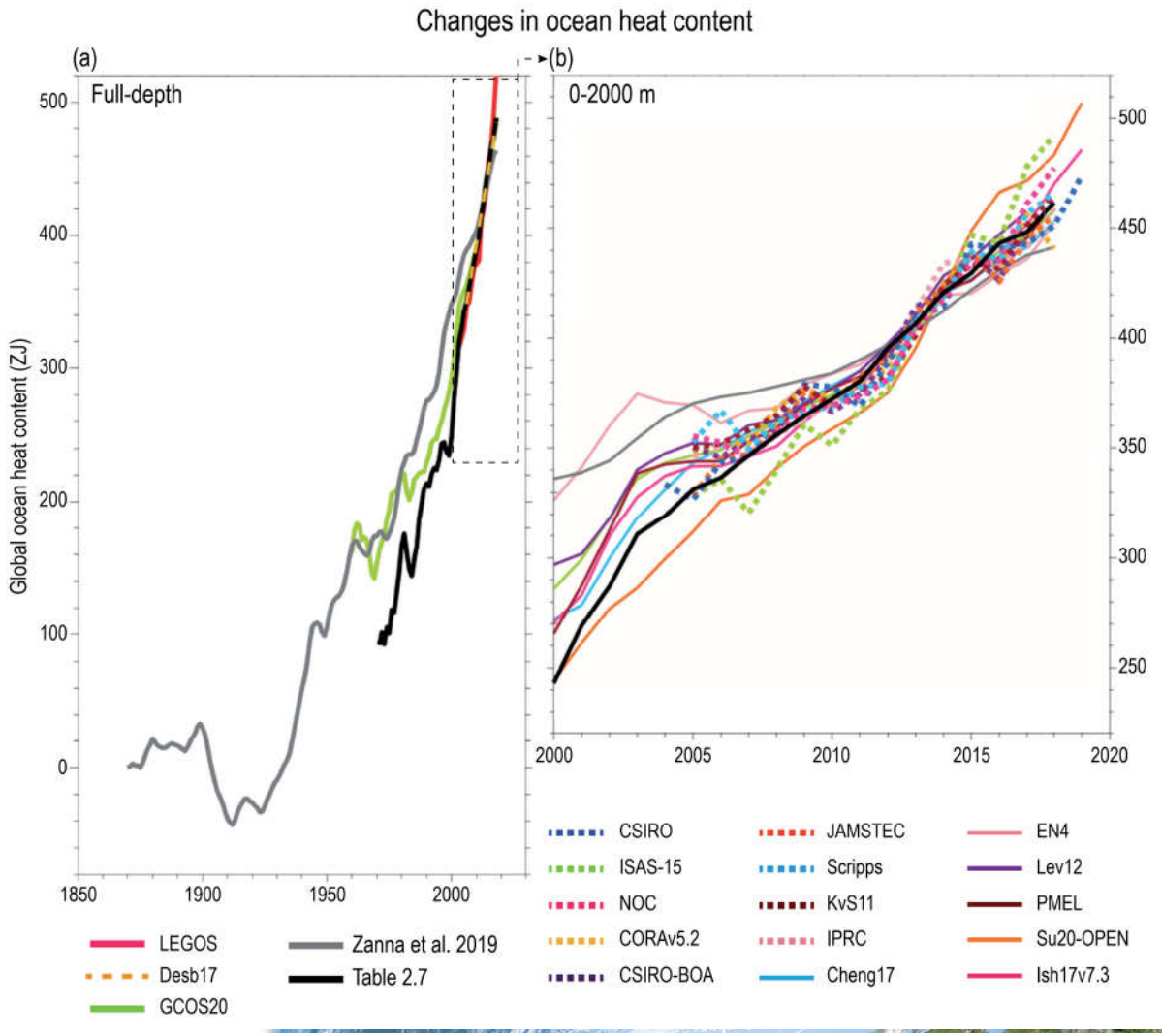

IPCC 2021, Chap. 2

Changes in ocean salinity

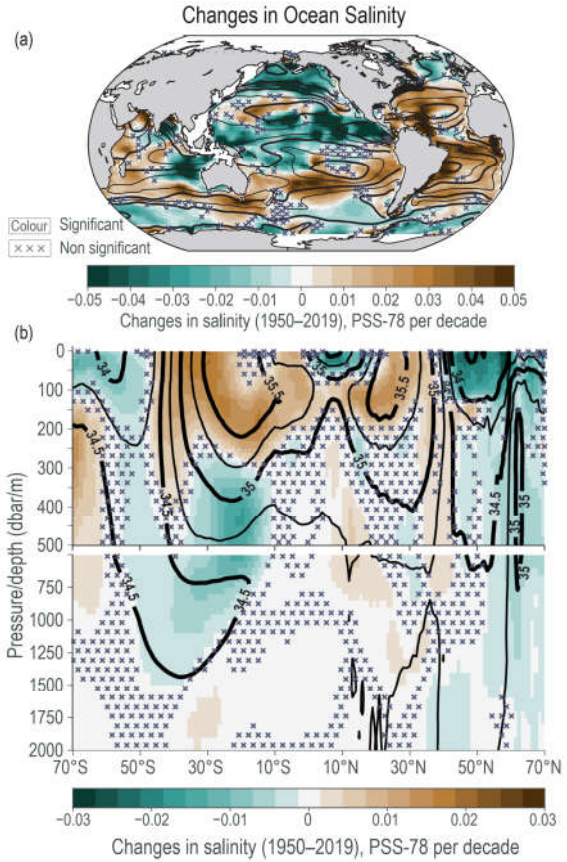

Figure 2.27 | Changes in ocean salinity. Estimates of salinity trends using a total least absolute differences fitting method for **(a)** global near-surface salinity (SSS) changes and **(b)** global zonal mean subsurface salinity changes. Black contours show the associated climatological mean salinity (either near-surface (a) or subsurface (b)) for the analysis period (1950–2019). Both panels represent changes in Practical Salinity Scale 1978 [PSS-78], per decade. In both panels green denotes freshening regions and orange/brown denotes regions with enhanced salinities ('×' marks denote non-significant changes). Further details on data sources and processing are available in the chapter data table (Table 2.SM.1).

IPCC 2021, Chap. 2

Changes in ocean salinity

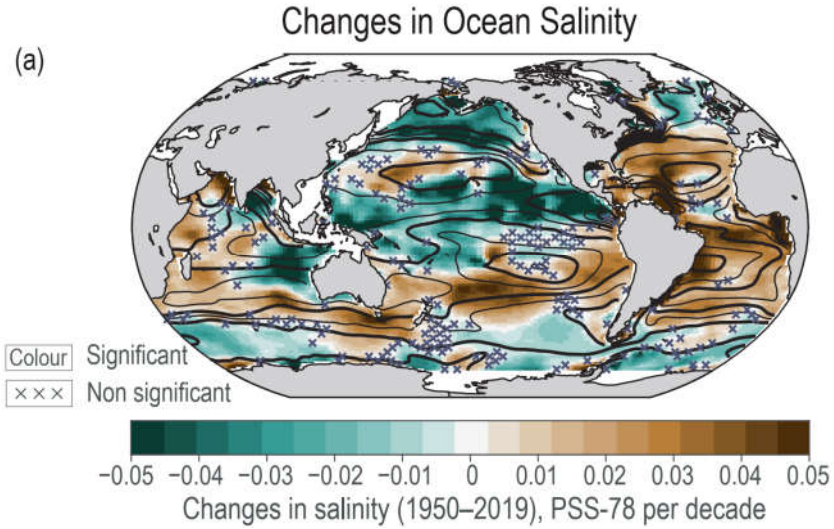

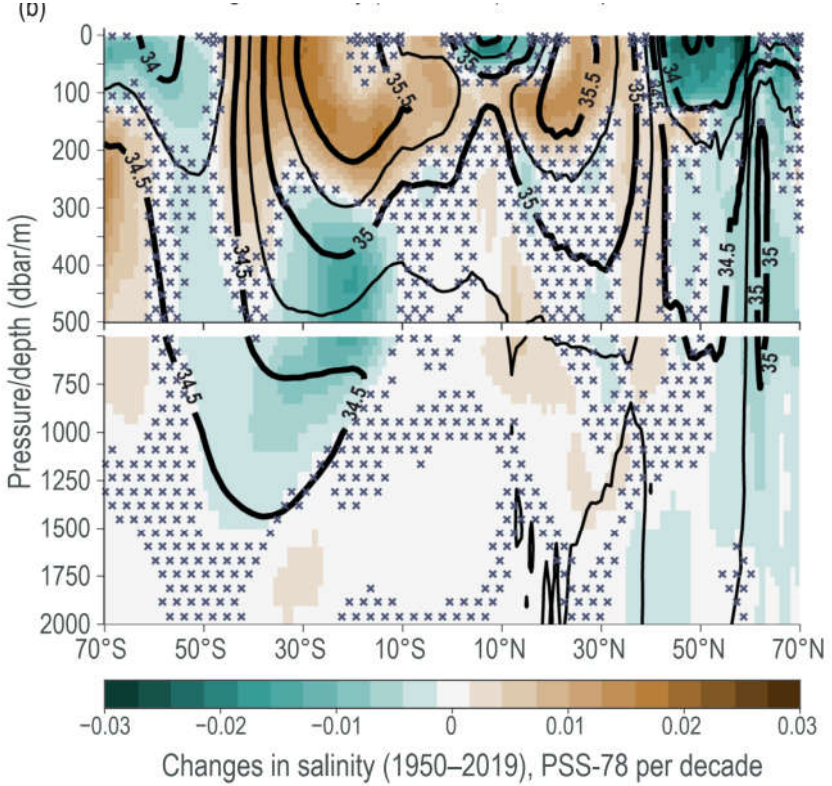

IPCC 2021, Chap. 2

Low latitude surface ocean pH over the last 65 million years

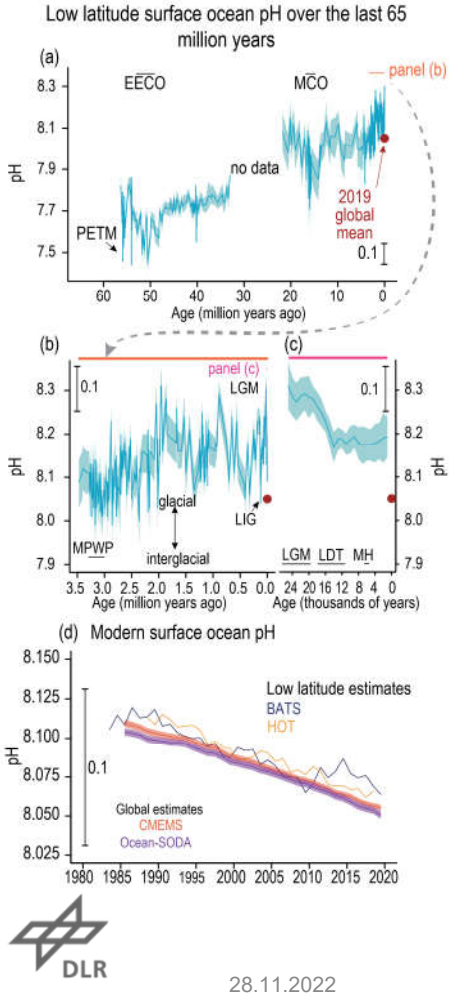

Figure 2.29 | Low-latitude surface ocean pH over the last 65 million years (65 Myr). (a) Low-latitude (30°N–30°S) surface ocean pH over the last 65 Myr, reconstructed using boron isotopes in foraminifera. **(b)** as (a) but for the last 3.5 Myr. Double headed arrow shows the approximate magnitude of glacial-interglacial pH changes. **(c)** Multisite composite of surface pH. In (a, b, c) uncertainty is shown at 95% confidence as a shaded band. Relevant paleoclimate reference periods (CCB2.1) have been labelled. Period windows for succeeding panels are shown as horizontal black lines in (a) and (b). **(d)** Estimated low-latitude surface pH from direct observations (BATS, HOT) and global mean pH (65°S–65°N) from two indirect estimates (CMEMS, OCEAN-SODA). Further details on data sources and processing are available in the chapter data table (Table 2.SM.1).

IPCC 2021, Chap. 2

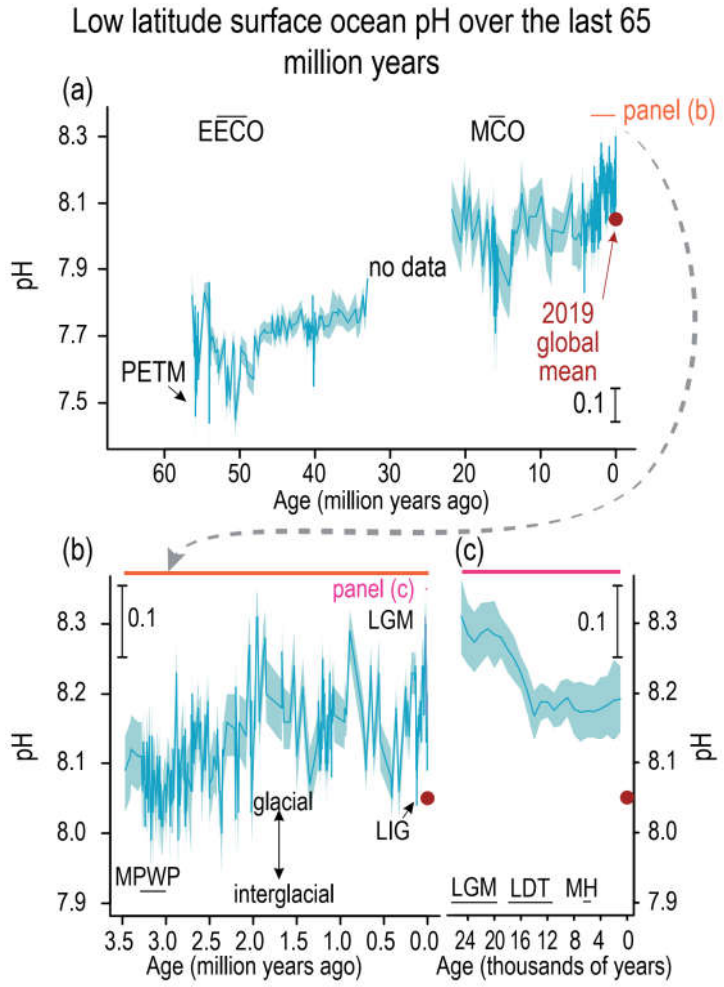

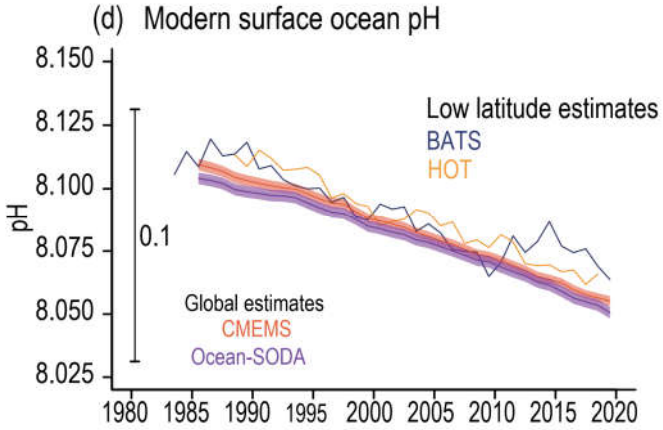

IPCC 2021, Chap. 2

Statements in the Executive Summary

Changes in Key Indicators of Global Climate Change (10)

Changes in the marine biosphere are consistent with large-scale warming and changes in ocean geochemistry (*high confidence*). The ranges of many marine organisms are shifting towards the poles and towards greater depths (*high confidence*), but a minority of organisms are shifting in the opposite directions. This mismatch in responses across species means that the species composition of ecosystems is changing (*medium confidence*). At multiple locations, various phenological metrics for marine organisms have changed in the last 50 years, with the nature of the changes varying with location and with species (*high confidence*). In the last two decades, the concentration of phytoplankton at the base of the marine food web, as indexed by chlorophyll concentration, has shown weak and variable trends in low and mid-latitudes and an increase in high latitudes (*medium confidence*). Global marine primary production decreased slightly from 1998–2018, with increasing production in the Arctic (*medium confidence*). {2.3.4.2}

IPCC 2021, Chap. 2

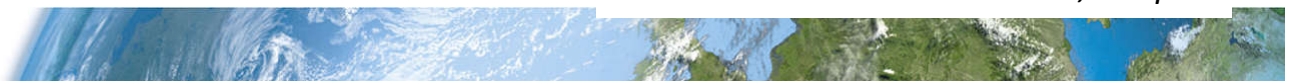

Changes in the amplitude of the seasonal cycle of CO_2

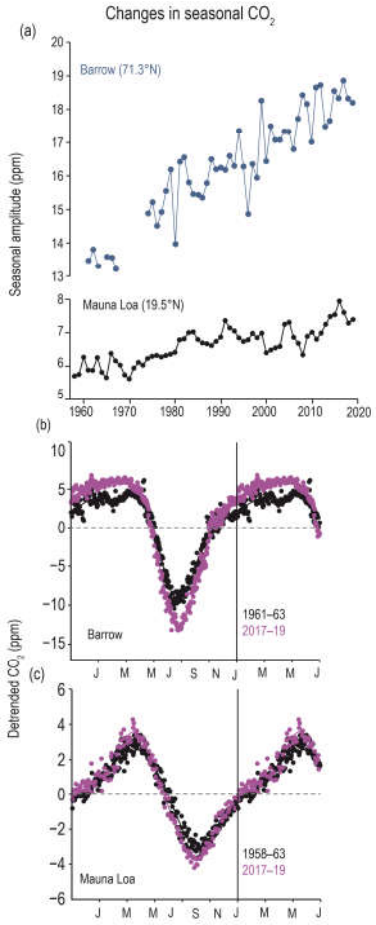

Figure 2.30 | Changes in the amplitude of the seasonal cycle of CO_2. **(a)** Observed peak-to-trough seasonal amplitude given by the day of year of downward zero crossing, of CO_2 concentration at Barrow (71°N, blue) and Mauna Loa (20°N, black). Seasonal CO_2 cycles observed at **(b)** Barrow and **(c)** Mauna Loa for the 1961–1963 or 1958–1963 and 2017–2019 time periods. The first six months of the year are repeated. Reprinted with permission from AAAS. Further details on data sources and processing are available in the chapter data table (Table 2.SM.1).

IPCC 2021, Chap. 2

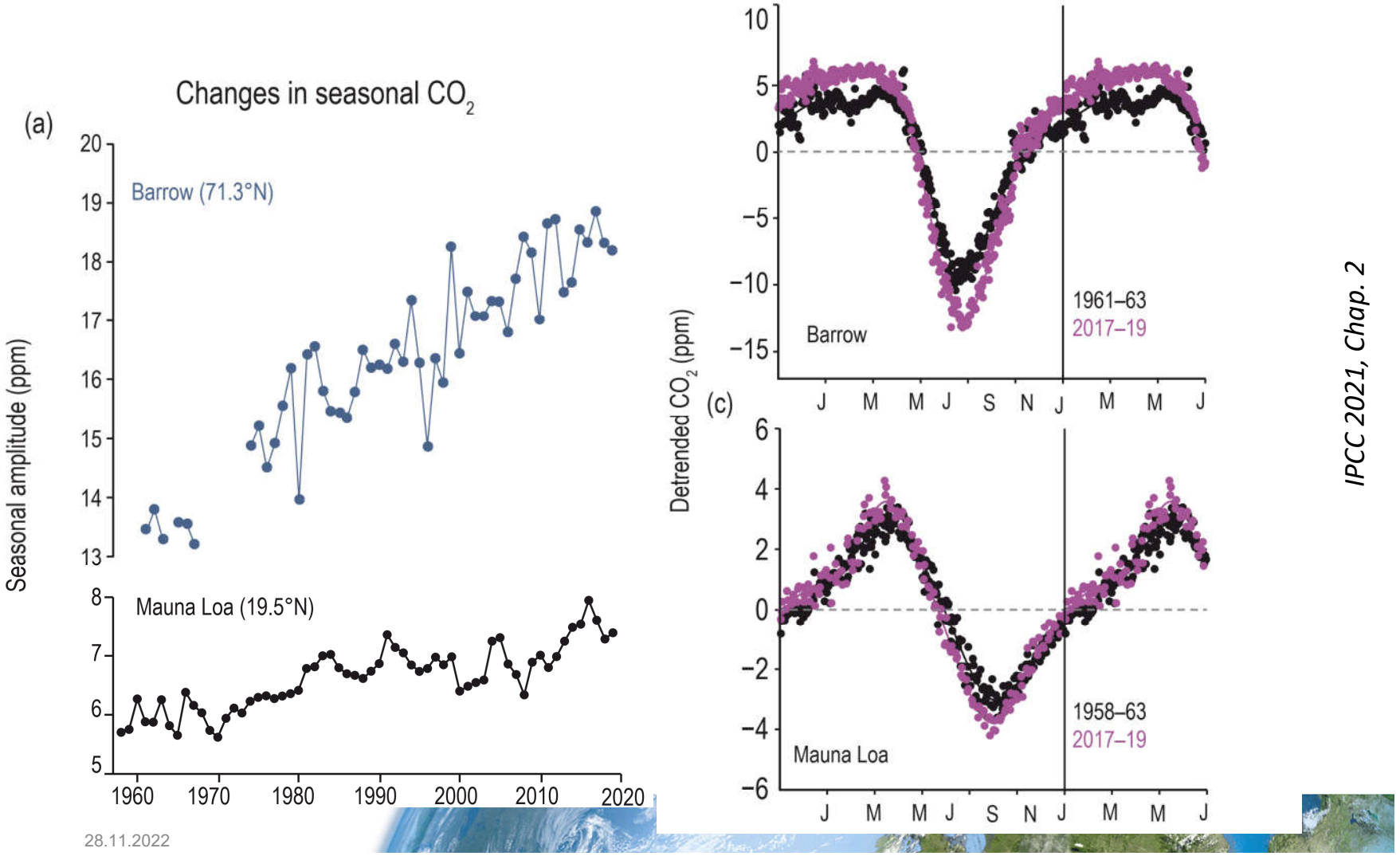

IPCC 2021, Chap. 2

Phytoplankton dynamics in the ocean

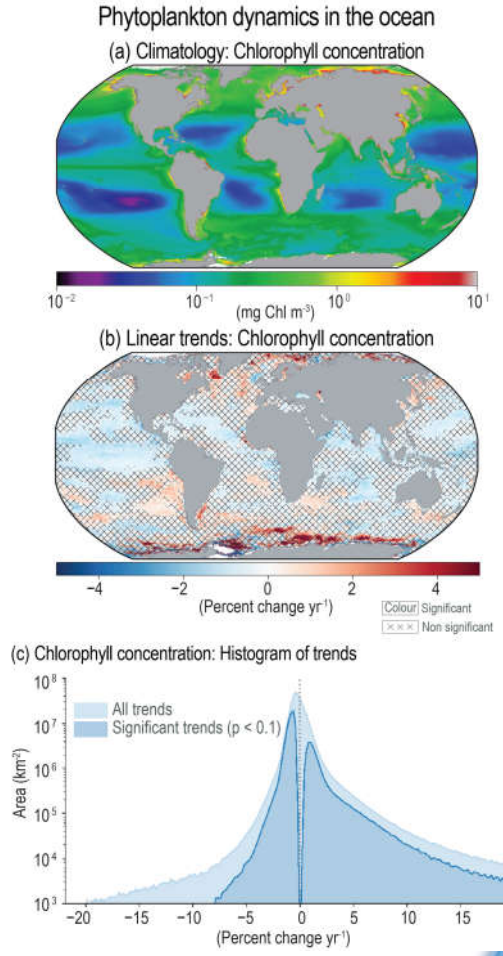

Figure 2.31 | Phytoplankton dynamics in the ocean. (a) Climatology of chlorophyll-a concentration derived from ocean-colour data (1998–2018); **(b)** Linear trends in chlorophyll concentration. Trends are calculated using OLS regression with significance assessed following AR(1) adjustment after Santer et al. (2008) ('×' marks denote non-significant changes). **(c)** Histogram of linear trends in chlorophyll concentration, after area weighting and with per-pixel uncertainty estimates based on comparison with in situ data. Further details on data sources and processing are available in the chapter data table (Table 2.SM.1).

IPCC 2021, Chap. 2

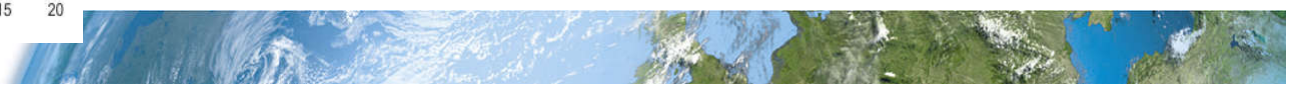

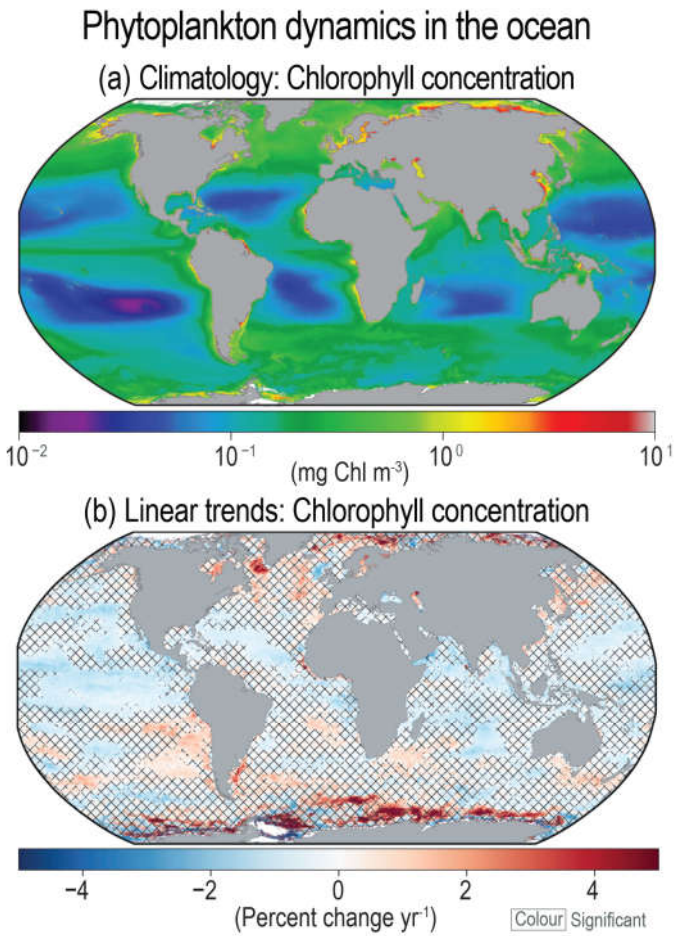

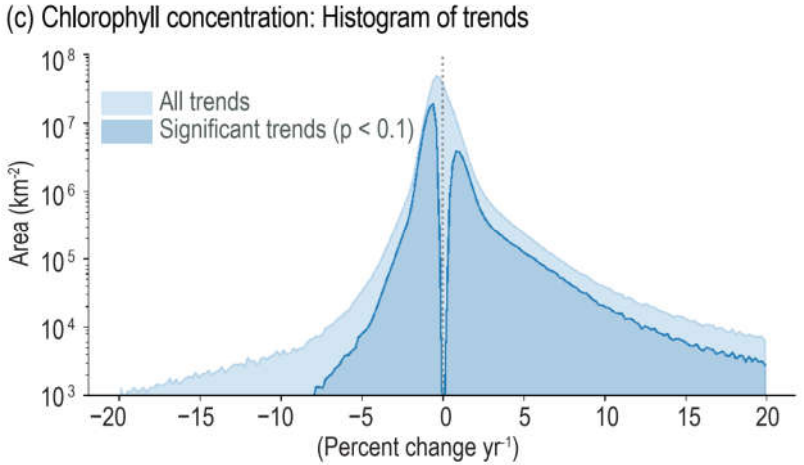

IPCC 2021, Chap. 2

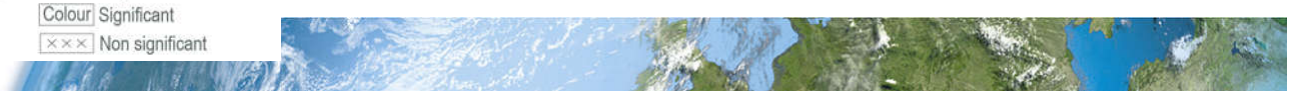

Statements in the Executive Summary

Changes in Key Indicators of Global Climate Change (11)

Changes in key global aspects of the terrestrial biosphere are consistent with large-scale warming (high confidence). Over the last century, there have been poleward and upslope shifts in the distributions of many land species (*very high confidence*) as well as increases in species turnover within many ecosystems (*high confidence*). Over the past half century, climate zones have shifted poleward, accompanied by an increase in the length of the growing season in the Northern Hemisphere extratropics and an increase in the amplitude of the seasonal cycle of atmospheric CO_2 above 45°N (*high confidence*). Since the early 1980s, there has been a global-scale increase in the greenness of the terrestrial surface (*high confidence*). {2.3.4.1, 2.3.4.3}

IPCC 2021, Chap. 2

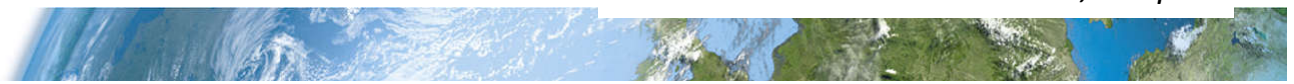

Phenological indicators of changes in growing season

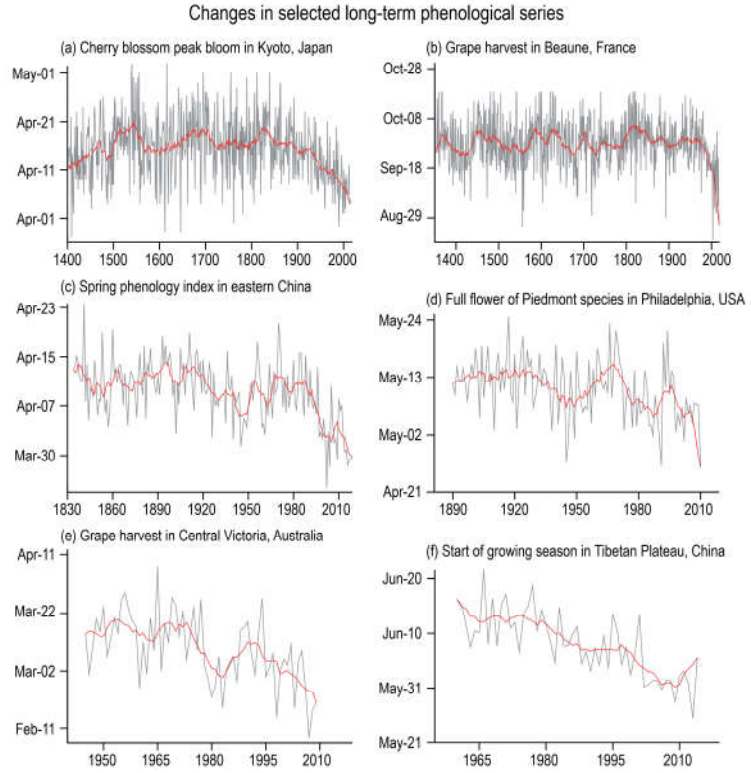

Figure 2.32 | Phenological indicators of changes in growing season. (a) Cherry blossom peak bloom in Kyoto, Japan; **(b)** grape harvest in Beaune, France; **(c)** spring phenology index in eastern China; **(d)** full flower of Piedmont species in Philadelphia, USA; **(e)** grape harvest in Central Victoria, Australia; **(f)** start of growing season in Tibetan Plateau, China. Red lines depict the 25-year moving average (top row) or the nine-year moving average (middle and bottom rows) with the minimum roughness boundary constraint of Mann (2004). Further details on data sources and processing are available in the chapter data table (Table 2.SM.1).

IPCC 2021, Chap. 2

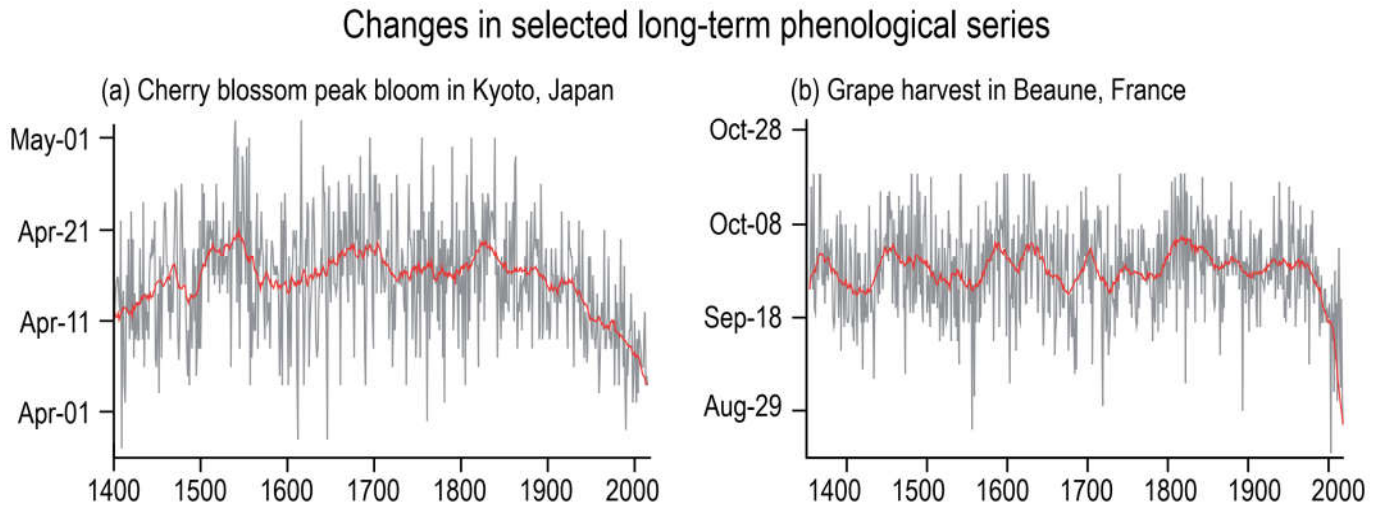

IPCC 2021, Chap. 2

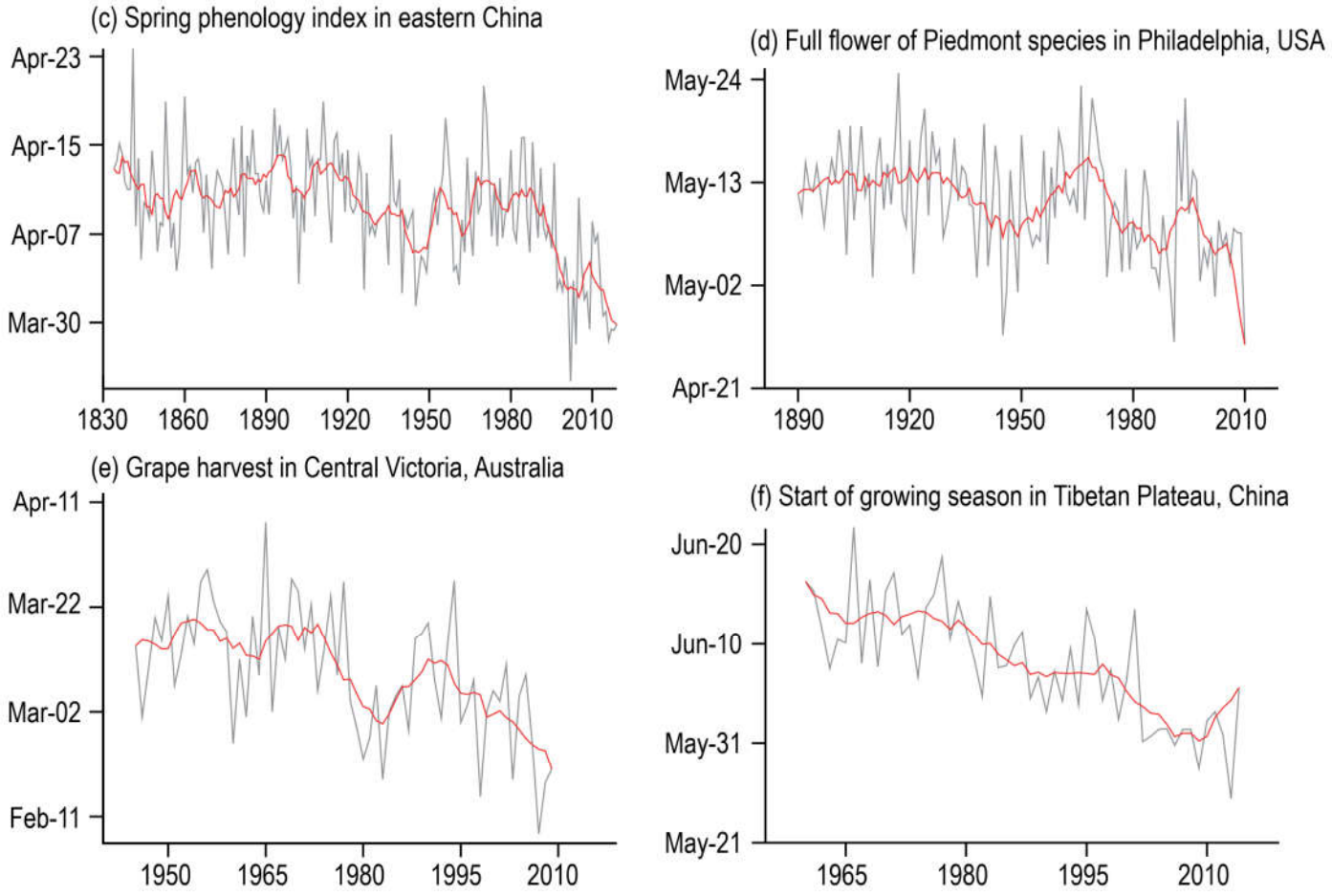

IPCC 2021, Chap. 2

Satellite-based trends in Fraction of Absorbed Photosynthetically Active Radiation (per decade) for 1998–2019

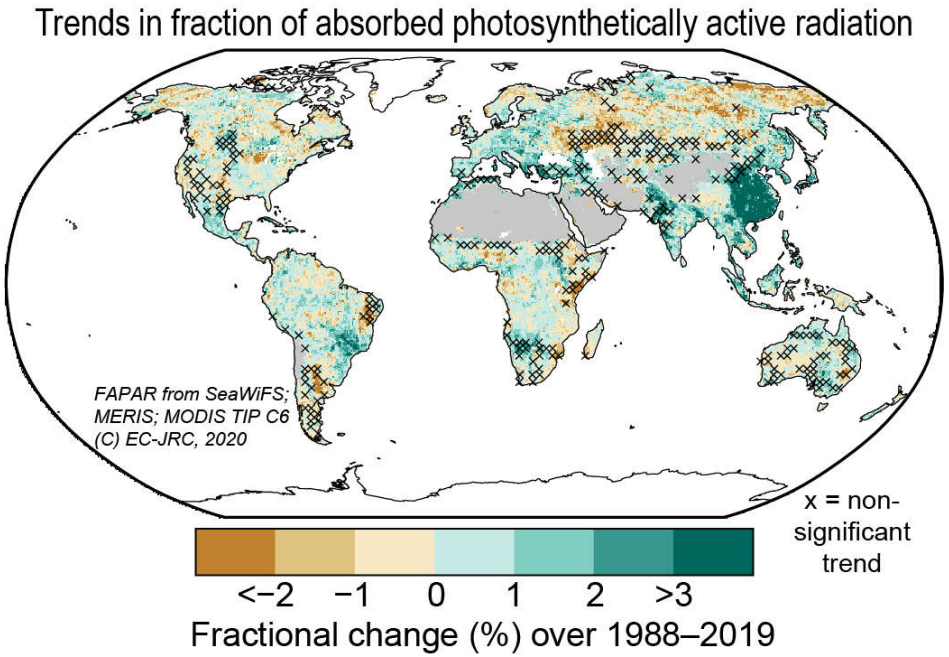

Figure 2.33: Satellite-based trends in Fraction of Absorbed Photosynthetically Active Radiation (per decade) for 1998–2019. Trends are calculated using OLS regression with significance assessed following AR(1) adjustment after Santer et al (2008b) ('x' marks denote non-significant trend). Unvegetated areas such as barren deserts (grey) and ice sheets (white) have no trend in FAPAR. Further details on data sources and processing are available in the chapter data table (Table 2.SM.1).

IPCC 2021, Chap. 2

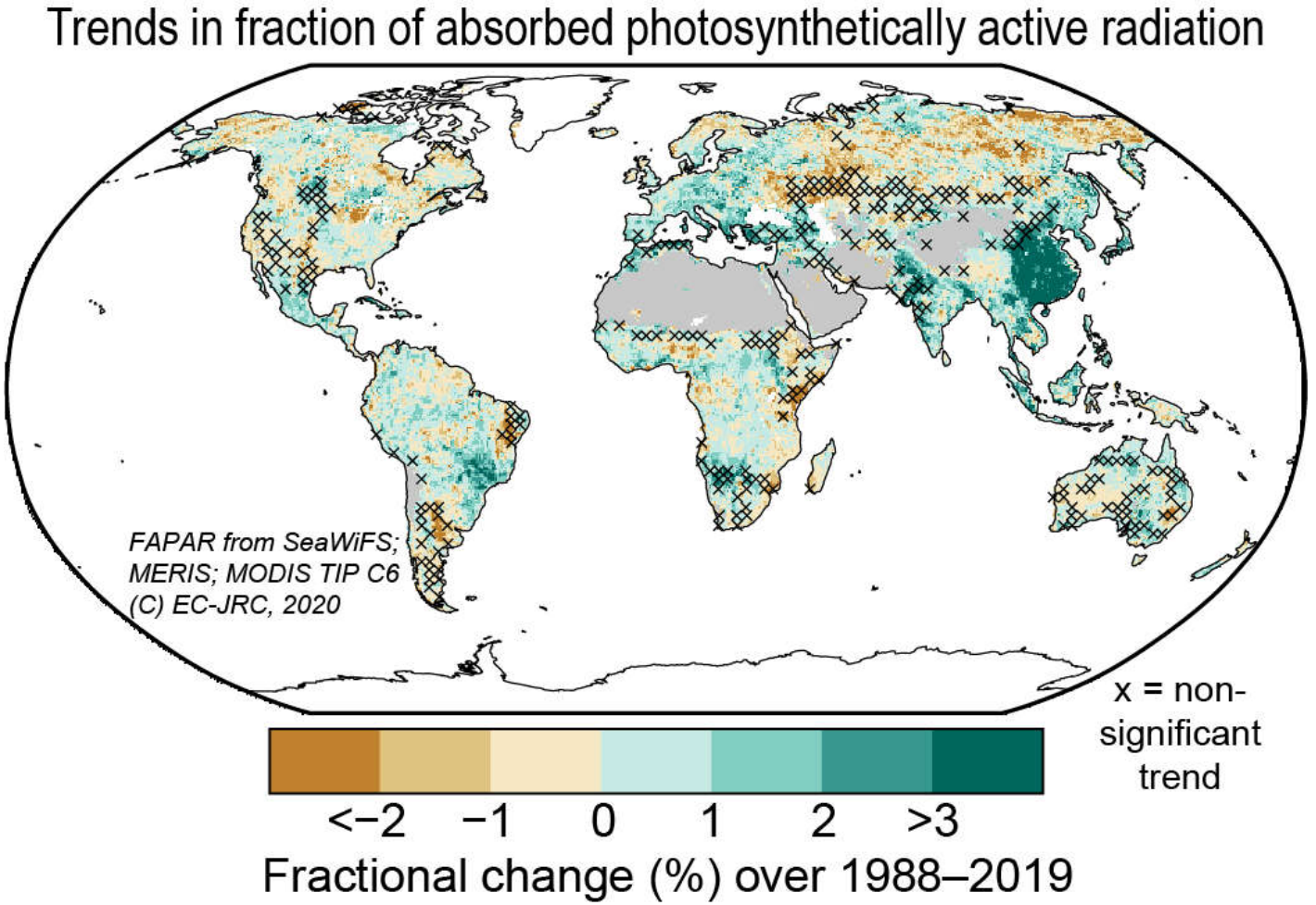

IPCC 2021, Chap. 2

Statements in the Executive Summary

Changes in Key Indicators of Global Climate Change (12)

During the Mid-Pliocene warm period (MPWP, 3.3–3.0 million years ago) slowly changing large-scale indicators reflect a world that was warmer than present, with CO_2 similar to current levels. CO_2 levels during the MPWP were similar to present for a sustained period, within a range of 360–420 ppm (*medium confidence*). Relative to the present, GMST, GMSL and precipitation rate were all higher, the Northern Hemisphere latitudinal temperature gradient was lower, and major terrestrial biomes were shifted northward (*very high confidence*). There is *high confidence* that cryospheric indicators were diminished and *medium confidence* that the Pacific longitudinal temperature gradient weakened and monsoon systems strengthened. {2.3, Cross-Chapter Box 2.4, 9.6.2}

IPCC 2021, Chap. 2

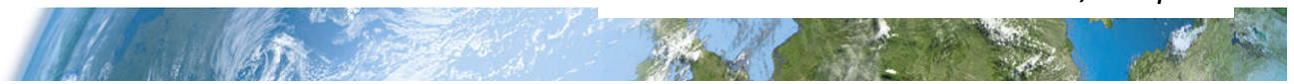

Selected large-scale climate indicators during paleoclimate and recent reference periods of the Cenozoic Era

Selected large-scale climate indicators from the Cenozoic era to the recent past

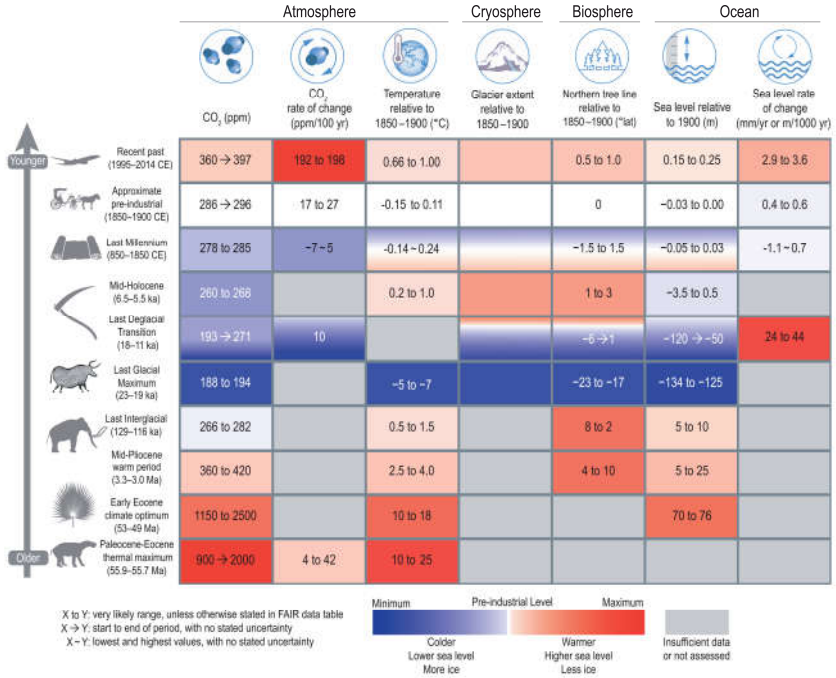

Figure 2.34 | Selected large-scale climate indicators during paleoclimate and recent reference periods of the Cenozoic Era. Values are based upon assessments carried out in this chapter, with *confidence* levels ranging from *low* to *very high*. Refer to Cross-Chapter Box 2.1 for description of paleoclimate reference periods and Section 1.4.1 for recent reference periods. Values are reported as either the *very likely* range (x to y), or best estimates from beginning to end of the reference period with no stated uncertainty (x → y), or lowest and highest values with no stated uncertainty (x ~ y). Temperature is global mean surface temperature. Glacier extent is relative and colour scale is inverted so that more extensive glacier extent is intuitively blue.

IPCC 2021, Chap. 2

Selected large-scale climate indicators from the Cenozoic era to the recent past

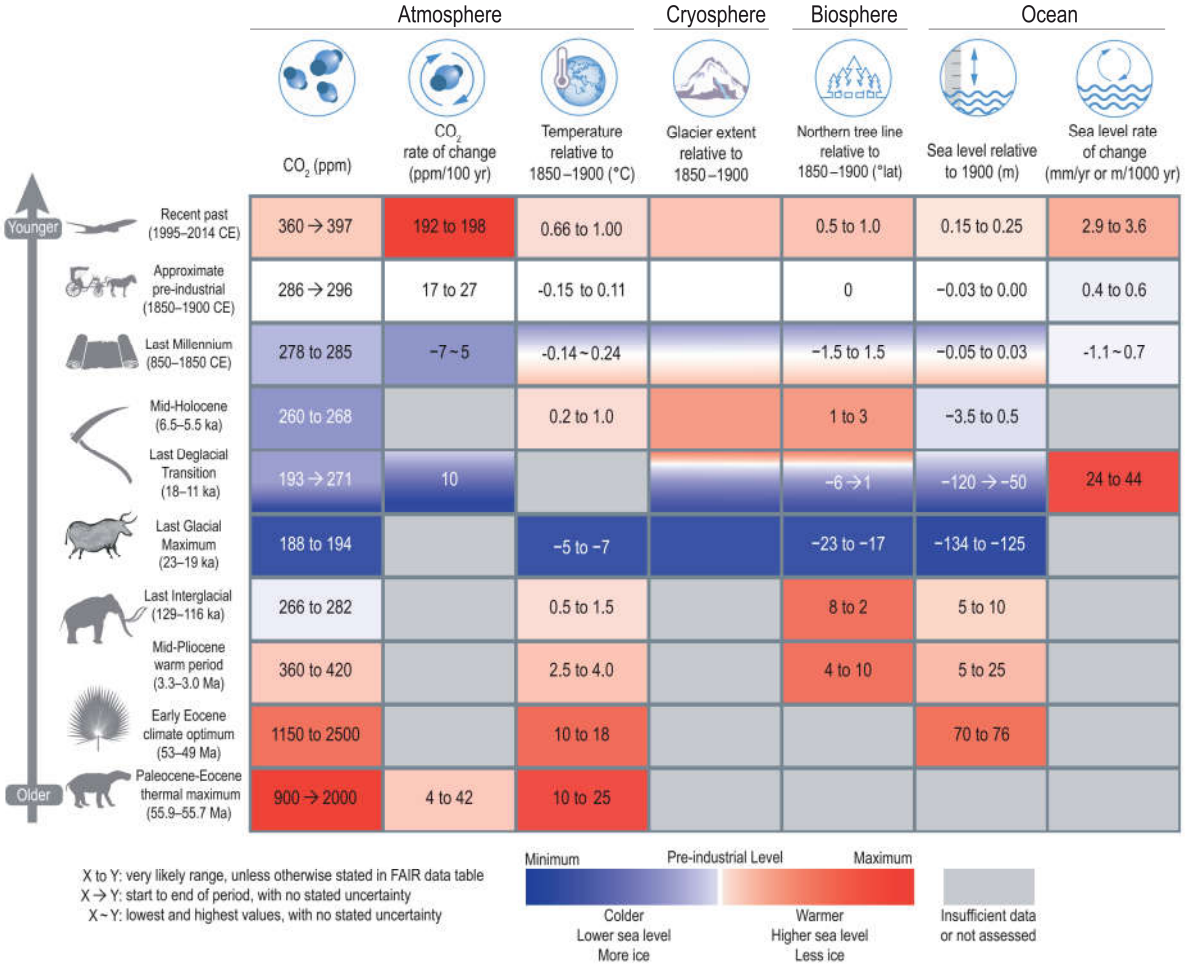

IPCC 2021, Chap. 2

Statements in the Executive Summary

Changes in Key Indicators of Global Climate Change (13)

Inferences from past climate states based on proxy records can be compared with climate projections over coming centuries to place the range of possible futures into a longer-term context. There is *medium confidence* in the following mappings between selected paleo periods and future projections: During the Last Interglacial, GMST is estimated to have been 0.5°C–1.5°C warmer than the 1850–1900 reference for a sustained period, which overlaps the low end of the range of warming projected under SSP1-2.6, including its negative-emissions extension to the end of the 23rd century [1.0–2.2] °C. During the mid-Pliocene Warm Period, the GMST estimate [2.5-4.0] °C is similar to the range projected under SSP2-4.5 for the end of the 23rd century [2.3-4.6] °C. GMST estimates for the Miocene Climatic Optimum [5–10] °C and 20 Early Eocene Climatic Optimum [10–18] °C, about 15 and 50 million years ago, respectively, overlap with the range projected for the end of the 23rd century under SSP5-8.5 [6.6–14.1] °C. {Cross-Chapter Box 2.1, 22 2.3.1, 4.3.1.1, 4.7.1.1}

IPCC 2021, Chap. 2

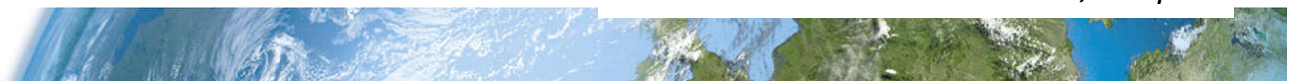

Climate indicators of the mid-Pliocene Warm Period (3.3–3.0 Ma) from models and proxy data

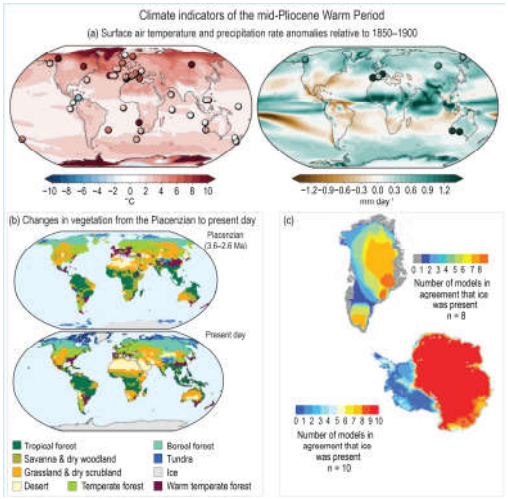

IPCC 2021, Chap. 2

Cross-Chapter Box 2.4, Figure 1 | Climate indicators of the mid-Pliocene Warm Period (MPWP; 3.3–3.0 million years ago, Ma) from models and proxy data. (a) Simulated surface air temperature (left) and precipitation rate anomaly (right) anomaly (relative to 1850–1900) from the Pliocene Model Intercomparison Project Phase 2 multi-model mean, including CMIP6 (n = 4) and non-CMIP6 (n = 12) models. Symbols represent site-level proxy-based estimates of sea-surface temperature for KM5c (n = 32), and terrestrial temperature (n = 8) and precipitation rate for the MPWP (n = 8). **(b)** Distribution of terrestrial biomes was considerably different during the Piacenzian Stage (3.6–2.6 Ma) (upper) compared with present-day (lower). Biome distributions simulated with a model (BIOME4) in which Pliocene biome classifications are based on 208 locations, with model-predicted biomes filling spatial gaps, and the present day, with the model adjusted for CO_2 concentration of 324 parts per million (ppm). **(c)** Ice-sheet extent predicted using modelled climate forcing and showing where multiple models consistently predict the former presence or absence of ice on Greenland (n = 8 total) and Antarctica (n = 10 total). Further details on data sources and processing are available in the chapter data table (Table 2.SM.1).

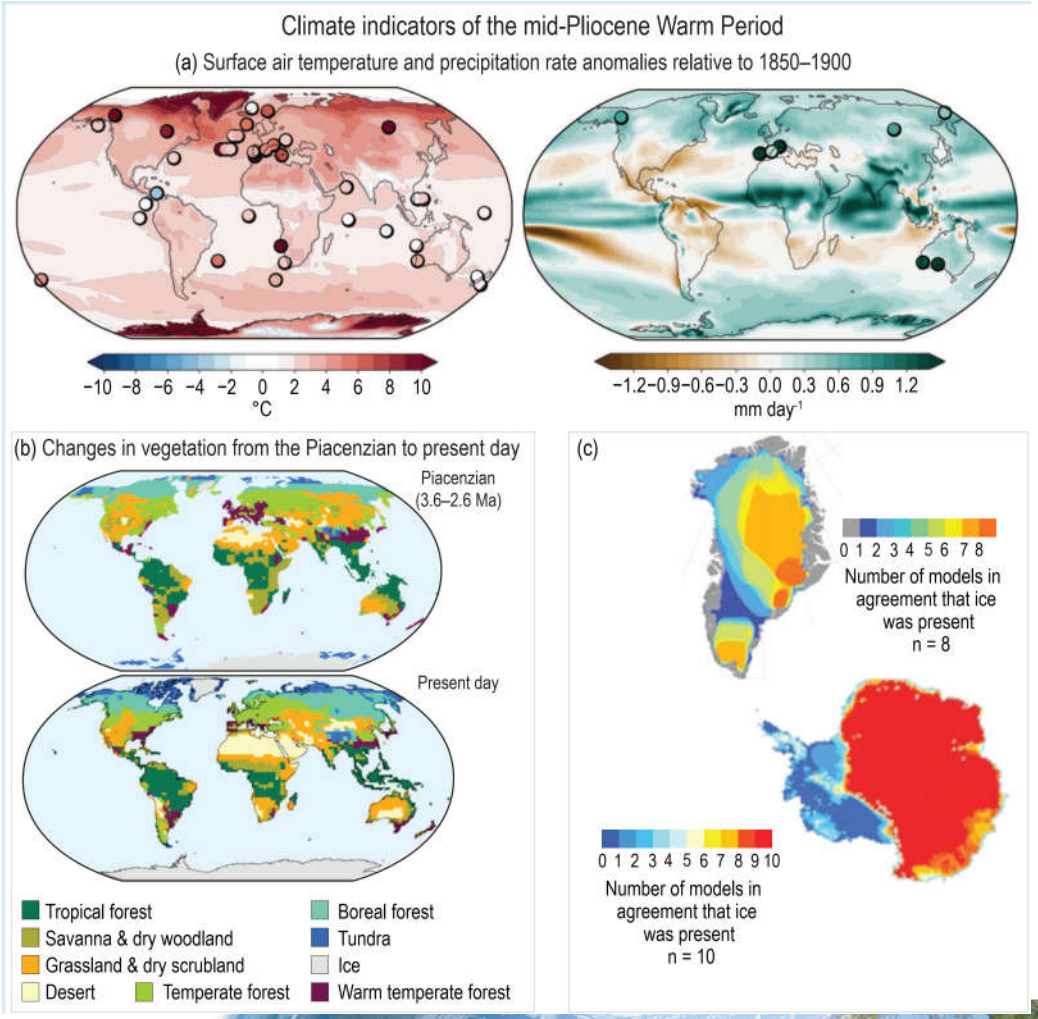
Climate indicators of the mid-Pliocene Warm Period
(a) Surface air temperature and precipitation rate anomalies relative to 1850–1900
−10 −8 −6 −4 −2 0 2 4 6 8 10
°C
−1.2 −0.9 −0.6 −0.3 0.0 0.3 0.6 0.9 1.2
mm day-1
(b) Changes in vegetation from the Piacenzian to present day
Piacenzian
(3.6–2.6 Ma)
Present day
Tropical forest
Savanna & dry woodland
Grassland & dry scrubland
Desert
Temperate forest
Boreal forest
Tundra
Ice
Warm temperate forest
(c)
0 1 2 3 4 5 6 7 8
Number of models in agreement that ice was present
n = 8
0 1 2 3 4 5 6 7 8 9 10
Number of models in agreement that ice was present
n = 10

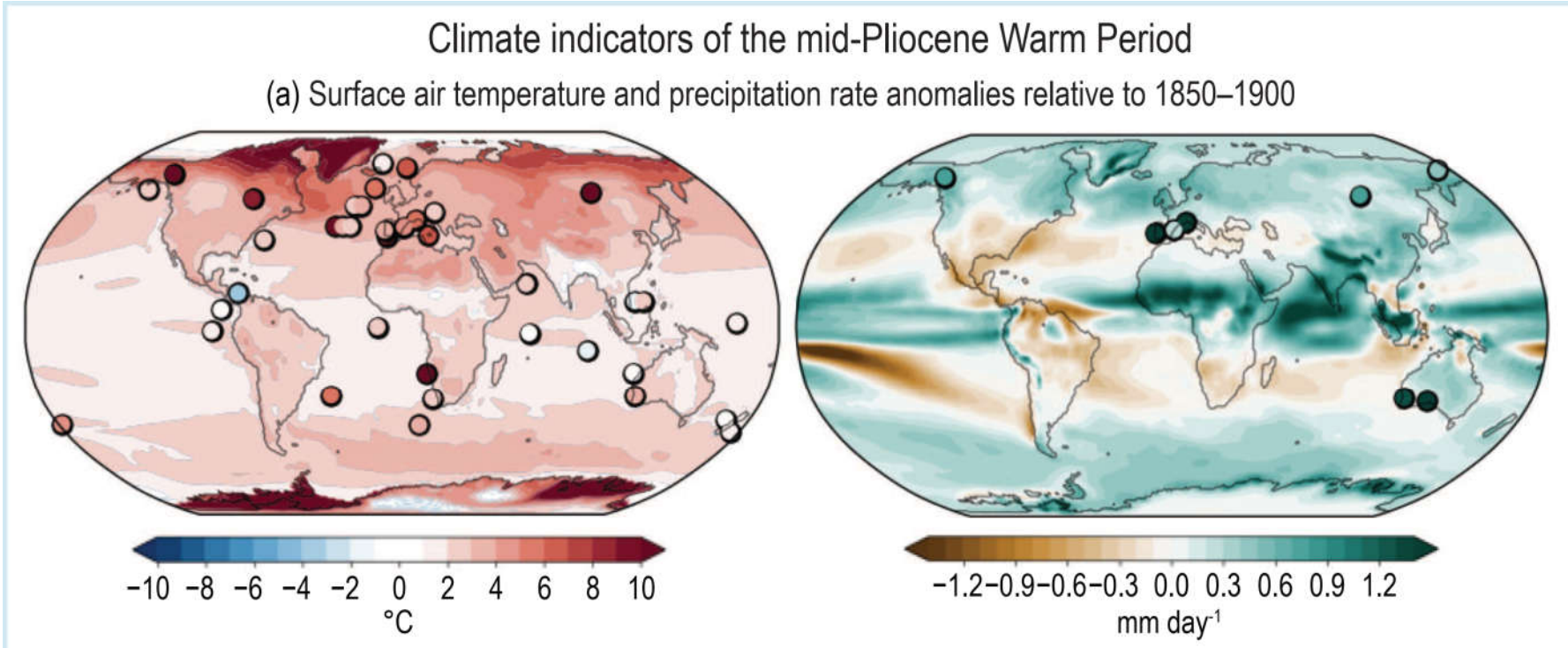

IPCC 2021, Chap. 2

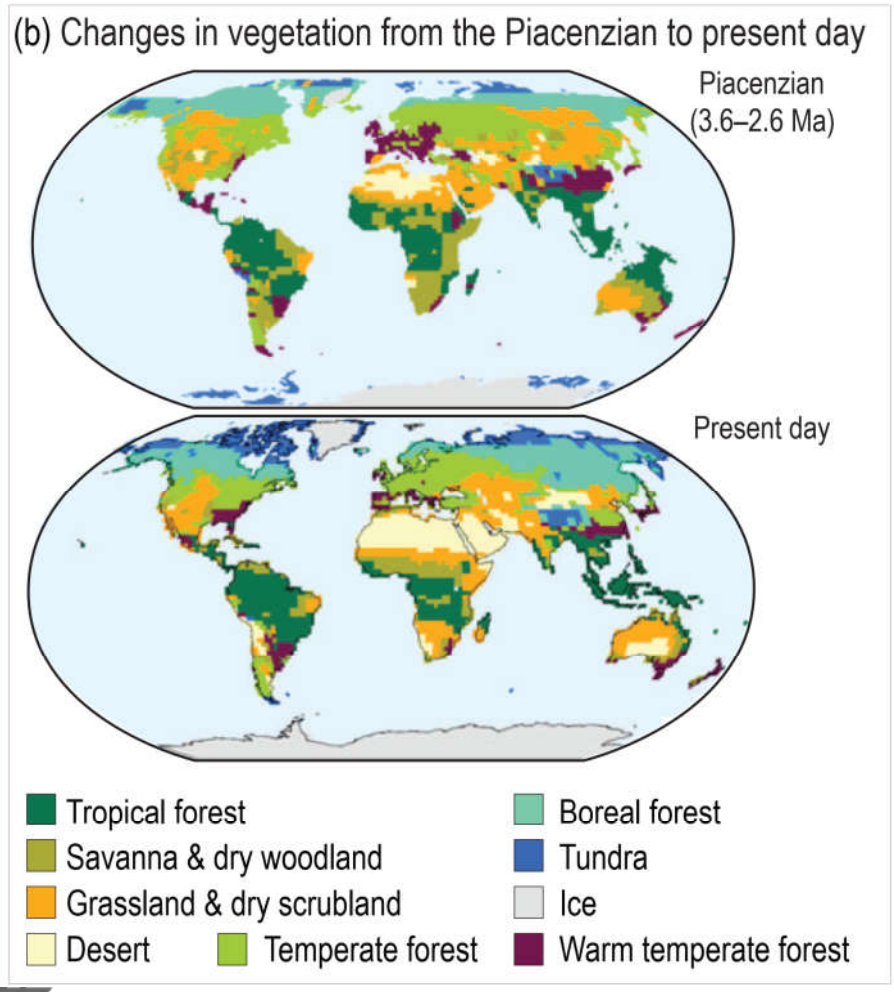

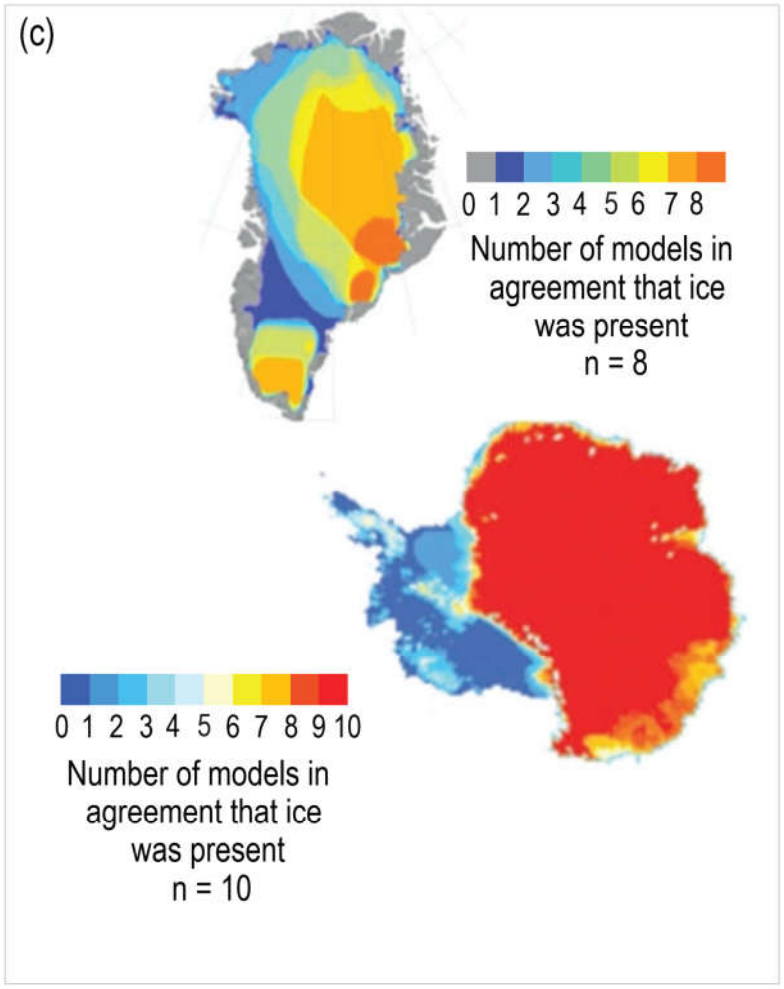

IPCC 2021, Chap. 2

Statements in the Executive Summary

Changes in Modes of Variability

Since the late 19th century, major modes of climate variability show no sustained trends but do exhibit fluctuations in frequency and magnitude at inter-decadal time scales, with the notable exception of the Southern Annular Mode, which has become systematically more positive (*high confidence*). There is *high confidence* that these modes of variability have existed for millennia or longer, but *low confidence* in detailed reconstructions of most modes prior to direct instrumental records. Both polar annular modes have exhibited strong positive trends toward increased zonality of midlatitude circulation over multi-decadal periods, but these trends have not been sustained for the Northern Annular Mode since the early 1990s (*high confidence*). For tropical ocean modes, a sustained shift beyond multi-centennial variability has not been observed for El Niño–Southern Oscillation (*medium confidence*), but there is *low evidence* and *low agreement* about the long-term behaviour of other tropical ocean modes. Modes of decadal and multi- decadal variability over the Pacific and Atlantic oceans exhibit no significant trends over the period of observational records (*high confidence*). {2.4}

IPCC 2021, Chap. 2

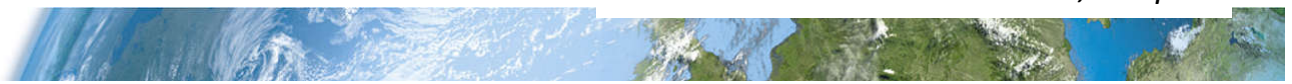

Southern Annular Mode (SAM) reconstruction over the last millennium

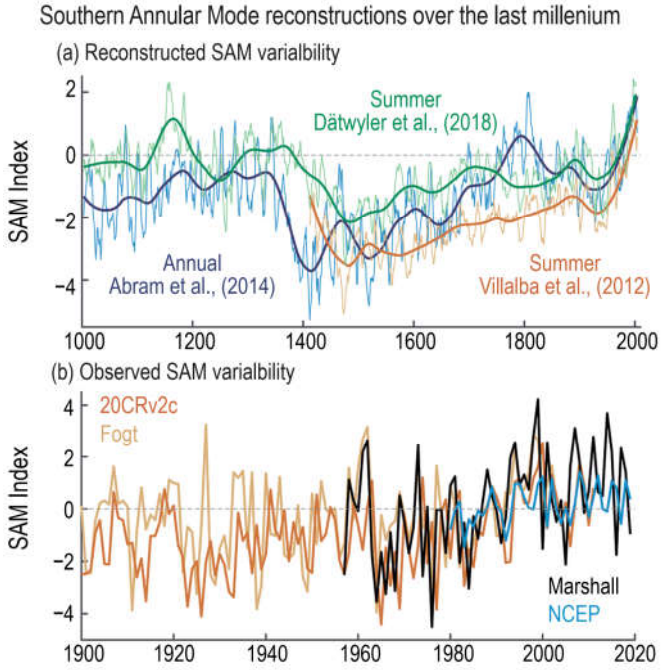

The Southern Annular Mode is usually defined as the difference in the zonal mean sea level pressure at 40°S (mid-latitudes) and 65°S (Antarctica)

IPCC 2021, Chap. 2

Figure 2.35 | Southern Annular Mode (SAM) reconstruction over the last millennium. (a) SAM reconstructions as seven-year moving averages (thin lines) and 70-year LOESS filter (thick lines). **(b)** Observed SAM index during 1900–2019. Further details on data sources and processing are available in the chapter data table (Table 2.SM.1).

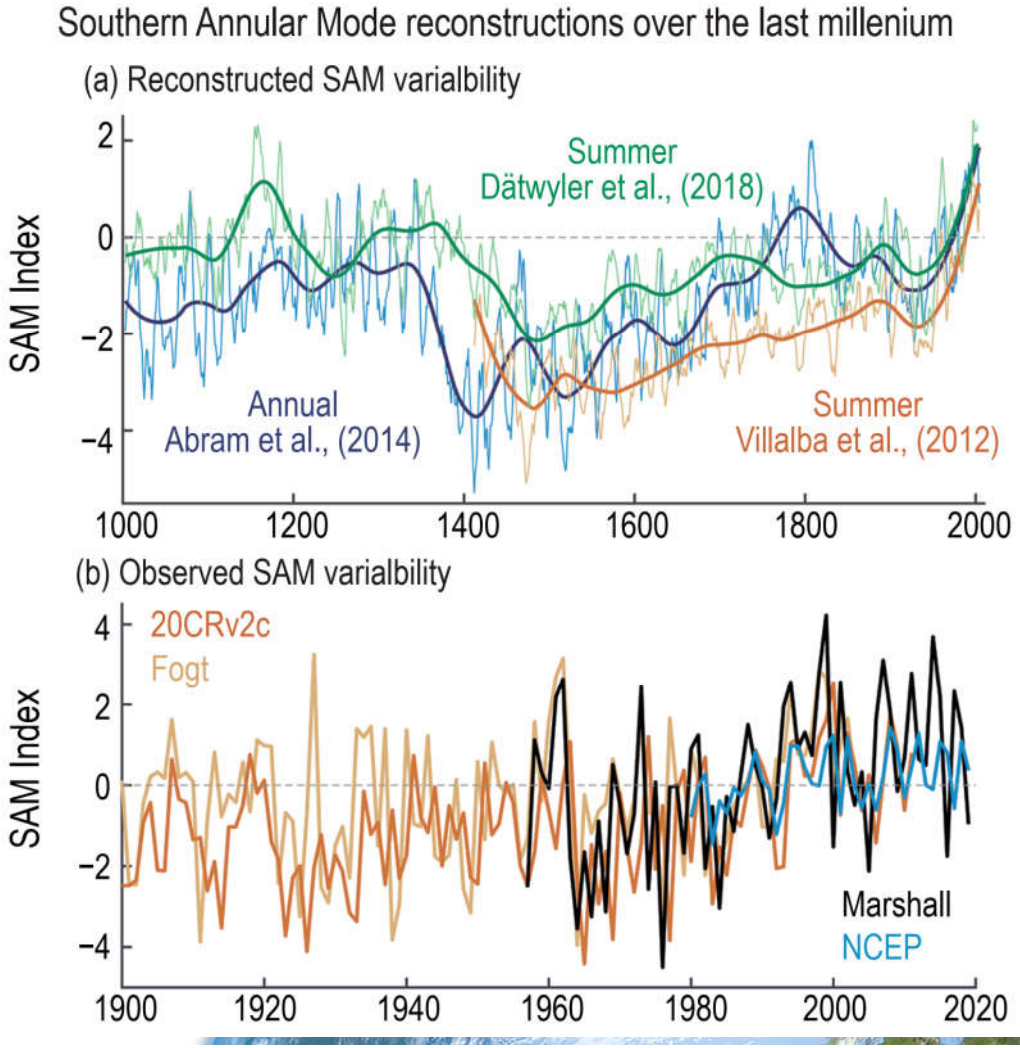

IPCC 2021, Chap. 2

Reconstructed and historical variance ratio of El Niño–Southern Oscillation (ENSO)

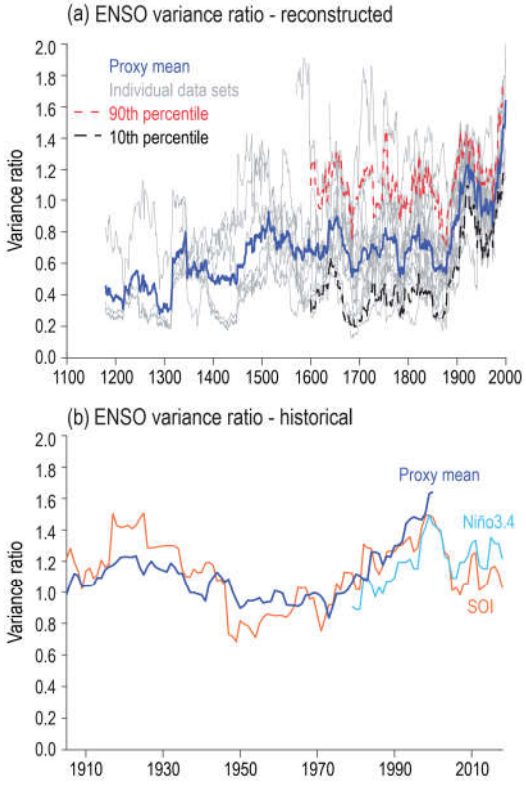

Figure 2.36 | Reconstructed and historical variance ratio of El Niño–Southern Oscillation (ENSO). (a) 30-year running variance of the reconstructed annual mean Niño 3.4 or related indicators from various published reconstructions. **(b)** Variance of June–November Southern Oscillation Index (SOI) and April–March mean Niño 3.4 (1981–2010 base period) along with the mean reconstruction from (a). Further details on data sources and processing are available in the chapter data table (Table 2.SM.1).

IPCC 2021, Chap. 2

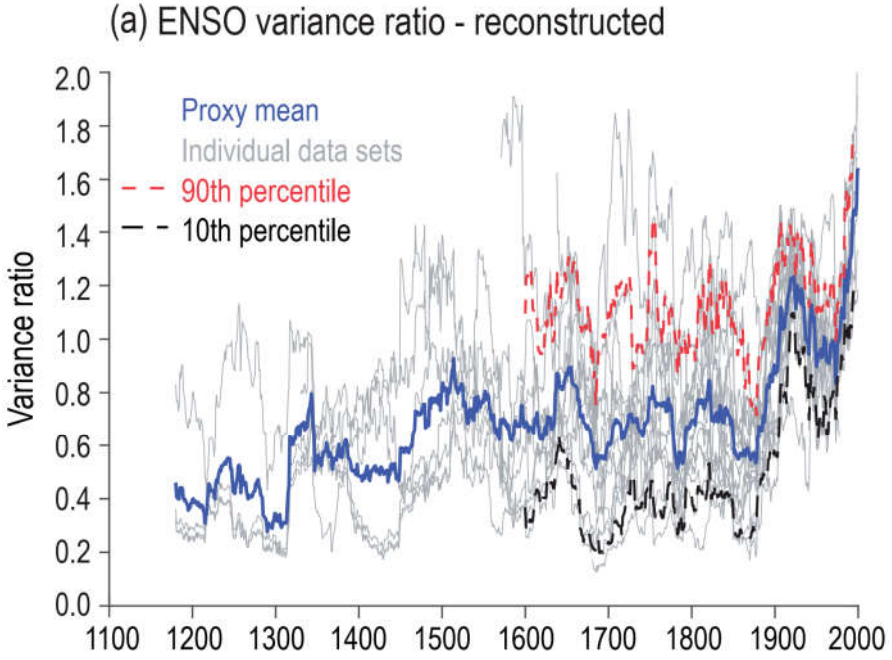

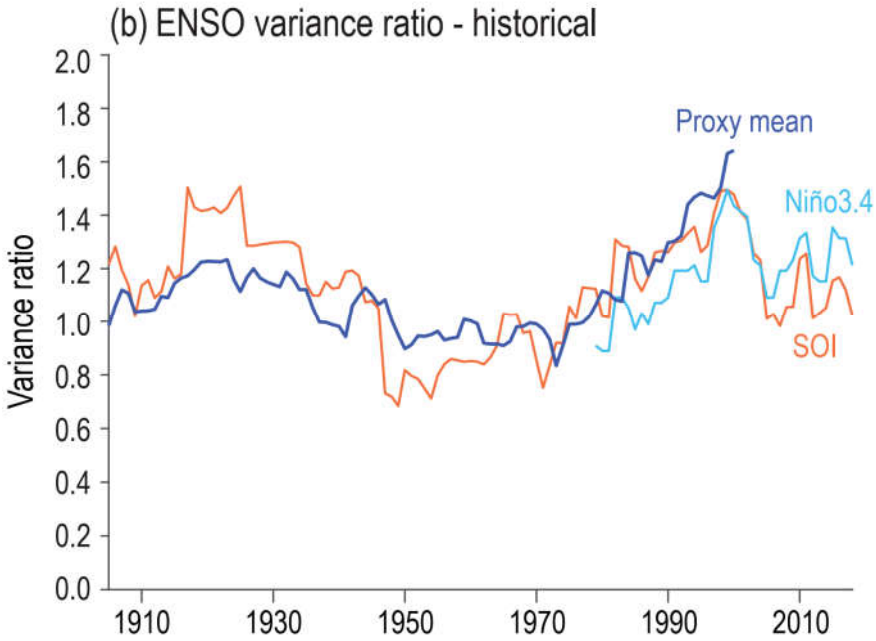

IPCC 2021, Chap. 2